

Design and Construction of a Supersonic Wind Tunnel

A Major Qualifying Project

Submitted to the Faculty

of

Worcester Polytechnic Institute

in partial fulfillment of the requirements for the

Degrees of Bachelor of Science

in Aerospace and Mechanical Engineering

by

Kelly Butler

David Cancel

Brian Earley

Stacey Morin

Evan Morrison

Michael Sangenario

March 16, 2010

Approved:

Prof. John Blandino, MQP Advisor

Prof. Simon Evans, MQP Co-advisor

Executive Summary

The goal of this project was to design and construct a small-scale, supersonic wind tunnel. The wind tunnel was intended to use the difference between atmospheric pressure and the pressure inside the vacuum chamber in WPI's Vacuum Test Facility (VTF) to achieve its desired flow velocities. A previous MQP already designed a small, supersonic wind tunnel, but it was designed for one specific Mach number. As such, it was decided that this project would aim to make a tunnel capable of achieving various test section Mach numbers. The completed wind tunnel was designed for educational and research purposes.

Previous MQP Work

The previous supersonic wind tunnel was designed by WPI alumnus Peter Moore. His tunnel was intended to achieve a test section Mach number of 3.68. The tunnel contours—the pieces that form the shape of the upper and lower sections through which the air flows—were solid pieces of aluminum with a fixed shape that was predetermined using the method of characteristics. Two end pieces were also designed, one that served as a connector to attach the wind tunnel to the vacuum chamber, and one with a ball valve used to control the flow of air into the tunnel after the chamber was pumped down to the appropriate pressure. Since Peter Moore was unable to finish the tunnel completely before he graduated, this project team also finished the tunnel assembly after all of its components were fabricated, tested it several times, and attempted to fix problems which arose.

Methodology and Design

Before any designing commenced for the second wind tunnel, calculations were performed for various states of operation to determine design restrictions and feasibility in terms of run-time, test section area, and desired Mach number. In addition to revealing additional

design constraints, the calculations confirmed the theory that adding a diffuser would increase run time. Another set of calculations were performed using isentropic flow and Mach-area relations in order to determine expected pressures and temperatures throughout the tunnel.

The tunnel designed for this project had a test section with similar cross sectional area to that of the previous tunnel, and also used the same ball valve end piece. Since this tunnel was intended to be capable of reaching several test section Mach numbers, the contour shape needed to be variable. The contours were thus designed of flexible polystyrene strips and secured to aluminum backbone pieces, support pieces that run the length of the tunnel. The sections of the contours for which adjustability was a necessity, such as the throat, expansion and straightening sections, and diffuser section, were controlled by pivoting screw adjustment mechanisms. As with the previous tunnel, the shape of the contour for a given Mach number was determined using the method of characteristics. The variable shape resulted in a changing contour length, so the tunnel was designed to have excess contour length extending into the vacuum chamber. A tensioning system was created to keep the polystyrene taught. The test section was held flat with linear slides, which allowed the contour to adjust its length when the throat and expansion sections are changed. Like its predecessor, this tunnel was designed as an indraft tunnel which exhausts into the vacuum chamber. Since the ball valve was positioned at the inlet of the tunnel and not between the tunnel and the vacuum chamber, the tunnel was forced to be pumped down to a low pressure with the vacuum chamber. As such, it was necessary to ensure that the tunnel was sealed against the atmosphere. Otherwise, the chamber would not have been able to reach its desired pressure. Sealing the tunnel was accomplished by attaching rubber O-ring to the edges of the contours and compressing the contours between the two acrylic side plates.

Results

The various runs of the tunnel from the previous MQP revealed severe leaking issues. Through modifications to the sealing gaskets and the use of side panel compression in subsequent runs, the leaking was drastically reduced. Successful sealing ideas were incorporated into the design of the second tunnel. The lowest pressure achieved with the first tunnel (static pressure just before opening of the inlet valve) was 17 Torr. The necessary interface components for the second tunnel were not completed in time to run it with the vacuum chamber. Mechanically, the tunnel operated as desired; the screw adjusters moved the contour properly, and the linear slide allowed the contour to move as designed.

Acknowledgements

The project group would like to thank the following individuals for their assistance on this project:

Prof. Blandino and Prof. Evans - for their continual guidance and advice throughout the project, and for pushing us to dig deeper and search for better solutions

Torbjorn (Toby) Bergstrom, Adam Sears, Neil Whitehouse and Erik Macchi - for their assistance in manufacturing

Michael Fagan - for his advice in designing for manufacturability and manufacturing techniques, and for donating his time and materials to the project

Barbara Furhman - for her help in ordering and receiving materials and helping us keep track of our budget

Hydro Cutter, Inc. - for providing water jet services to the project

Table of Contents

Executive Summary	i
Previous MQP Work	i
Methodology and Design	i
Results	iii
Acknowledgements	iv
Table of Contents	v
List of Figures	viii
List of Tables	xi
1 Introduction	1
2 Background	2
2.1 Introduction to Wind Tunnels	2
2.2 Introduction to Compressible Flow Regimes	2
2.3 Method of Characteristics	5
2.3.1 Characteristics	5
2.3.2 Unit Processes	7
2.3.3 Design of Supersonic Wind Tunnel Nozzles	8
2.3.4 Method of Characteristics Procedure	11
2.4 Supersonic Wind Tunnel Design	13
2.4.1 Supersonic Wind Tunnel Types	14
2.4.2 Supersonic Diffusers	18
2.4.3 Variable Geometry	19
2.5 Vacuum Technology	21

2.6	Psychrometrics/Condensation	22
2.7	Diagnostics and Flow Visualization	27
2.7.1	Presure Measurements	27
2.7.2	Shadowgraph Imaging	31
2.8	Previous Work (Peter Moore's Tunnel)	32
3	Methodology	35
3.1	Initial Calculations	35
3.1.1	Facility and Model Assumptions	35
3.1.2	Intermittent Test Duration	36
3.1.3	Steady State Operation	41
3.1.4	Diffuser Effects on Intermittent Test Time	48
3.1.5	Condensation	52
3.2	Variable Contour Ideation	56
3.2.1	Axially Shifting Contour Tunnel	56
3.2.2	Constant Force Spring Tunnel	57
3.3	Method of Characteristics Calculations	59
3.4	Detailed Design	61
3.4.1	Large Flange	61
3.4.2	Wind Tunnel	65
4	Testing	70
4.1	Peter Moore's Tunnel	70
4.1.1	Test One: Systemic Leaks	70
4.1.2	Test Two: Thicker Gaskets	74
4.1.3	Test Three: Pinched Gaskets & Screw Hole Leakage	75
4.1.4	Test Four: Backbone Corner Leakage	76
4.2	Variable Geometry Tunnel Construction	76

4.3 Large Flange Manufacturing	81
5 Recommendations	83
5.1 Sealing the Tunnel	83
5.2 Axially Shifting Tunnel Design	84
5.3 Ball Valve Assembly	84
5.4 Shadowgraph Imagery	85
References Cited	86
A Assembly Procedure	88
B Part and Assembly Drawings	89
C MOC MATLAB Code	100
D MOC Config: Mach 2.5	108
E MOC Config: Mach 3.68	109
F MOC Config: Mach 4.0	110
G Bill of Materials	111
H Effect of Probe Introduction	112
I Pressure Diagnostics	115
J Psychrometrics Data	120

Certain materials are included under the fair use exemption of the U.S. Copyright Law and have been prepared according to the fair use guidelines and are restricted from further use.

List of Figures

2.1	Notation for point-to-point method of characteristics calculations	6
2.2	Supersonic flow in a two-dimensional diverging channel	9
2.3	Incident wave reflected off flat wall	9
2.4	Supersonic flow in a two-dimensional diverging channel	9
2.5	Example Characteristic Mesh	10
2.6	Continuous Wind Tunnel	15
2.7	Blowdown Wind Tunnel	15
2.8	Indraft Wind Tunnel	17
2.9	Axial Shifting Tunnel Diagram	21
2.10	The Vacuum Chamber/VTF	22
2.11	Pressure vs. Pump Speed of Vacuum Pump	23
2.12	Moisture Content in Atmospheric Air	25
2.13	Pressure Effects on Dew Point	26
2.14	Change in Dew Point due to Axial Position Compared to Change in Temperature	26
2.15	Pitot Tube	29
2.16	Pitot-Static Tube	30
2.17	Pitot-Static Tube in Supersonic Flow	30
2.18	Professor Evans' Shadowgraph Setup	31
3.1	Intermittent Indraft Tunnel Test Time Calculation Flowchart	39
3.2	Test Time vs. Throat Height	40
3.3	Test Time vs. Throat Height at Mach 2.20	40
3.4	Continuous Operation Scenarios	42
3.5	Throat and Test Section Height vs. Mach No. for Normal Shock at End of Test Section	44

3.6	Throat and Test Section Height vs. Mach No. for Matched Condition Flow	44
3.7	Continuous Test Flowchart with Normal Shock at End	46
3.8	Continuous Test Flowchart for Matched Condition	47
3.9	Diffuser Test Time Calculation Flowchart	49
3.10	Test Time Increase vs. Throat Height Ratio for Mach 2.0	50
3.11	Test Time Increase vs. Throat Height Ratio for Mach 3.5	51
3.12	Maximum Achievable Mach Number with No Supercooling Allowed	53
3.13	Maximum Achievable Mach Number with 55°F of Supercooling	53
3.14	Standard Schematic for Dryer	54
3.15	Axially Shifting Tunnel	57
3.16	Constant Force Spring	58
3.17	Constant Force Spring Tunnel Sketch	59
3.18	Expansion and Straightening Section Contour for Mach 2.5	60
3.19	Expansion and Straightening Section Contour for Mach 3.68	60
3.20	Expansion and Straightening Section Contour for Mach 4.0	60
3.21	Rendering of Standard Flange with 4 inch Viewport	61
3.22	Deformation of 8"x3/8" Thick Acrylic Disk Under 1 atm	63
3.23	Deformation of 9.5"x1" Thick Acrylic Disk Under 1 atm	63
3.24	Large Flange Window Recess	64
3.25	Large Flange Final Design	65
3.26	Tunnel Exploded View	66
3.27	Contour Adjuster	67
3.28	Spring Contour Tensioning System	68
3.29	Side Plate Screw Attachment	69
3.30	"Quad" O-Ring Profile	69
4.1	T1 Assembled on VTF	71
4.2	Tape on flange side gasket	72

4.3	Valve End Gasket	73
4.4	VTF End Gasket	73
4.5	T1 Caulking	75
4.6	Throat block profile	77
4.7	Throat Block Fixturing	78
4.8	Complete Tunnel Assembly	80
4.9	Sideplate Gap at Throat	80
4.10	Damaged Carbide Inserts	82
B.1	Adjuster Pivot	89
B.2	Side Plate Drawing	90
B.3	Adjuster Assembly	91
B.4	Chamber Flange	92
B.5	Window Clamp	93
B.6	Window Glass	94
B.7	Diffuser Block	95
B.8	Large Flange	96
B.9	Polystyrene Block	97
B.10	Screw Bracket	98
B.11	Complete Tunnel Drawing	99
H.1	Mach Number vs. Probe Diameter	113
H.2	Reduction in Mach Number vs. Area Reduction Due to Probe	114
I.1	Pressure (psia) vs. Error	118
I.2	Transducer Box Lid View	119
I.3	Transducer Box Views	119

List of Tables

2.1	MOC Example Expansion Section for 6° Divergence	14
4.1	Compounds Used for T2 Assembly	79
G.1	Bill of Materials: Tunnel Parts	111
G.2	Bill of Materials: Assembly Items	111
H.1	T1 Parameters Used for Analysis	113
I.1	Omega Pressure Transducer Specifications	116
I.2	Error Data for Omega PX137-015AV Pressure Transducer	118
J.1	Amount Supercooled vs. Relative Humidity	120
J.2	Maximum Achievable Mach Number with No Supercooling	121
J.3	Maximum Achievable Mach Number with 55°F Supercooling	122
J.4	Maximum Achievable Mach Number with 180°F Supercooling	123
J.5	Maximum Achievable Mach Number with 320°F Supercooling	124

1. Introduction

The goal of this project was to design and construct a small-scale supersonic wind tunnel with a test section area on the order of 20-50 cm². The tunnel was designed to work in conjunction with Worcester Polytechnic Institute's Vacuum Test Facility (VTF). The use of a vacuum chamber to produce the pressure difference to drive the wind tunnel flow makes the tunnel an in-draft style wind tunnel. The tunnel was intended to be more flexible than a previous MQP design, allowing for a variable contour shape and selectable test section Mach number. The finished product was intended for educational and research purposes through the application of flow visualization and other diagnostics.

In order to achieve the project goals, several objectives had to be met. First and foremost, the group had to learn about and understand the different types of supersonic wind tunnels as well as their component parts and functions. Compressible flow theory had to be used to estimate attainable test times given numerous budgetary, scheduling, and technical design constraints (i.e. facility pumping speed, chamber flange dimension, etc.). Several design alternatives had to be considered in detail, followed by the selection of a design that best met the given constraints. In order to determine the ideal shape of the tunnel expansion and straightening section contour, the group had to learn about and apply the method of characteristics (MOC). The last design objective was to research and develop several ideas for creating variable tunnel geometry contours. After all of this, the final objective was to generate complete solid models of the design, fabricate, and finally test the wind tunnel. From that point, the wind tunnel would be available to study properties of external and internal supersonic flow over solid bodies and internal flows.

2. Background

In order to better understand the process of designing and constructing a supersonic wind tunnel, it is important to understand various types of existing wind tunnels and how they function. Additionally, it is critically important to understand the properties of the flow through these tunnels in order to successfully achieve supersonic flow as well as to ensure that the flow is uniform and otherwise conditioned for testing purposes. This chapter provides some background in compressible flow regimes, information about existing wind tunnel hardware and designs, and previous work done in this research area.

2.1 Introduction to Wind Tunnels

A wind tunnel is a device designed to generate air flows of various speeds through a test section. Wind tunnels are typically used in aerodynamic research to analyze the behavior of flows under varying conditions, both within channels and over solid surfaces. Aerodynamicists can use the controlled environment of the wind tunnel to measure flow conditions and forces on models of aircraft as they are being designed. Being able to collect diagnostic information from models allows engineers to inexpensively tweak designs for aerodynamic performance without building numerous fully-functional prototypes. In the case of this project, the wind tunnel will serve as an educational and research tool to analyze basic flow principles.

2.2 Introduction to Compressible Flow Regimes

In fluid mechanics, low speed flows (where kinetic energy is negligible compared to the thermal energy) approximate an incompressible fluid with minimally varying density. Relatively high speed flows (kinetic energy comparable to the thermal energy), on the other hand, may be characterized by significant density changes. The high flow velocities used in

this project go hand-in-hand with large pressure gradients. These large pressure gradients, which ultimately drive the flow, lead to continuously varying flow properties (i.e., temperature, pressure, density, velocity, etc.). Discontinuous variation in those properties can occur if the pressure gradients are large enough, such as across a shock wave. When discussing compressible flow, the Mach number M is often conveniently used to denote the different flow regimes. In supersonic flow, the values of the Mach number correspond to the local flow properties at the point of interest. The Mach number non-dimensionalizes the local flow velocity to the local speed of sound:

$$M = \frac{V}{a} \quad (2.1)$$

Where a is the local speed of sound that depends on the local temperature, the universal gas constant, and the ratio of specific heats.

Subsonic Flow ($M < 1$)

A flow in which the velocity at every point is less than that of sound is defined as *subsonic flow*, i.e. $M < 1$. This flow is generally characterized by smooth streamlines and continuously varying flow properties in the case of laminar flow, though non-smooth streamlines do exist in the turbulent case (e.g. flow in the wake behind a ball). The presence of a body in the flow is “felt” far upstream of the body where the initially straight, parallel streamlines begin to deflect. When the Mach number is less than about 0.3, density changes can be neglected and the flow is assumed to be incompressible. When the Mach number is greater than 0.3, variations in density become more important, and the flow is considered compressible. The subsonic regime is loosely defined with a free stream in which $M_\infty < 1$ [1].

Transonic Flow ($0.8 < M < 1$)

Transonic flow is a special case of subsonic flow. The transonic flow field is characterized by regions of mixed flow where there may have been a shock incident on a surface yielding supersonic flow upstream but subsonic flow immediately behind it. In most situations, shocks

can be considered negligibly thin compared to any other length scale in the flow (thicknesses on the order of 10^{-5} cm are typical). In addition, despite the fact that the Mach number lies between 0.8 and 1, the analytical solution of the conservation equations is much more difficult since neither the elliptic equations used to solve problems in the subsonic regime nor the hyperbolic equations that govern the supersonic flow regime are strictly applicable for the transonic flow regime.

Supersonic Flow ($M < 1$)

A flow field in which the free stream Mach number is greater than unity ($M_\infty > 1$) is defined as *supersonic flow*. In this flow field, the local fluid velocity can be much greater than the local speed of sound. Mach 5 or above qualifies as *hypersonic flow*, which is another regime altogether. In supersonic flows, the presence of a body in the flow is not “felt” until the oblique or normal shock it has created is encountered. This shock results from the coalescence of highly compressed air around the body. This is the flow regime that the wind tunnel in this project aims to create.

Shock Waves

The supersonic flow regime invariably results in the presence of shock waves. Shock waves are formed to preserve continuity at a boundary. The boundary may be a physical one, such as a wall, or a boundary in the fluid (i.e. a slip line or contact surface) such as outside an under-expanded rocket engine nozzle cruising at a relatively high altitude. These shocks may be oblique shock waves or normal shock waves depending on the flow velocity and other physical parameters. A normal shock wave is a special case of an oblique shock wave in which the wave angle relative to the unperturbed flow direction is equal to 90° . Oblique shocks are compression waves. Expansion waves occur as a result of a pressure drop in the flow which increases the velocity, and hence the Mach number. Compression waves operate in precisely the opposite way, decreasing the upstream velocity as a result of an increase in local flow

pressure. A shock wave, whether normal or oblique, is a special case of a compression wave in which the pressure variation becomes discontinuous (and no longer isentropic).

2.3 Method of Characteristics

The physical conditions of a two-dimensional, steady, isentropic, irrotational flow can be expressed mathematically by the nonlinear differential equation of the velocity potential. The method of characteristics is a mathematical formulation that can be used to find solutions to the aforementioned velocity potential, satisfying given boundary conditions for which the governing partial differential equations (PDEs) become ordinary differential equations (ODEs). The latter only holds true along a special set of curves known as characteristic curves, which will be discussed in the next section. As a consequence of the special properties of the characteristic curves, the original problem of finding a solution to the velocity potential is replaced by the problem of constructing these characteristic curves in the physical plane. The method is founded on the fact that changes in fluid properties in supersonic flows occur across these characteristics, and are brought about by pressure waves propagating along the Mach lines of the flow, which are inclined at the Mach angle to the local velocity vector.

2.3.1 Characteristics

Characteristics are unique in that the derivatives of the flow properties become unbounded along them. On all other curves, the derivatives are finite. Characteristics are defined by three properties as detailed by John and Keith [2]:

Property 1 A characteristic in a two-dimensional supersonic flow is a curve or line along which physical disturbances are propagated at the local speed of sound relative to the gas.

Property 2 A characteristic is a curve across which flow properties are continuous, although

they may have discontinuous first derivatives, and along which the derivatives are indeterminate.

Property 3 A characteristic is a curve along which the governing partial differential equations(s) may be manipulated into an ordinary differential equation(s).

For the purposes of notation, if one is considering a point P, the point which connects to P by a right-running characteristic¹ line is considered A, and the point connecting with a left-running line is considered point B, as shown in Figure 2.1. Right-running characteristics are considered to be type I, or C_I lines. Similarly, left-running characteristics are considered to be type II, or C_{II} lines.

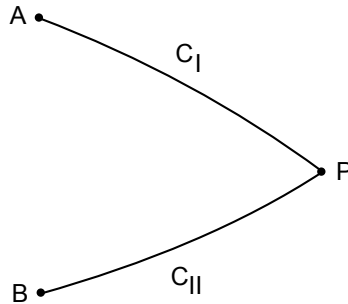


Figure 2.1: Notation for point-to-point method of characteristics calculations

The numerical technique involves the calculation of the flow field properties at discrete points in the flow resulting from a Taylor series expansion of these flow properties [2]. For specific boundary conditions, one constructs, in a stepwise fashion, a “characteristics net” of whatever spatial resolution one would like. One can start with a coarse net and obtain solutions with successively finer nets until two successive solutions agree to a desired decimal

¹Right-running characteristic: A characteristic line which slopes downward to the right. The opposite applies for a left-running characteristic.

accuracy. The reader is referred to References [1] and [2] for a rigorous derivation of the technique and examples of its application.

Since all practical calculations utilize a finite number of grid points, such numerical solutions are subject to truncation error, due to the neglect of higher order terms. Moreover, the flow field calculations are subject to round-off error because all digital computers round off each number to a certain number of significant figures. The Mach wave pattern as determined by the method of characteristics strongly agrees with that produced by Schlieren imaging [2]. Accurate numerical results can be obtained if the first two of the following three precautions are taken in the calculations, and the third precaution is taken in real-time while running the experiment:

1. Avoid very large, adverse pressure gradients.
2. The wall streamline should be displaced by an amount equal to a carefully computed boundary layer thickness.
3. If possible, any large initial boundary layer should be removed via suction.

Finally, it should be noted that the solution of a general two dimensional supersonic flow problem, for which the method of characteristics is applicable, is often easier to obtain than the solution of a similar problem in subsonic flow, where no such procedure exists. This further establishes the utility of the method of characteristics.

2.3.2 Unit Processes

All flow patterns can be synthesized in terms of corresponding wave patterns with the repeated application of a few unit processes. A unit process is a certain calculation procedure for determining flow conditions encountered by a characteristic. As described in Reference [2], “When a characteristic of one family extends into a flow field, it can encounter (1) a characteristic of another family, (2) a boundary, (3) a free surface, or (4) a shock wave.” For details on the computational procedure for each of these situations, the reader is referred to the book by John and Keith [2].

2.3.3 Design of Supersonic Wind Tunnel Nozzles

It is critical that the stream entering the test section of a wind tunnel be uniform and parallel in order to record valid test data. This requirement becomes more difficult to achieve as the Mach number of the flow increases from the subsonic regime to the supersonic regime where shock waves may form. The design of the divergent portion of the supersonic nozzle contour, in particular the straightening section, is extremely important for this reason. The shape of the expansion contour is largely arbitrary and depends somewhat on the shape of the sonic line². It has been demonstrated that theoretical results obtained from the method of characteristics, with the assumption of a near linear sonic line, match quite well to experimental values [2]. Also, it is undesirable to have compression shocks in the nozzle, due to boundary layer behavior. Since large pressure gradients arise through these shocks, the shock interaction with the boundary layer can cause irregularities in the flow and even flow separation. Therefore, the Prandtl-Meyer flow in the straightening section should seek to avoid the formation of oblique shock waves.

For this project, the method of characteristics was utilized to design a contour shape that produces test section flows that are free of shocks. To accomplish this, an initial channel divergence angle is chosen for the expansion region of the contour where the channel simply expands as a linearly diverging section, as pictured in Figure 2.2.

Immediately downstream of this section, the channel walls begin to straighten out, gradually becoming horizontal to turn the flow straight and produce uniform streamlines. In normal circumstances, when an incident wave impinges upon a flat wall, that wave is reflected off at an angle, as shown in Figure 2.3.

In the case of the straightening section, the wall of the contour is turned exactly through the wave turning angle α at the point at which the wave meets the wall, as shown in Figure 2.4.

²Sonic Line: A curve in a flow along which the Mach number equals unity. For wind tunnel nozzles, this exists somewhere in the throat and is usually nonlinear

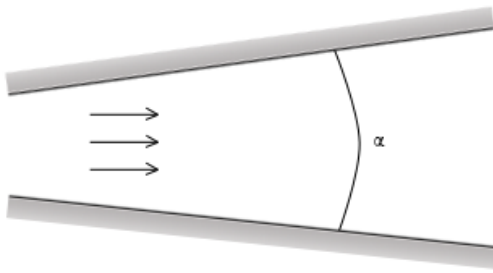


Figure 2.2: Supersonic flow in a two-dimensional diverging channel

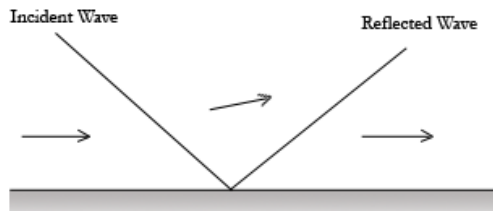


Figure 2.3: Incident wave reflected off flat wall

Turning the wall in this manner cancels the reflected wave by eliminating the need for it. The angled wall satisfies the boundary condition, as it causes flow to run parallel to the wall.

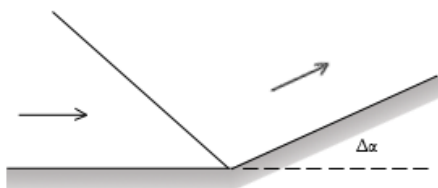


Figure 2.4: Supersonic flow in a two-dimensional diverging channel

The characteristic net employed in the calculations for this project finds numerous points at which to turn the wall contour to create a continuous smooth curve of wave cancellations.

Calculations of the characteristic “net” started with a sample spreadsheet recreating an example method of characteristics calculation presented in John and Keith’s *Gas Dynamics* [2]. The example consisted of a 12° diverging channel with an initial Mach number of 2 at the inlet. Because the channel was symmetrical, only the top half was considered (for a half-angle divergence of 6°). The arced initial value line (or “sonic line”) from which the rest of the flow field calculations are carried out was divided into four points having divergence increments of 2° between 0 and 6° . The spreadsheet was designed to match the initial 18 point example in the book, then further expanded to calculate all 32 points in the example expansion region shown in Figure 2.5.

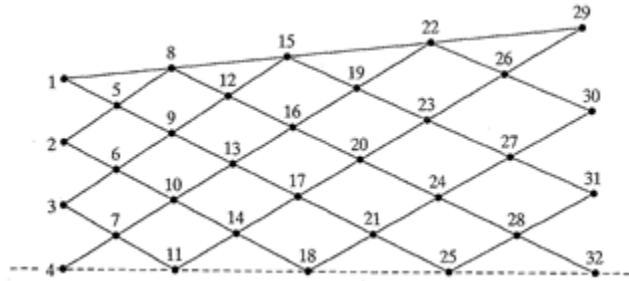


Figure 2.5: Example Characteristic Mesh (Ref. [2], ©2006, Pearson Prentice Hall)

After this was complete, the example mesh was then extended to create the straightening section, which was not present in the example. In this section, each local angle of each wall point was chosen to coincide with the local flow angle in order to cancel out the reflected Mach wave. Knowing the local angle of the wall as a function of axial position along the tunnel, the contour is fully defined. This region—the straightening section—ensures that test section flow is free of shocks.

2.3.4 Method of Characteristics Procedure

As previously mentioned, calculations began by dividing the initial value line into four increments to represent increasing angles of divergence. Points 1 through 4 were assigned α values of 6° , 4° , 2° , and 0° respectively. The Prandtl-Meyer angle ν was then calculated using the Prandtl-Meyer function (Equation 2.2 with known initial Mach numbers).

$$\nu(M) = \sqrt{\frac{\gamma+1}{\gamma-1}} \tan^{-1} \sqrt{\frac{\gamma-1}{\gamma+1} (M^2 - 1)} - \tan^{-1} \sqrt{M^2 - 1} \quad (2.2)$$

After this, C_I and C_{II} were calculated using Equations 2.3 and 2.4.

$$C_I = \nu + \alpha \quad (2.3)$$

$$C_{II} = \nu - \alpha \quad (2.4)$$

From here, the Mach angle μ was found by Equation 2.5.

$$\mu = \sin^{-1} \frac{1}{M} \quad (2.5)$$

The y-coordinate of point 1 in the example is arbitrarily chosen to be 1 “unit” (a physical dimension corresponding to the throat half-height), and therefore the x-coordinate $x_1 = y_1/\tan \alpha$. From these points, the radius of the initial value line is determined by Equation 2.6.

$$R_{IVL} = \sqrt{x_1^2 + y_1^2} \quad (2.6)$$

The coordinates of the other first four points were then calculated using $x = R_{IVL} \cos \alpha$ and $y = R_{IVL} \sin \alpha$, to form a curved sonic line.

After the first four points, further calculations followed a slightly different course. For these points, calculations began by using Equations 2.3 and 2.4 to calculate C_I and C_{II} for each subsequent point, referring to the ν and α values for the appropriate upstream points

as detailed in Figure 2.1. Values for ν and α were then calculated using Equations 2.7 and 2.8.

$$\alpha = \frac{C_I - C_{II}}{2} \quad (2.7)$$

$$\nu = \frac{C_I + C_{II}}{2} \quad (2.8)$$

Microsoft Excel’s “Goal Seek” feature was used to solve for the Mach number M at the point using the solution for ν from Equation 2.2. The angle μ was again found by Equation 2.5. For non-boundary points, the slopes of the characteristic lines leading to the point in question were calculated using Equations 2.9 and 2.10.

$$m_I = \tan \left[\frac{(\alpha - \mu)_A + (\alpha - \mu)}{2} \right] \quad (2.9)$$

$$m_{II} = \tan \left[\frac{(\alpha + \mu)_B + (\alpha + \mu)}{2} \right] \quad (2.10)$$

This equation averages the values of $(\alpha - \mu)$ and $(\alpha + \mu)$ for the point itself and the corresponding upstream point to produce a more accurate result. The x-coordinate of the point was calculated using Equation 2.11.

$$x = \frac{y_A - y_B + m_{II}x_B - m_Ix_A}{m_{II} - m_I} \quad (2.11)$$

The y-coordinate can then be calculated using whichever of the following two equations is more convenient for a given point:

$$y = y_A + m_I(x - x_A) \quad (2.12)$$

$$y = y_B + m_{II}(x - x_B) \quad (2.13)$$

If the point in question lies on a boundary, whether it lies on the contour itself or the

centerline, α is known. It corresponds to either the predetermined divergence angle of the section or the horizontal centerline ($\alpha = 0^\circ$). In these cases, different equations must be used. Equation 2.14 is used to calculate C_I for points on the centerline, while Equation 2.15 is used to calculate C_{II} for points along the contour. The slopes of type I characteristics of contour points were calculated using Equation 2.16. Likewise, the slopes of type II characteristics for centerline points were calculated using Equation 2.17.

$$C_I = \nu_A + \alpha_B = \nu_P + \alpha_P \quad (2.14)$$

$$C_{II} = \nu_B - \alpha_B = \nu_P - \alpha_P \quad (2.15)$$

$$m_I = \tan \alpha \quad (2.16)$$

$$m_{II} = \tan \alpha \quad (2.17)$$

This process continued throughout the entirety of the expansion section and the straightening section. In the straightening section, however, the α values of the points forming the contour were taken to be equal to the α value of that point's corresponding B point (as labeled in Figure 2.1), which ultimately turned the flow back to completely horizontal flow.

Table 2.1 shows how a simple spreadsheet program can be configured to calculate discrete points in the flow. This shows only the expansion portion of the algorithm, using the equations and processes presented above.

2.4 Supersonic Wind Tunnel Design

Supersonic flow brings many new challenges in design, from developing the required pressure differential to drive the high speed flows to preventing shocks from forming in the test section. There are many aspects of supersonic wind tunnels which must be analyzed and carefully considered throughout the design process. In developing a new tunnel, the facility constraints and other design constraints must all be considered in determining what may be

Table 2.1: MOC Example Expansion Section for 6° Divergence^a

Point	α deg	ν deg	C_I deg	C_{II} deg	M	μ deg	$\alpha + \mu$ deg	$\alpha - \mu$ deg	m_I	m_{II}	x	y
1	6	26.3798	32.3798	20.3798	2	30	36	-24	-	-	9.5144	1.0000
2	4	26.3798	30.3798	22.3798	2	30	34	-26	-	-	9.5435	0.6673
3	2	26.3798	28.3798	24.3798	2	30	32	-28	-	-	9.5609	0.3339
4	0	26.3798	26.3798	26.3798	2	30	30	-30	-	-	9.5668	0.0000
5	5	27.3798	32.3798	22.3798	2.0360	29.4173	34.4173	-24.4173	-0.4496	0.6798	9.8264	0.8597
6	3	27.3798	30.3798	24.3798	2.0360	29.4173	32.4173	-26.4173	-0.4922	0.6299	9.8504	0.5162
7	1	27.3798	28.3798	26.3798	2.0360	29.4173	30.4173	-28.4173	-0.5364	0.5822	9.8625	0.1721
8	6	28.3798	34.3798	22.3798	2.0730	28.8420	34.8420	-22.8420	0.1051	0.6906	10.1221	1.0639
9	4	28.3798	32.3798	24.3798	2.0730	28.8420	32.8420	-24.8420	-0.4585	0.6403	10.1530	0.7100
10	2	28.3798	30.3798	26.3798	2.0730	28.8420	30.8420	-26.8420	-0.5014	0.5921	10.1716	0.3552
11	0	28.3798	28.3798	28.3798	2.0730	28.8420	28.8420	-28.8420	-0.5459	0.0000	10.1778	0.0000
12	5	29.3798	34.3798	24.3798	2.1105	28.2822	33.2822	-23.2822	-0.4258	0.6510	10.4695	0.9160
13	3	29.3798	32.3798	26.3798	2.1105	28.2822	31.2822	-25.2822	-0.4676	0.6023	10.4951	0.5500
14	1	29.3798	30.3798	28.3798	2.1105	28.2822	29.2822	-27.2822	-0.5109	0.5557	10.5079	0.1834
15	6	30.3798	36.3798	24.3798	2.1477	27.7500	33.7500	-21.7500	0.1051	0.6623	10.8005	1.1352
16	4	30.3798	34.3798	26.3798	2.1477	27.7500	31.7500	-23.7500	-0.4351	0.6132	10.8335	0.7576
17	2	30.3798	32.3798	28.3798	2.1477	27.7500	29.7500	-25.7500	-0.4773	0.5661	10.8533	0.3790
18	0	30.3798	30.3798	30.3798	2.1477	27.7500	27.7500	-27.7500	-0.5209	0.0000	10.8600	0.0000

^a Bold entries indicate known information for the given point.

most feasible to construct.

2.4.1 Supersonic Wind Tunnel Types

In order to better understand wind tunnel operation and to determine the best approach to take for this project, three types of wind tunnels were researched. Each approach, continuous, blowdown, and indraft, has its advantages and disadvantages, making certain wind tunnels more suitable for some purposes than others. Given the available resources, this project's focus was ultimately on the indraft design despite the advantages of both the blowdown and continuous types.

Continuous wind tunnels are essentially a closed-circuit system and can be used to achieve a wide range of Mach numbers [3]. They are designed so that the air that passes through the tunnel does not exhaust to the atmosphere; instead, it enters through a return passage and is cycled through the test section repeatedly as pictured in Figure 2.6. This type of wind tunnel is beneficial because the operator has more control of the conditions in the test section than with other approaches since the tunnel is cut off from the environmental conditions once running. In comparison to other wind tunnel types, continuous wind tunnels have superior flow quality due to the different facets of the tunnel's construction. The turning vanes in the corners and flow straighteners near the test section ensure that relatively uniform flow passes

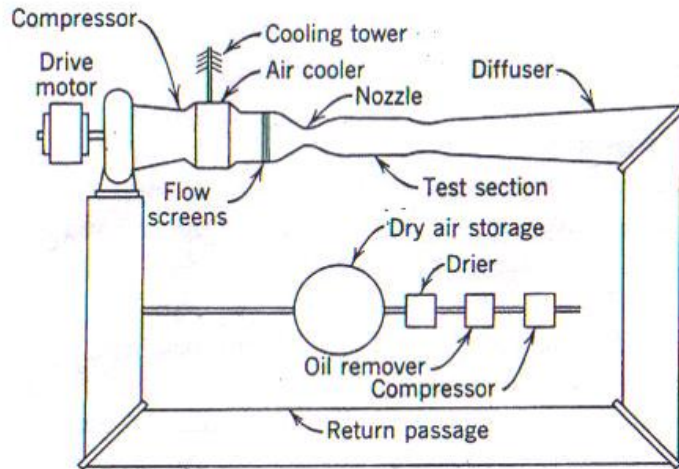


Figure 2.6: Continuous Wind Tunnel (Ref. [3], ©1965, John Wiley & Sons, Inc.)

through the test section [4]. Continuous tunnels also operate relatively quietly. Finally, the testing conditions can be held constant for extended periods of time [3], and the overall time for each run is typically longer than with other approaches. Unfortunately, some continuous tunnel designs require two or more hours to reach the desired pressure, and their construction is complicated and expensive [3]. The latter point made a continuous wind tunnel a poor choice for this project, as adequate facilities were not available to support such a device.

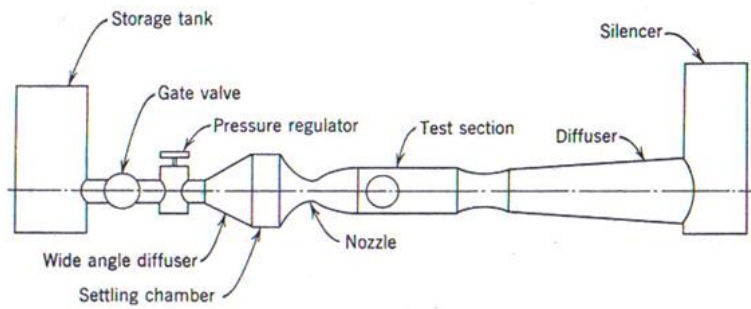


Figure 2.7: Blowdown Wind Tunnel (Ref. [3], ©1965, John Wiley & Sons, Inc.)

Blowdown tunnels were also researched (see Figure 2.7). They can have a variety of different configurations and are generally used to achieve high subsonic and mid-to-high supersonic Mach numbers [3][5]. Blowdown tunnels use the difference between a pressurized

tank and the atmosphere to attain supersonic speeds. They are designed to discharge to the atmosphere, so the pressure in the tank is greater than that of the environment in order to create flow from the tank out of the tunnel. In one configuration, known as a “closed” blowdown tunnel, two pressure chambers are connected to either side of the tunnel [5]. In this configuration, one chamber would contain a high pressure gas and the other chamber would be at a very low pressure. At the beginning of a run, valves are opened at each chamber, and the pressure differential causes air to flow in the direction of the lower pressure until the two chambers have reached equilibrium. The test section is positioned at the end of the supersonic nozzle. Many blowdown tunnels have two throats, with the second throat being used to slow supersonic flow down to subsonic speeds before it enters the second chamber.

In other types of blowdown wind tunnels, the low pressure chamber is removed, and the tunnel discharges directly into the atmosphere, as with Figure 2.7. There are several advantages to blowdown tunnels: they start easily, are easier and cheaper to construct than other types, and have “superior design for propulsion and smoke visualization” [5]. Blowdown tunnels also have smaller loads placed on a model as a result of the faster start time. These tunnels, however, have a limited test time. As a consequence, faster, more expensive measuring equipment is needed. They can also be noisy. This design was determined to not be the best choice for this project; a high pressure chamber would have been needed, which would have resulted in costs that would have significantly exceeded the project budget.

The final type researched, and the approach taken for this project, was the intermittent indraft tunnel (see Figure 2.8). Intermittent indraft wind tunnels use the difference between a low pressure tank and the atmosphere to create a flow [3]. A vacuum tank is pumped down to a very low pressure, and the other end of the tunnel is open to the atmosphere. When the desired vacuum pressure is reached, a valve is opened, and air rushes from outside the tunnel, in through the test section, into the vacuum chamber. The end of the run occurs when the pressure differential is no longer great enough to drive the tunnel at the desired test section Mach number [3]. One of the benefits of an indraft tunnel is that the stagnation

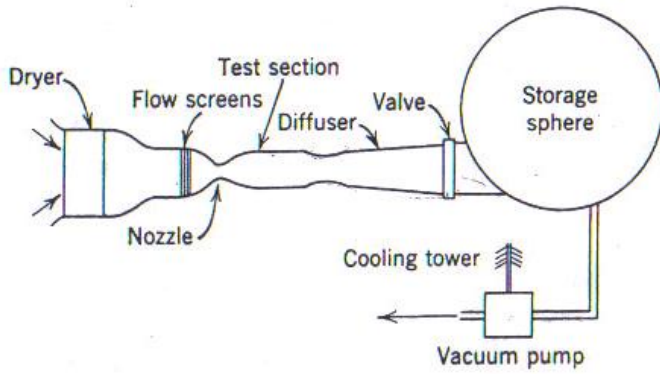


Figure 2.8: Indraft Wind Tunnel (Ref. [3], ©1965, John Wiley & Sons, Inc.)

temperature can be considered constant throughout a run. Additionally, the flow is free of contaminants from equipment used by other wind tunnel types. For example, there is no need for the pressure regulators required by blowdown tunnels. In comparison to other types of tunnels, indraft tunnels can operate at higher Mach numbers before a heater is necessary to prevent flow liquefaction during expansion. Lastly, using a vacuum is safer than using high pressures. High pressure tanks face the risk of exploding, while the reversed pressure differential of a vacuum chamber only results in the risk of an implosion. Indraft tunnels typically have nine major components: a vacuum tank, pump, test section, diffuser, settling chamber, nozzle, one or two valves (between the test section and tank), and a drier. One of the major disadvantages of indraft wind tunnels is that they can be up to four times as expensive as their blowdown counterparts [3]. Additionally, the Reynolds number for a particular Mach number can be varied over a greater range with a blowdown tunnel. Finally, while indraft tunnels are capable of running without air driers, they may only do so up to Mach 1.6 without condensation. In order to address this problem, air can be slowly dried and stored in a balloonet over time, or it can be dried as it is used. Because WPI's Vacuum Test Facility (VTF) was available for use, it was decided that it was most feasible from the standpoint of both cost and ease of fabrication, to design and build an indraft tunnel for this project.

2.4.2 Supersonic Diffusers

The role of a supersonic diffuser is to take the supersonic gas from a wind tunnel's test section and slow it down to a subsonic velocity at the exit plane in order to reduce the overall pressure differential needed to operate the tunnel. The function of a diffuser is to slow down the flow with as little loss in total pressure as possible [1]. If the entire process was perfectly isentropic, the ratio of total pressures would be unity. This situation would imply the possibility of a perpetual motion machine, which is impossible. Since the flow is assumed to be nearly isentropic and the total pressure loss is low, a diffuser ultimately reduces the minimum pressure ratio required to drive the tunnel. As a result of this reduction, supersonic tunnels that use pressurized (or evacuated) systems to drive air flow, such as the indraft type, can achieve longer test durations for a given initial pressure difference. Without a diffuser, these low pressures would normally cause any other tunnel to unstart, meaning the throat would un-choke and the flow would be subsonic. The diffuser makes operation at these low pressures possible.

As discussed earlier, the style of wind tunnel used in this project is the indraft type, which uses an evacuated chamber to drive the flow of air through the tunnel. Given initial research into this style of wind tunnel, test durations were found to be on the order of tens of seconds. The installation of a supersonic diffuser would be advantageous in order to attain longer test times. Achieving longer test durations would allow more time to conduct experiments and analyze flow diagnostics. Calculations had to be done to determine the required diffuser area ratio for different Mach numbers of interest to analyze its overall effectiveness in terms of extending test duration. The flow is not perfectly isentropic due to boundary layers caused by friction and non-ideal conditions which introduce losses. As a rule of thumb, diffuser throat area must be larger than that of the nozzle to allow the throat to swallow shock waves [1]. Once the dimensions of the desired throat areas were obtained, test durations could be derived from the mass flow and a series of pressure ratios. These calculations proved important because they showed that diffusers, in terms of this project, provide at

most a 3 second increase in test time.

2.4.3 Variable Geometry

There are two parameters in supersonic wind tunnels which are commonly made variable, both of which are area ratios. The first is the driving parameter for speed in any supersonic wind tunnel: the area ratio between the first (nozzle) throat and test section. It is advantageous to be able to adjust this ratio over a range to achieve a varying test section Mach number, allowing for a wider range of testing capabilities. The second ratio is that of the diffuser throat area to the nozzle throat area. As discussed previously, the minimum allowable diffuser throat size is larger than the nozzle throat size for steady-state operation, due to tunnel starting requirements. A variable area diffuser enables the diffuser throat to be constricted to the optimum size once the shock has been swallowed.

Variable area diffusers are more prevalent than variable nozzle throats because they are significantly simpler to manufacture and operate. Shocks downstream of the test section are irrelevant in most tunnels, since they do not affect the flow in the test section. This means that adjustable diffusers can be made mechanically simple, as the specific contour shape is unimportant. For each Mach number, there exists an Area-Mach relationship that describes the minimum diffuser area based on the area of the first throat and the ratio of total pressures.

A variable geometry diffuser provides the flexibility to precisely select exact diffuser dimensions to maximize its efficiency and thus its effectiveness in lengthening test times. If the nozzle has variable geometry as well, a variable geometry diffuser would allow the most efficient operation of the wind tunnel over a greater range of Mach numbers as it would be able to adapt to the Area-Mach relations. In terms of scale model testing, a variable geometry diffuser would allow the diffuser to be opened, enabling wedges and various other scale models to be inserted into the test section from downstream, and then readjusted once the models were in position.

In reality, the “maximum” diffuser efficiency³ is never attainable with a fixed diffuser, since it requires a throat too small to successfully start the tunnel. Variable diffusers can circumvent this by allowing the diffuser throat to change size after the tunnel has been started. This is only useful in tunnels with test durations long enough to allow adequate time to adjust the diffuser mid-run.

It is important in most supersonic tunnels to keep the test section as free of shocks as possible. The contour of the throat and expansion section is critical to maintaining a smooth flow through the test section, and any variable geometry in that region must reflect that. This means that, unlike a variable diffuser, the nozzle throat must curve gently, without sharp turns or corners. Depending on how exact the Mach number in the section must be, the contours may also have to closely match lines specified by the method of characteristics.

Lockheed Martin operates a large-scale supersonic wind tunnel which uses a flexible steel sheet to match an exact contour and keep the flow in the test section uniform and shock-free [6]. Hydraulic jacks spaced along the nozzle contours hold the steel sheet in place during operation, but they can be adjusted in between tests to vary the test section speed. The disadvantage is that this type of mechanism is mechanically complex and requires an involved process to re-adjust.

Asymmetric wind tunnels are unique in that they possess two different contours which, when axially translated in relation to one another (Figure 2.9), can accelerate air much like their more traditional symmetric counterparts.

This type of tunnel allows easier manipulation of Mach numbers at any given time, even during operation. A simple axial translation of one of the contour surfaces results in a change in characteristic throat area and a consequent change in area ratios, causing a change in the Mach number. For other traditional variable geometry wind tunnels, various points along

³Anderson [1] defines diffuser efficiency as the ratio of the actual total pressure ratio across the diffuser (P_{d0}/P_0) to the total pressure ratio across a hypothetical normal shock wave at the location of the test section Mach number (P_{02}/P_{01}). A diffuser efficiency of 1 denotes a normal shock diffuser. With this definition, the diffuser efficiency can exceed unity indicating better pressure recovery than one could obtain with just a normal shock.

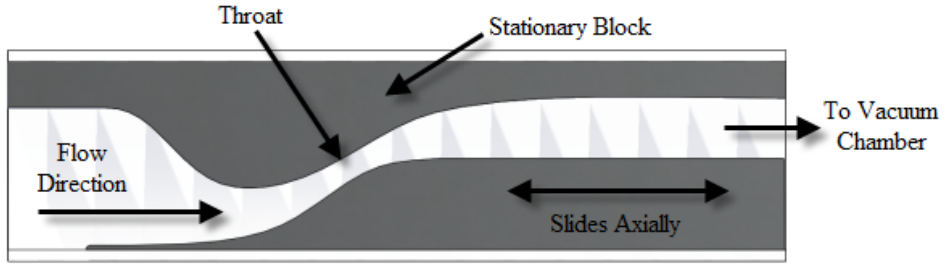


Figure 2.9: Axial Shifting Tunnel Diagram

the control surfaces must be accurately adjusted to follow the method of characteristics to change the area relations and to ensure a shock-free environment.

The most attractive feature of an asymmetric wind tunnel is the simplicity of its mechanics, as it only requires sliding one contour back and forth along the tunnel's axis to change the throat size. However, according to research done by the U.S Air Force, asymmetric wind tunnels need to be twice as long as their symmetric counterparts and the boundary layers that exist within the test section are thicker than normal [7]. Because they are twice as long, asymmetric wind tunnels may not be the best choice if space is an issue. At the University of Michigan, researchers have reported that they have not encountered any difficulties with the increased thickness in the boundary layer even after several years of operation of their asymmetric tunnel [7]. Another potential drawback of this tunnel type is that it has a limited range of motion and achievable Mach values before the shocks generated can no longer be cancelled out and begin to propagate in the test section area and make experimental data useless.

2.5 Vacuum Technology

The Vacuum Test Facility (VTF) used for this project has three main components: a vacuum chamber, a two-part pumping system, and a cryopump. The stainless steel vacuum chamber is 50 inches in diameter by 72 inches long (see Figure 2.10).



Figure 2.10: The Vacuum Chamber/VTF

It has several small flange ports with viewing windows around its cylindrical section, and a large port with a blank cover on the door. The port covers can be removed, allowing for the attachment of experiments or diagnostic equipment. For this work (which does not require very high vacuum, the chamber is pumped down using a system comprised of a rotary mechanical pump and a positive displacement blower. Combined, they can pump over 560 liters/s and reach a vacuum of 10^{-2} to 10^{-3} Torr (see Figure 2.11 for complete pumping speed information).

For achieving even higher vacuums, the cryopump is used. The cryopump is a 20 inch CVI TM500 capable of achieving pressures in the range of 10^{-4} to 10^{-7} Torr, and provides pumping speeds of up to 10,000 liters/s for nitrogen, 8500 liters/s for argon, and 4600 liters/s for xenon. The facility uses Pirani and hot cathode vacuum gauges.

2.6 Psychrometrics/Condensation

Significant temperature and pressure gradients arise in the flow through a converging-diverging nozzle as the flow transitions from a subsonic to a supersonic regime. As a result, supersonic wind tunnel design and its effectiveness rely heavily on the control and monitoring of the vapor content in the air. Psychrometrics is the study of the relationship between the mixture of dry air and water in a vapor state [3]. The study of psychrometrics involves basic

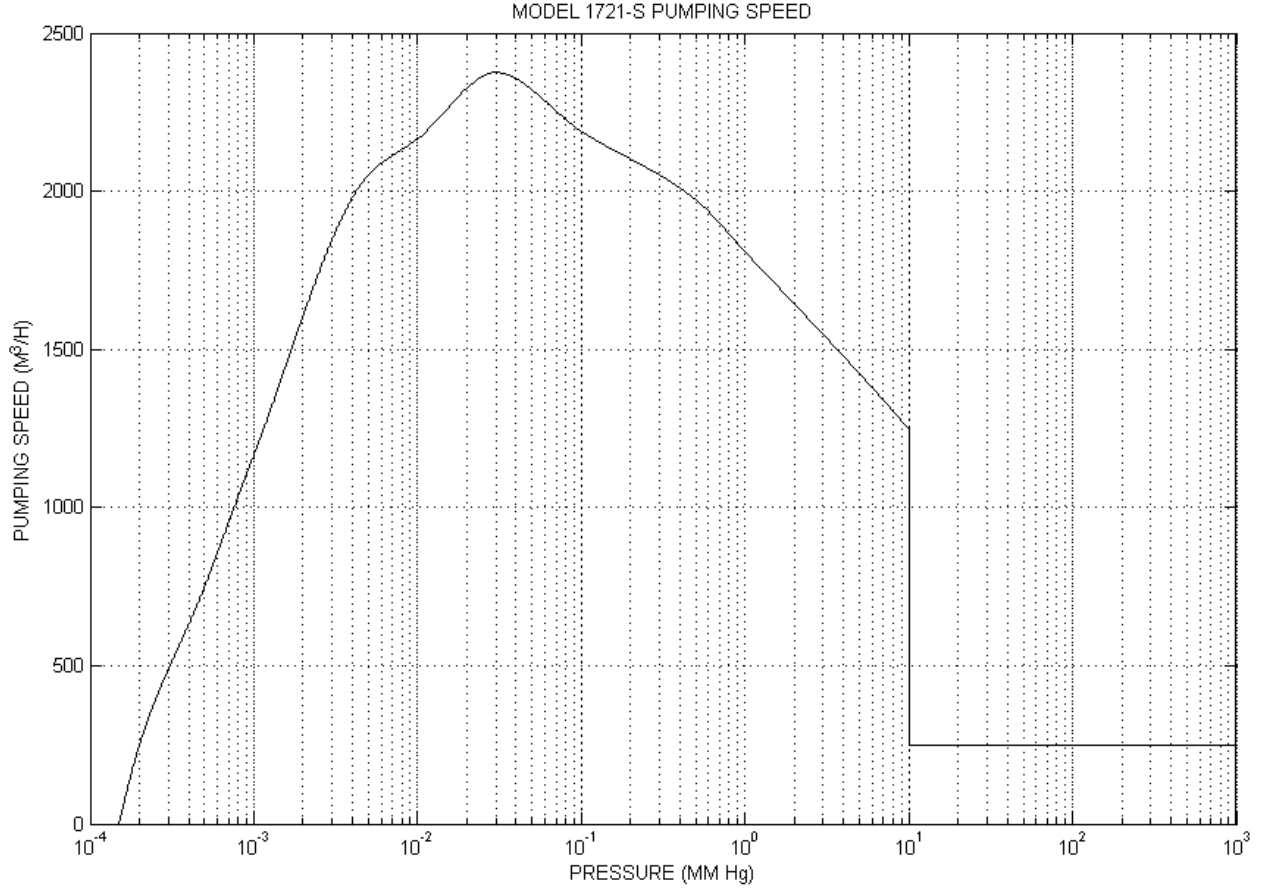


Figure 2.11: Pressure vs. Pump Speed of the Vacuum Pump [8]

knowledge of some thermodynamic concepts such as relative humidity, dew point temperature, and pressure. Relative humidity is defined as the ratio of the mole fraction of water vapor, at a given temperature and pressure, to the mole fraction of saturated air, at the same temperature and pressure. Relative humidity is denoted as a percentage. The dew point temperature is defined as the temperature at which the mole fraction of water vapor, at a given temperature and relative humidity, will saturate the air and cause the vapor to condense out of the air [9]. To find the dew point temperature, Equation 2.18 is used.

$$p_{v1} = \phi * p_g \quad (2.18)$$

For an initial temperature, the partial pressure of the ambient air (p_g) can be found using

the Properties of Saturated Water (Liquid-Vapor). In Equation 2.18, p_g is the pressure of the moist air (i.e. the mixture of air and water vapor). When this is multiplied by the relative humidity ϕ , one obtains the partial pressure of water vapor in the mixture p_{v1} . In practice, one can use a measured relative humidity and the pressure of moist air in the reservoir (ambient pressure for an indraft tunnel) along with Equation 2.18 to calculate the partial pressure of water vapor in the reservoir. A saturated vapor table can then be consulted to find the saturation temperature corresponding to this partial pressure. This temperature is the dew point (Shapiro [9], Appendix A-2E).

Figure 2.12, reproduced from Pope's book [3] on high speed wind tunnel testing, shows how the amount of moisture contained within atmospheric air is a function of both relative humidity and the dry bulb temperature⁴. As can be seen, air at higher temperature and relative humidity is capable of holding greater amounts of moisture per pound of dry air. As air is accelerated to supersonic speeds, it cools as it is isentropically expanded. Conditions may be such that the air may reach temperatures below its dew point, which is known as "supercooling" [3]. If this happens, the concern is that moisture will condense out of its vapor phase and cause fog to appear within the tunnel. If condensation were to occur, it would induce irregularities in the flow characteristics, compromising any data being collected.

Four parameters determine whether or not condensation will occur during wind tunnel operation. The first parameter is the amount of moisture contained within the air. This can be found given the initial temperature and relative humidity of the ambient air within the laboratory. Two additional parameters to be considered are the static temperature and pressure seen by the gas as it is accelerated to a supersonic state. The fourth and final parameter is that of time, specifically the time for the process of heat transfer to cool the air [3].

At supersonic speeds, the static temperature of air decreases with increasing Mach number. Using isentropic flow tables (such Table A.1 in Reference [1]), the ratio of total tem-

⁴Dry bulb temperature is the temperature as measured by a thermometer that is shielded from both radiation and moisture[9]

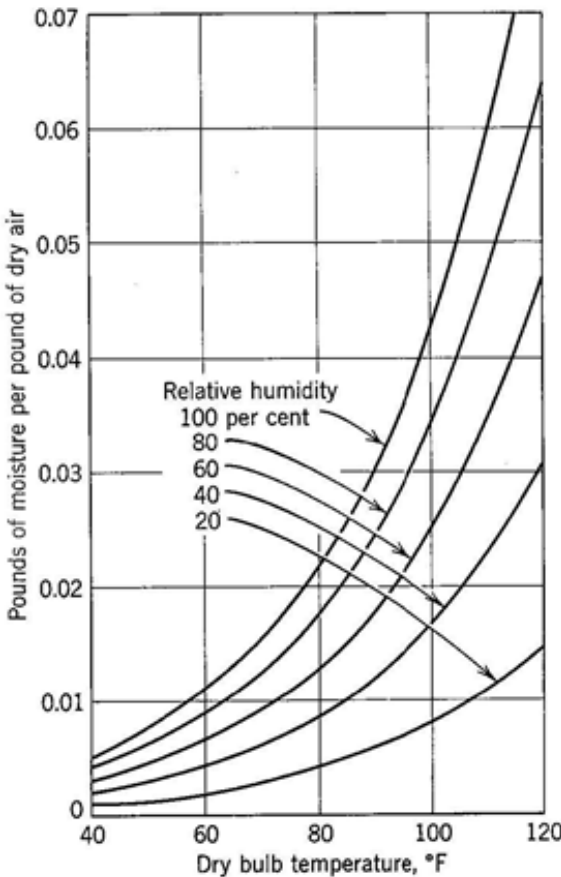


Figure 2.12: Moisture Content in Atmospheric Air (Ref. [3], ©1965, John Wiley & Sons, Inc.)

perature to static temperature can be found for a given Mach number, assuming isentropic flow. These temperatures can easily fall below the dew point temperature of atmospheric air at high Mach numbers and induce condensation.

Condensation is also dependent upon the changes in pressure that occur as air is accelerated to supersonic speeds. When viewing the isentropic flow tables, it can be seen that the ratio of total pressure to static pressure increases more dramatically at higher Mach numbers than does the temperature ratio. Figure 2.13 shows that as pressure is reduced the dew point temperature is also reduced. In terms of preventing condensation, this effect is advantageous.

Figure 2.14 illustrates how the change in temperature as a function of axial position in

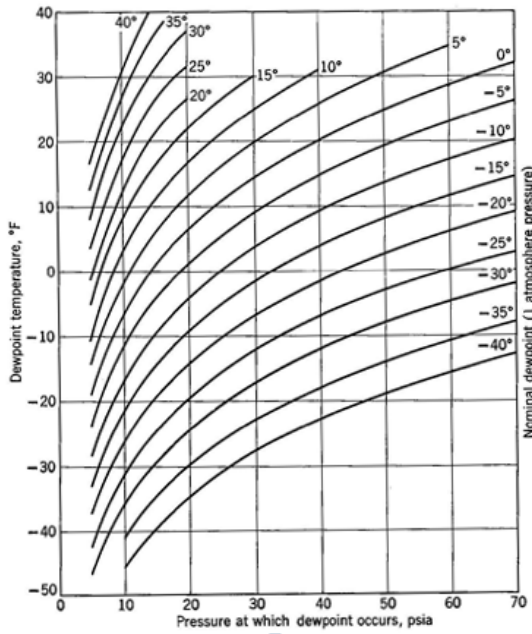


Figure 2.13: Pressure Effects on Dew Point (Ref. [3], ©1965, John Wiley & Sons, Inc.)

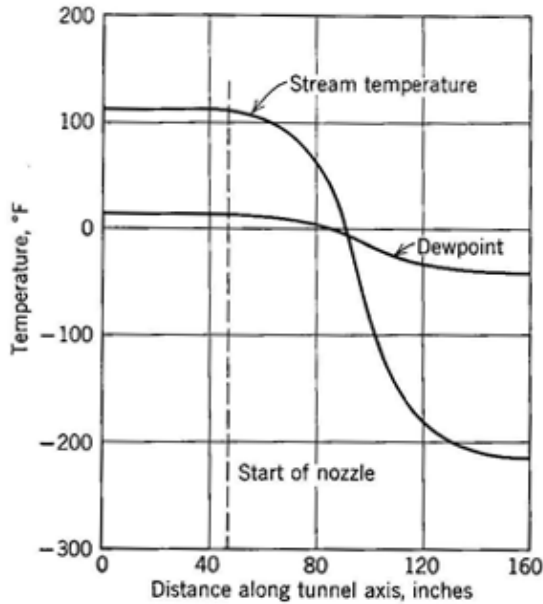


Figure 2.14: Change in Dew Point due to Axial Position Compared with Change in Temperature: $M=2.56$, $T_f=110^\circ\text{F}$, $P_t=25 \text{ psia}$ (Ref. [3], ©1965, John Wiley & Sons, Inc.)

the tunnel is greater than the subsequent change in dew point due to the change in pressure.

The conclusion is that the effect of temperature change is the limiting factor in terms of

anticipating condensation and will be discussed further in Section 3.1.5 [3].

2.7 Diagnostics and Flow Visualization

In order to analyze the flow through the test section and around models being tested, equipment must be used to provide quantitative and qualitative measurements of some of the flow properties. Numerical pressure measurements can be obtained via the use of pressure ports and Pitot probes mounted in and along the flow. Pressure measurements allow for the determination of local Mach numbers at various locations in the flow [2]. Additionally, it can often be useful to be able to visualize the changes in flow properties. This can be done optically through such methods as shadowgraph imaging. Shadowgraph imaging works on the principle that light refraction through a medium is dependent upon the density of that medium. The flow characteristics can be visualized through the observation of the refraction of light directed through the test section [2].

2.7.1 Pressure Measurements

The purpose of this project was to construct a wind tunnel capable of producing supersonic flows. As such, being able to determine the Mach number reached in the test section was essential to confirm successful operation. This is usually done with a method similar to that used by aircraft to determine their flight speeds. Diagnostic equipment measures the static and stagnation pressure of the air, and the velocity or Mach number can be calculated using the appropriate equations [10]. Aircraft diagnostic equipment consists primarily of Pitot-static probes; wind tunnels, however, can use simpler Pitot probes and static pressure taps.

Static Pressure Measurements

In gas dynamics, static pressure is the pressure one would measure if moving along with a fluid element at the same velocity [2]. Devices designed for measuring static pressure are placed perpendicular to the flow direction and are positioned so as not to cause any flow disturbances. The device most often used for measuring the static pressure in a wind tunnel is static pressure port: a hole drilled through the side of the tunnel, connected via tubing to a measurement device such as a transducer or manometer. The hole must be small, with a diameter less 20% of the boundary layer thickness, and must be free of any roughness or obstructions to avoid disrupting the flow [2].

Stagnation Pressure Measurements

In contrast to static pressure, stagnation or total pressure is measured when a flow is brought to rest isentropically (corresponding to full pressure recovery) [2]. The most common devices used to measure stagnation pressure are called Pitot tubes. They have three critical components: the tip, the body, and the measuring device. The body is a narrow tube, and is generally bent at a right angle and inserted into the flow through a hole in the side of the wind tunnel (see Figure 2.15).

The body is aligned directly parallel to the flow, with the tip upstream of the body and facing directly into the flow; due to the tip's positioning and shape, the flow velocity ideally reaches zero isentropically in the tube. The pressure of the gas at rest is then measured by a manometer or gauge. The Mach number can be determined from the relationship between static and stagnation pressures measured at a given point in the flow through Equation 2.19.

$$\frac{P_0}{P} = \left(1 + \frac{\gamma - 1}{2} M^2\right)^{\frac{\gamma}{\gamma - 1}} \quad (2.19)$$

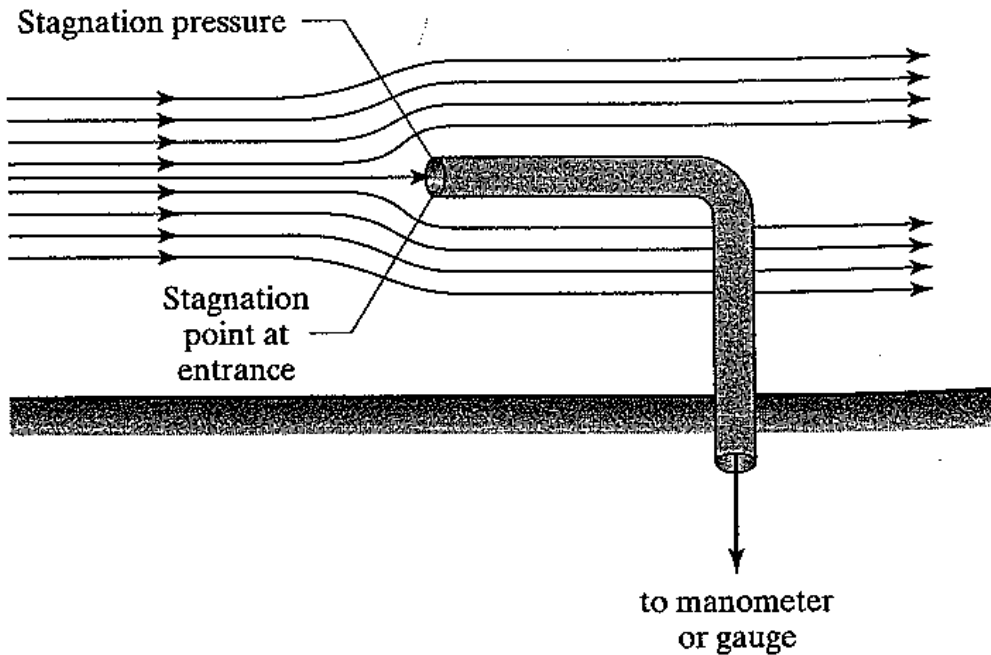


Figure 2.15: Pitot Tube (Ref. [3], ©1965, John Wiley & Sons, Inc.)

Pitot-Static Tubes and Supersonic Flow

Many wind tunnels use a Pitot-static combination tube to measure both types of pressures (see Figure 2.16) [2]. Pitot-static tubes contain nested tubes: the inner tube measures the stagnation pressure while the outer tube simultaneously measures the static pressure. The static pressure tubes are connected to holes on the surface of the outer tube, perpendicular to the flow, and the inner tube is connected to the tip as with a simple Pitot tube. When designing the tip for a subsonic Pitot or Pitot-static tube, there are a wide variety of options. If the flow of interest is supersonic, however, the design options are more limited.

In a supersonic flow, a Pitot-static probe will act as a blunt-nosed body, which will cause a detached bow shock in front of the tip (see Figure 2.17). As a result, the stagnation pressure measured at the tip of the probe is the stagnation pressure of the flow behind the incident normal shock. Equation 2.20, derived in Reference [3] by combining normal shock relations and isentropic flow relations, can be used to determine the Mach number.

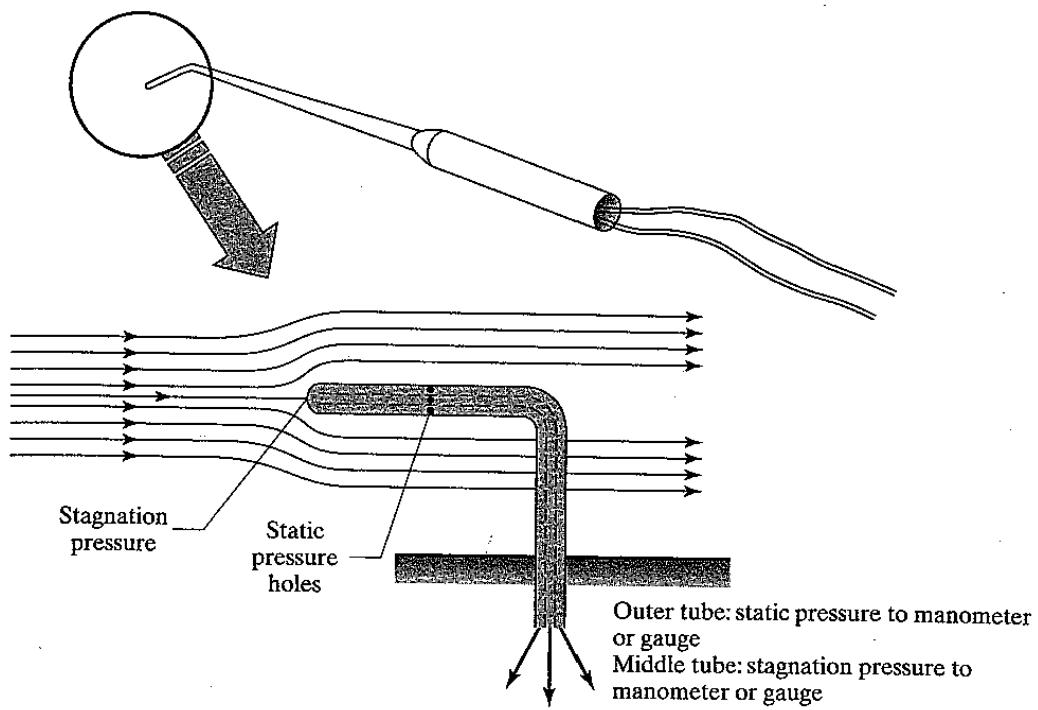


Figure 2.16: Pitot Static Tube (Ref. [3], ©1965, John Wiley & Sons, Inc.)

$$\frac{P_{02}}{P_1} = \frac{\gamma + 1}{2} \left[\frac{(\gamma + 1)^2 M_1^2}{4\gamma M_1^2 - 2(\gamma - 1)} \right]^{\frac{1}{\gamma-1}} \quad (2.20)$$

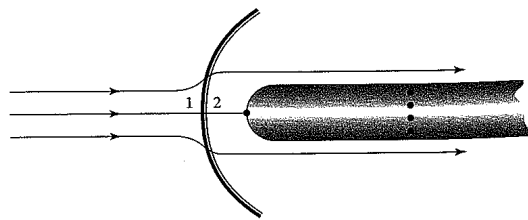


Figure 2.17: Pitot Static Tube in Supersonic Flow (Ref. [3], ©1965, John Wiley & Sons, Inc.)

2.7.2 Shadowgraph Imaging

The shadowgraph is a very simple, inexpensive imaging technique that is well-suited to flows with strong shocks, and therefore sudden changes in density [2]. The system consists of a screen, lens, and a light source. Light travels from the point source to the lens, by which it gets collimated before passing into the test section as nearly parallel beams of light. The light then gets refracted as it passes through the density gradients in the flow, and is then projected onto the screen on the opposite side of the test section. The refracted light is displayed on the screen as shadows, illustrating the density changes in the flow [2].

In past experiments with supersonic wind tunnels, project co-advisor Prof. Simon Evans used a shadowgraph system to visualize shocks [11]. His setup involved a xenon lamp, a condensing lens, a knife edge, a parabolic mirror, and a camera. The condensing lens focused the light from the lamp into a point source, and the knife further sharpened the edge of the point source to reduce blurring of the final image. The parabolic mirror channeled parallel light rays through the test section to the camera, which produced the image. The complete setup is shown in Figure 2.18. Prof. Evans' shadowgraph setup would have been the basis for an optical diagnostic for this project had budgetary constraints not been an issue.

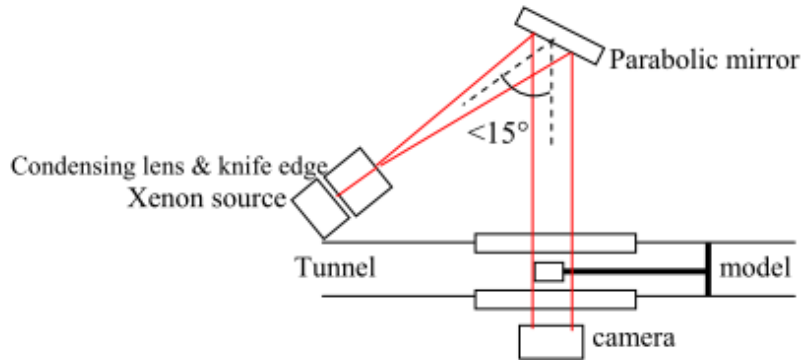


Figure 2.18: Professor Evans' Shadowgraph Setup [11]

2.8 Previous Work (Peter Moore's Tunnel)

A former WPI student, Peter Moore completed a related Major Qualifying Project [12] over the summer of 2009. The goal of Moore's project was to design and build a fixed geometry supersonic wind tunnel for use in the laboratory. His wind tunnel, also an indraft/draw-down type, uses the same vacuum chamber to create the necessary pressure differential to achieve supersonic flow. He worked with all the same design constraints as the current project, such as creating an interface with existing flanges on the vacuum chamber, sustaining supersonic flow for a specified time period, and keeping costs within the given budget.

To design the fixed geometry supersonic nozzle used in his tunnel, Moore made use of the contours calculated by the method of characteristics. The method of characteristics, also used in this project, has previously been described in Section 2.3. As was the case for this project, Moore also determined that it was necessary to operate the tunnel intermittently. This decision was made for several practical and economic reasons.

Moore also researched several other mechanisms that could be used on both blowdown and indraft tunnels to increase run times, but found them unsuitable for his objectives. One of the mechanisms examined was a pre-programmed electronic PID controller and the other was a diffuser. The PID controller is a Proportional-Integral-Derivative controller that would operate the smooth opening and closing of the isolation valve in a blowdown supersonic wind tunnel. Having a PID controller would regulate the airflow to prevent overshoot of stagnation pressure and limit oscillations caused by fast opening valves [12]. The purpose of having a PID controller is to maximize the runtime as well as to minimize transient inefficiencies. Some of the transient inefficiencies associated with the interaction between laminar-turbulent transition and shockwave-boundary layer interactions are largely unknown [12]. For the particular design and use of Moore's tunnel it was deemed that these transient inefficiencies would be negligible, therefore, making the use of a pre-programmed PID controller unnecessary.

Moore also determined that a diffuser would not extend test times long enough to be a

practical addition, due to the fact that the tunnel would be exhausting directly into the vacuum chamber. Moore states, “Considering that the tunnel will be exhausting into a vacuum, the flow will initially be underexpanded and as the tank pressure rises will be overexpanded, and finally a shock will travel up the test section to end the test. It is only during this last time interval, when the shocks form inside the, tunnel that a diffuser would extend test time.” It was later determined over the course of this project that a diffuser would appreciably increase the testing time by increasing the minimum pressure required in the vacuum chamber to run the tunnel. The purpose of diffusers is discussed in depth in Section 2.4.2.

The method of characteristics is an important tool used in determining flow characteristics at distinct points in a flow field. Moore’s exploration of the method of characteristics with John and Keith’s *Gas Dynamics* [2] was enlightening and helpful for work on this project. Moore’s results from the method of characteristics were compared to the results obtained from calculations performed for this project.

Moore performed many initial calculations to determine feasible test section areas, throat areas, and run times which would then help to determine the final design and the contour shape. Some parameters were not in his control, such as the size and pumping capacity of the vacuum chamber, which were important considerations in determining test duration. He primarily used MATLAB for these calculations. Once he settled on the specific parameters he wanted, then he needed to design and fabricate the components of the wind tunnel.

The design went through a few different iterations due to geometric restrictions, as well as manufacturability concerns. One such consideration involved parts in which the transition from a round cross-section to a rectangular cross-section or vice versa needed to be made. In one iteration, the necessary transition from the ball valve to the test section resulted in it being moved to the upstream end of the tunnel. Other constraints included the existing geometry of the vacuum chamber ports and flanges. There were also a couple of design iterations involving the method of characteristics through a trial and error process to design

the tunnel contour. The final design included a ball valve, aluminum rectangular entry flange, the tunnel contours, two acrylic side walls, and the end piece which would attach to the vacuum chamber port. Moore designed all of parts using SolidWorks, except for the ball valve which was purchased prefabricated.

In conclusion, Peter Moore designed and fabricated a supersonic wind tunnel, though he was never able to test it during his time at WPI. His project examined the essential features required to achieve steady, sustained supersonic flow: the contours. Most of his time working on this project was dedicated to working with the method of characteristics calculations to determine a suitable contour design to produce the desired Mach numbers. In the interest of completing his project in a reasonable amount of time, some initial objectives were deemed to be out of the scope of the project, such as the treatment of condensation. Consequently, future work was left to be done, such as assembling the tunnel, testing, and designing test equipment to be integrated into the tunnel.

3. Methodology

Before any of the tunnel designing could be started, preliminary assumptions needed to be established and preliminary calculations needed to be performed. The next step was to consider various tunnel options, select one, and design the tunnel. Finally, an attachment flange needed to be designed that would successfully attach the tunnel to the vacuum chamber.

3.1 Initial Calculations

Before any detailed designs could be seriously considered, many calculations and feasibility studies were performed to determine the functional limitations of any designs, as well as to provide performance benchmarks for comparison with the final product. Many of the eventual design decisions were based on the findings of these initial studies.

3.1.1 Facility and Model Assumptions

Multiple calculations were performed to determine the run-time and area limitations on the final wind tunnel design, as well as to provide a numerical basis for making design decisions concerning factors such as the test section height and desired Mach numbers. Because the tunnel is limited in functionality and shape by the vacuum chamber and other facilities with which it interfaces, certain parameters, assumptions, and relations hold true for all calculations.

The VTF's vacuum chamber determines two basic driving parameters: tank volume ($V_T = 2.32 \text{ m}^2$) and chamber starting pressure ($P_i = 50 \text{ milliTorr}$). In addition, the current attachment flanges on the chamber limit the tunnel's maximum attachment area to approximately 40 cm^2 . The width of the tunnel was assumed to be a constant 1.5 in (3.81 cm), equal to that of the previous tunnel designed and built by Peter Moore. This assumption allowed for comparison between the calculated results for each tunnel.

The calculations assumed an isentropic flow in the tunnel and a polytropic filling process in the tank. Additionally, air was assumed to be an ideal gas with a specific heat ratio of $\gamma = 1.4$, entering the tunnel at standard atmospheric conditions ($P_0 = 101$ kPa, $T_0 = 288$ K). Combining the isentropic assumption with the ideal gas assumption allows for the use of the isentropic Mach-Area relations within the tunnel. Test section Mach numbers between 1 and 5 were evaluated, with Mach 5 being considered the practical upper limit of operation. Lastly, because a supersonic wind tunnel requires a choked throat, the mass flow rate is considered to be constant through the tunnel at all points of operation.

3.1.2 Intermittent Test Duration

For any tunnel with limited run times, the duration of a run is of vital importance, as it imposes limitations on the type of tests that can be performed, as well as what sensing and diagnostic equipment is feasible to use. Ultimately, the goal of this calculation was to derive this test time as a function of the test section Mach number and throat height. Design decisions such as tunnel size and speed were then based on the possible durations of each run.

The calculation for intermittent test time duration assumed that the test section ends where it meets the tank flange, and that there was no diffuser. A run was considered to start when the valve opened, allowing air to flow through the tunnel, and to end when a normal shock coalesces at the intersection of the test section with the vacuum chamber. After this normal shock forms, it starts to move back through the test section. The shock's speed and position would not be known, causing any data gathered during this time to be unusable. This end condition was chosen such that the calculated test duration will encompass the full range of time for which conditions in the test section are known. Equation 3.6 is used to calculate the time for the chamber to fill from the initial pressure to the chamber pressure at the test ending condition.

The first step in determining the intermittent test duration was to find the end pressure

in the tank required to create a normal shock. This shock is a function only of the test section Mach number and reservoir stagnation pressure. Isentropic relations were used to find the test section static pressure, using Equation 3.1.

$$P = P_0 \left(1 + \frac{1 - \gamma}{2} M^2 \right)^{\frac{\gamma-1}{\gamma}} \quad (3.1)$$

From the test section Mach number, the normal shock pressure ratio was used to find the end pressure in the tank P_e with Equation 3.2.

$$P_e = P_0 \left[1 + \frac{2\gamma}{\gamma+1} (M^2 - 1) \right] \quad (3.2)$$

This yielded the first parameter needed for the final test time equation. Next, the throat height was calculated using the Mach-Area relations to determine the throat area as a function of the test section area, using Equations 3.3 and 3.4.

$$\frac{A_t}{A^*} = \frac{1}{M} \left[\frac{2}{\gamma+1} \left(1 + \frac{\gamma-1}{2} M^2 \right) \right]^{\frac{\gamma+1}{2(\gamma-1)}} \quad (3.3)$$

$$A^* = \left(\frac{A^*}{A_T} \right) A_T \quad (3.4)$$

Although the previous test calculation is a function of the throat area, the limiting factor in the physical tunnel is the test section size, as it must fit on the attachment flange. For this reason, the test section area was chosen to be the driving variable.

The last required parameter before for the test time calculation was the mass flow rate \dot{m} , which is a constant due to choked flow in the throat. Equation 3.5 gives the mass flow rate for choked flow of an ideal gas, which is a function of the stagnation conditions and the gas constant R , equal to 287 kJ/kg-K for air.

$$\dot{m} = \frac{P_0 A^*}{\sqrt{T_0}} \sqrt{\frac{\gamma}{R} \left(\frac{2}{\gamma+1} \right)^{\frac{\gamma+1}{\gamma-1}}} \quad (3.5)$$

Equation 3.6 is presented by Pope and Goin as the test duration of a supersonic indraft tunnel [3]. It is a function of \dot{m} and P_e as derived above, the tank parameters of volume V_T and initial pressure P_i , and the thermodynamic parameters R , the polytropic coefficient n , and the tank end temperature T_e . Because the tank filling process happens quickly, it is assumed to be an adiabatic process where $T_e = \gamma T_0$. The polytropic coefficient was chosen to be 1.15 [3]. Figure 3.1 shows a schematic flow chart of the calculation process.

$$t = \frac{V_T P_e}{\dot{m} R T_e} \left[1 - \left(\frac{P_i}{P_e} \right)^{\frac{1}{n}} \right] \quad (3.6)$$

For the purposes of presenting the results, five Mach numbers were chosen to represent the range of flow speeds expected to be achievable with this tunnel. For each chosen Mach number, a curve was generated by varying the test section height between 0.26 and 10.76 cm (0.10 to 4.25 in).

The preliminary calculations showed that the maximum test time for the given constraints scales as a power function of the throat height. Test times increased markedly when the throat height was very small, but tended to vary only slightly towards the upper limits of throat and test section size as seen in Figure 3.2. The graph is presented in semi-log scale to provide higher resolution in the shorter time test time range.

Within the range of test section Mach numbers between 1 and 5, attainable test times ranged from 1 second to almost 2 minutes. For moderately sized test sections—those on the order of 5.8 cm high (about half of the theoretical maximum test section allowable for the smaller VTF attachment flange)—maximum test times between 3 and 5 seconds are possible. Figure 3.3 shows the test time and test section height as a function of throat height for a test section Mach number of 2.20.

One of the most significant conclusions drawn from the results is that, for the same test section size, higher test Mach numbers are more conducive to longer test times. This is a direct result of the larger ratio between throat area and test section area that results from

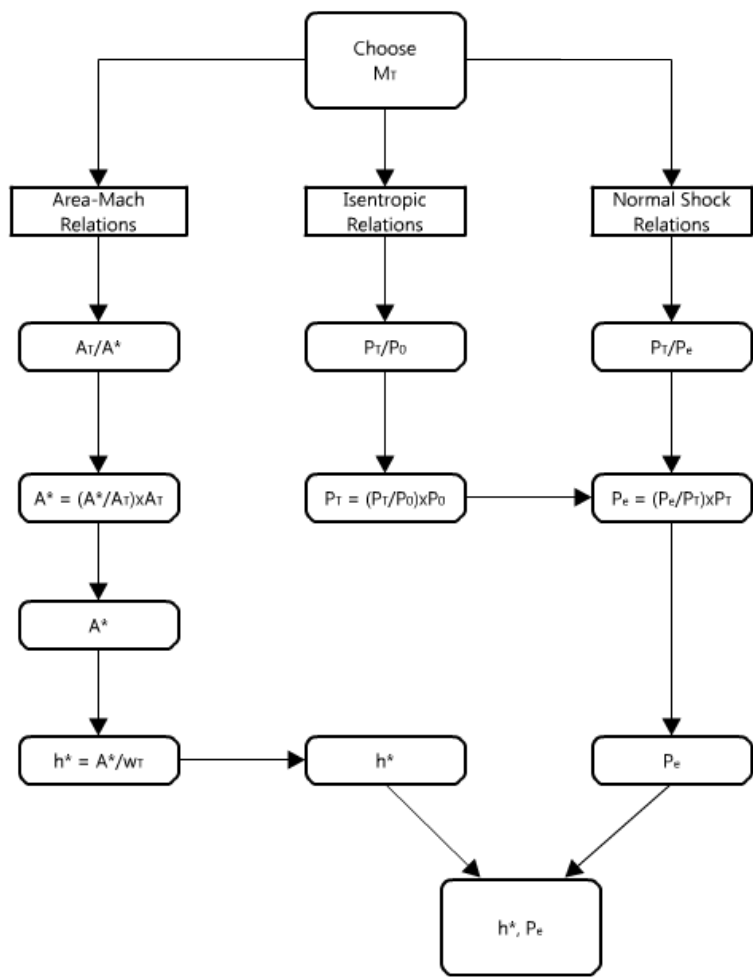


Figure 3.1: Intermittent Indraft Tunnel Test Time Calculation Flowchart

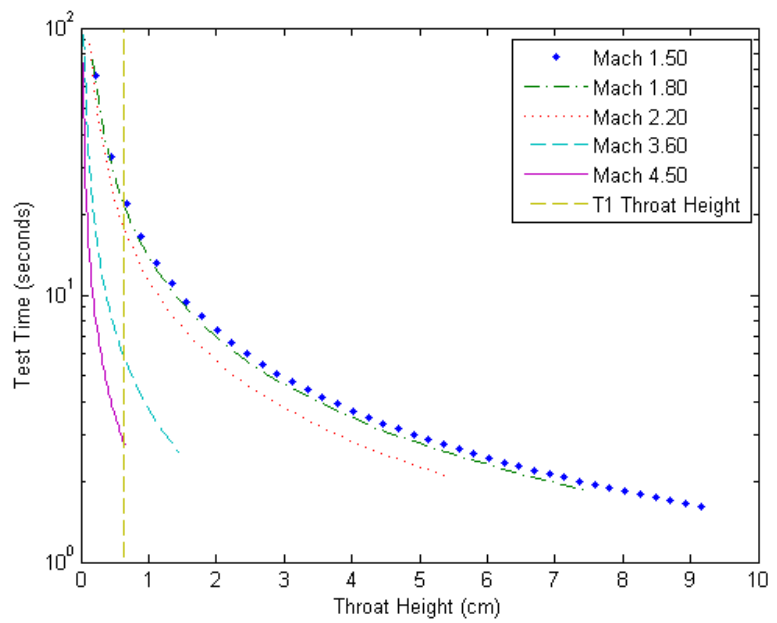


Figure 3.2: Test Time vs. Throat Height

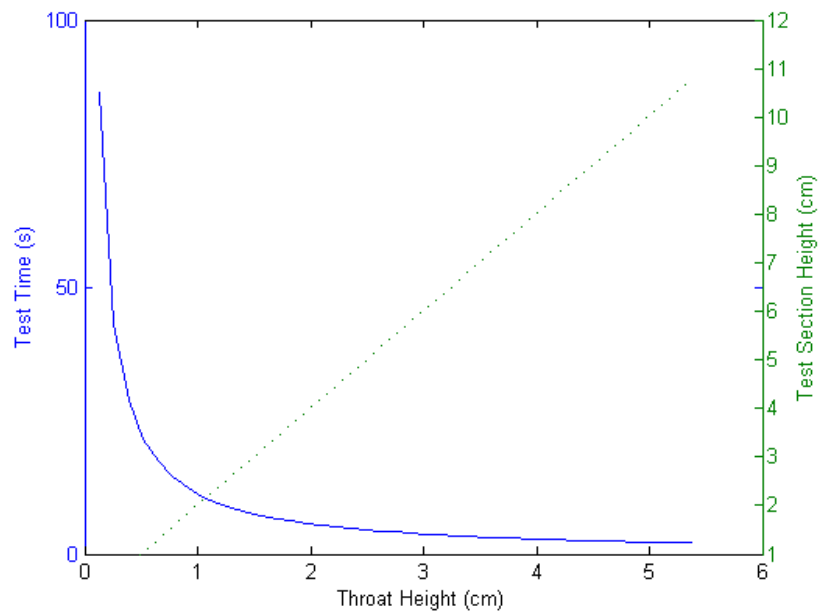


Figure 3.3: Test Time vs. Throat Height at Mach 2.20

higher Mach numbers. For the same size test section, a higher test Mach number will require a smaller throat, and thus a lower mass flow rate to remain choked. This results in a longer time to reach the final tank pressure before the test ends.

These preliminary results provided a basis for picking the design Mach numbers and test section size. Further investigation into condensation effects and boundary layers were necessary before final design decisions could be made.

3.1.3 Steady State Operation

Having the ability to run a supersonic wind tunnel indefinitely has numerous advantages over intermittent operation. All else equal, being able to run a test indefinitely is significantly better than only running for a few seconds, especially since it takes several seconds to open the valve and stable operating conditions may not be reached in just a few seconds. With continuous operation, however, comes many constraints that may be too significant to feasibly design a tunnel. These factors made careful analysis of the requirements for continuous operation very important to the final outcome of the project.

For the purposes of basic analysis, it was assumed that there was no diffuser after the test section, so that the test area discharged directly into the vacuum chamber. For the first set of calculations, the steady state condition was assumed to be that of a stationary shock at the end of the test section just before the exit plane to the vacuum chamber, as shown in Figure 3.4a. For the second set of calculations, a matched condition flow with no shocks in the test section was assumed, as illustrated in Figure 3.4b.

In order to calculate the throat and test section heights for the case of continuous operation, an algorithm was used that employed the Area-Mach relation, isentropic flow relations, normal shock relations, and the choked flow equation. To begin, a specified test section Mach number was chosen. From there, the Area-Mach relation was used to determine A_t/A^* (the ratio of the test section area to the throat area), isentropic relations were used to determine P_t/P_o (the ratio of test section pressure to stagnation pressure), and normal shock relations

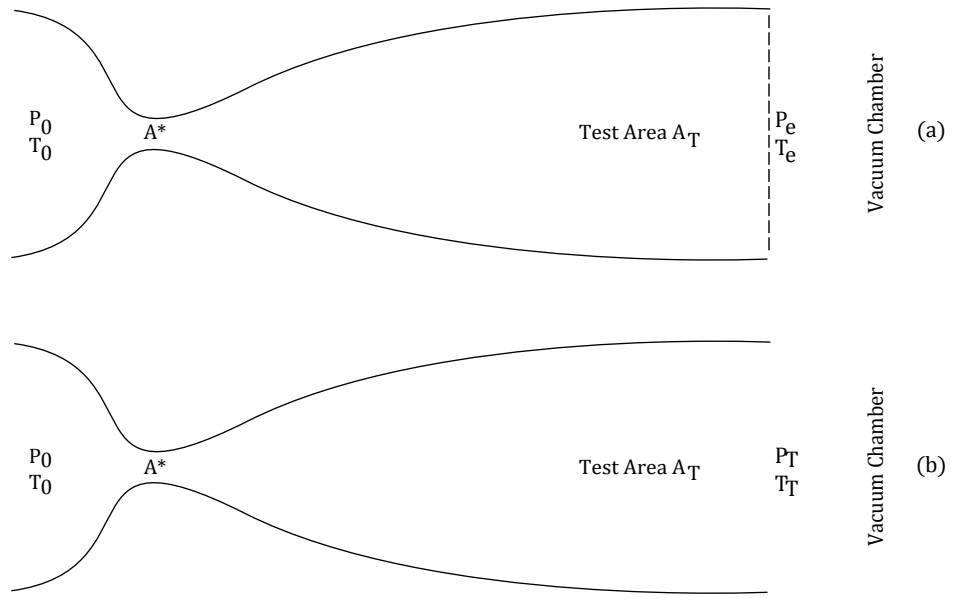


Figure 3.4: (a) Shock at end of test section (b) Matched condition flow

were used to determine P_t/P_e (the ratio of the test section pressure to the vacuum/exit pressure). From the first pressure ratio, the test section pressure was calculated using the fact that the stagnation pressure is equal to atmospheric pressure by design. Using the test section pressure, the second pressure ratio (P_t/P_e) gave the pressure at the exit for the normal shock case. The exit pressure allowed the second half of the calculations required to be performed.

The assumption $T_e = \gamma T_o$ (with $\gamma = 1.4$ and $T_o = 65^\circ\text{F}$ room temperature), which applies to an adiabatic process that relies on the fact that the internal energy in the full tank will be equal to the stagnation enthalpy flowing into the tank, was used to determine the temperature at the exit plane. Since the pressure at the exit had already been calculated, the Ideal Gas Law was used to determine the density of the air at that location. Using the pumping speed data for the Stokes blower (see Figure 2.11), the volumetric flow rate corresponding to the exit pressure was determined. Since $\dot{m} = V\rho$, the mass flow rate was calculated and used in

the choked flow equation rearranged to solve for A^* .

$$A^* = \frac{\dot{m}\sqrt{T_0}}{P_0} \left(\sqrt{\frac{\gamma}{R} \left(\frac{2}{\gamma+1} \right)^{\frac{\gamma+1}{\gamma-1}}} \right)^{-1} \quad (3.7)$$

The stagnation pressure was assumed to be atmospheric pressure and the stagnation temperature to be room temperature. Then, using the ratio A_t/A^* that was determined in the first step, the throat area for the chosen Mach number was determined. Dividing this value of the throat area by the width of the tunnel (1.5 in) gave the height. The calculations were repeated using Mach numbers between 1.2 and 5 in increments of 0.2. A flowchart of the calculation procedure is presented in Figure 3.7.

In order to calculate the test section and throat heights for the matched condition, a methodology very similar to the previously described calculations was employed. Again the calculations began by choosing a Mach number, and A_t/A^* and P_t/P_o were determined using the Area-Mach relation and isentropic flow relations respectively. From there, the pressure in the test section was used as the pressure at the exit to determine the density of the air at the exit. This enabled the exit mass flow rate to be calculated, and thus A^* via Equation 3.7. The test section area was determined by using A_t/A^* , and then dividing by the predetermined width of the tunnel (1.5 in) to calculate the height. A flowchart of this calculation procedure is presented in Figure 3.8.

The most significant conclusion that came from the calculations is that a continuous operation supersonic wind tunnel is not a feasible design concept for this project. For the conditions that create a shock at the end of the test section, it was found that the test section heights ranged from 0.07 cm to 0.15 cm between Mach 1.2 and Mach 5. Even the largest possible test section height for continuous operation is impractically small. Figure 3.5 shows the variation of the throat and test section heights as a function of the Mach number.

The results of the calculations indicated that the pressures required to drive the flow would not be nearly as low as our vacuum chamber is capable. At pressures around 6 Torr,

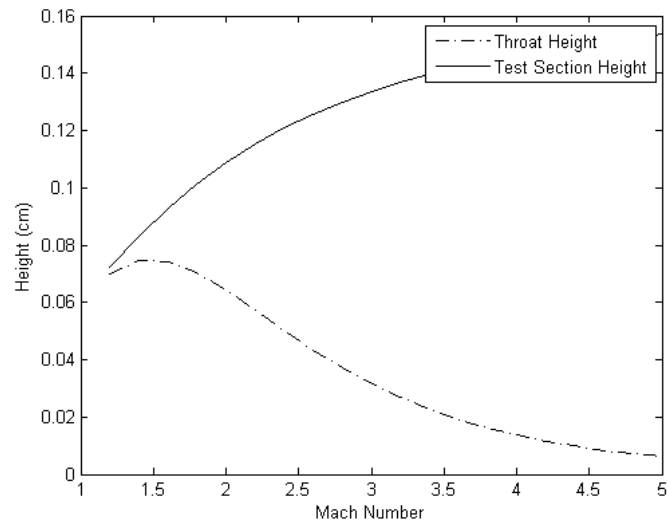


Figure 3.5: Throat and Test Section Height vs. Mach No. for Normal Shock at End of Test Section

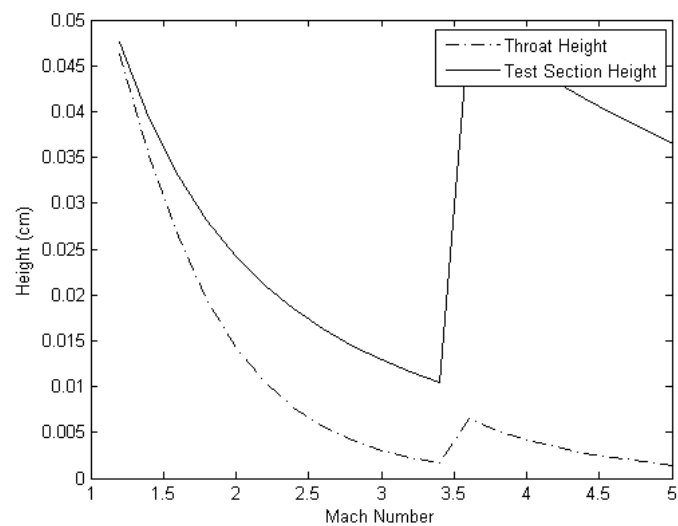


Figure 3.6: Throat and Test Section Height vs. Mach No. for Matched Condition Flow

the roots blower turns on to further lower the pressure in the chamber, but pressures required for continuous operation only reach as low as 42 Torr for test section speeds of Mach 5. For this condition, the roots blower would never turn on. The second set of calculations was performed to see if the pumping speed would be sufficient to maintain a matched condition at the exit plane (i.e. one without a normal shock).

For the matched flow case, the pressures were low enough in the vacuum chamber for the roots blower to start (represented by a jump in the plot in Figure 3.6) and pump the pressure down further. Despite this, the allowable test section and throat heights with the matched condition were smaller than those with the shock at the end of the test section. In this case, test section heights ranged from 0.03 to 0.04 cm, as shown in Figure 3.6. This effectively ruled out the continuous supersonic wind tunnel option for this project.

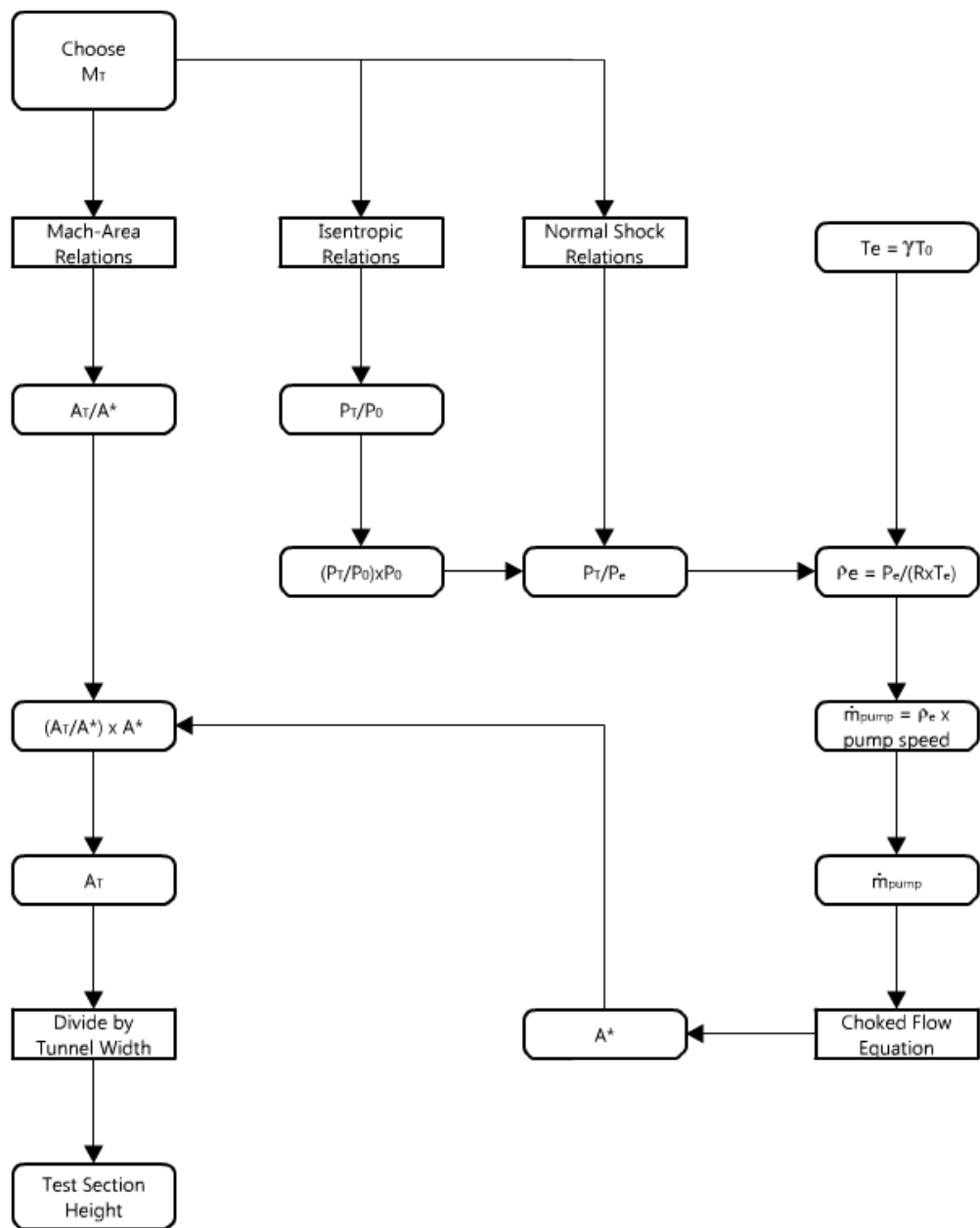


Figure 3.7: Continuous Test Flowchart with Normal Shock at End

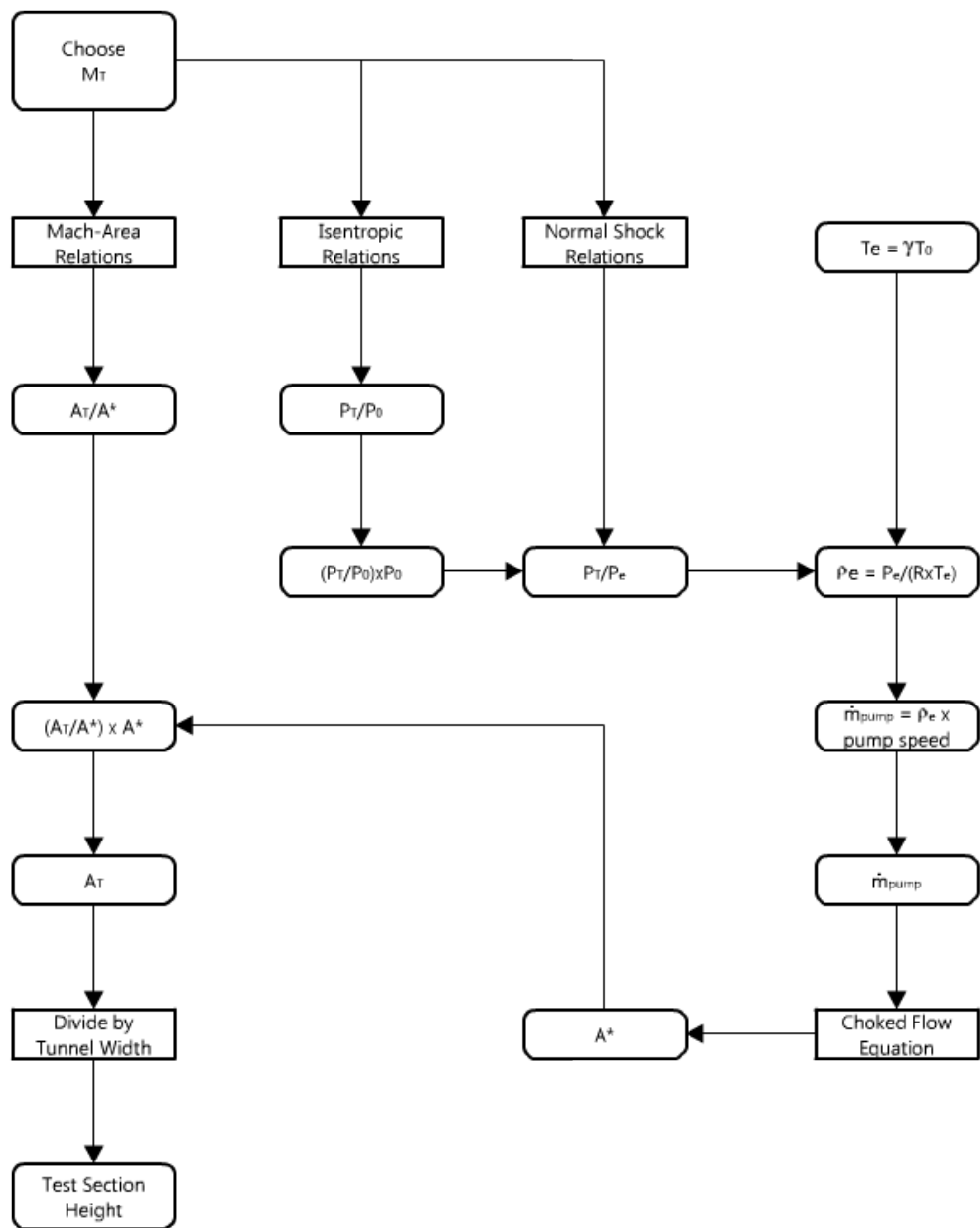


Figure 3.8: Continuous Test Flowchart for Matched Condition

3.1.4 Diffuser Effects on Intermittent Test Time

Run times for indraft style wind tunnels are dependent on the size of the vacuum chamber driving the flow. Due to the size of the vacuum chamber being used in this project, calculations indicated that test times would be on the order of tens of seconds. As a way to extend test times, the addition of a diffuser was evaluated. A diffuser's function (described more in depth in Section 2.4.2) is to slow the flow of air from the test section to a lower Mach number exhausting into the vacuum chamber, thereby reducing the overall pressure difference required. This results in an increase in the final back pressure which can result in longer test durations. In order to make a comparison, run times without a diffuser were calculated first. The calculations were done for intermittent operation, as previous calculations indicated that testing will need to be intermittent. Here, the behavior of the tunnel's test duration as a function of the characteristic throat size and the diffuser dimensions were explored. These calculations defined the final design of the wind tunnel, in terms of its dimensions, test section Mach number, and the desired test duration.

To mathematically model the process, the tank was assumed to be evacuated to some initial pressure, P_i , and allowed to fill through a choked nozzle to some final pressure, P_e . The final pressure was taken to be the pressure at which a normal shock is located at the exit plane of the diffuser, just before it travels back through the diffuser throat and enters the test section. Once the shock moves past the diffuser and into the test section the test would be over and any further data would be considered invalid. Like the intermittent test time calculation previously presented, the mass flow rate is obtained with Equation 3.5 for choked flow, and the ending temperature $T_e = \gamma T_0$.

In order to determine the test duration, a test section Mach number (M_T) and test section area (A_T) first had to be chosen. From isentropic flow relations, the Mach number yielded the area ratio. With the test area known, a value for A^* was found. Given this value along with P_0 and T_0 , the mass flow rate was calculated. The minimum diffuser throat height was then obtained with normal shock relations. Once these values were calculated, a Mach

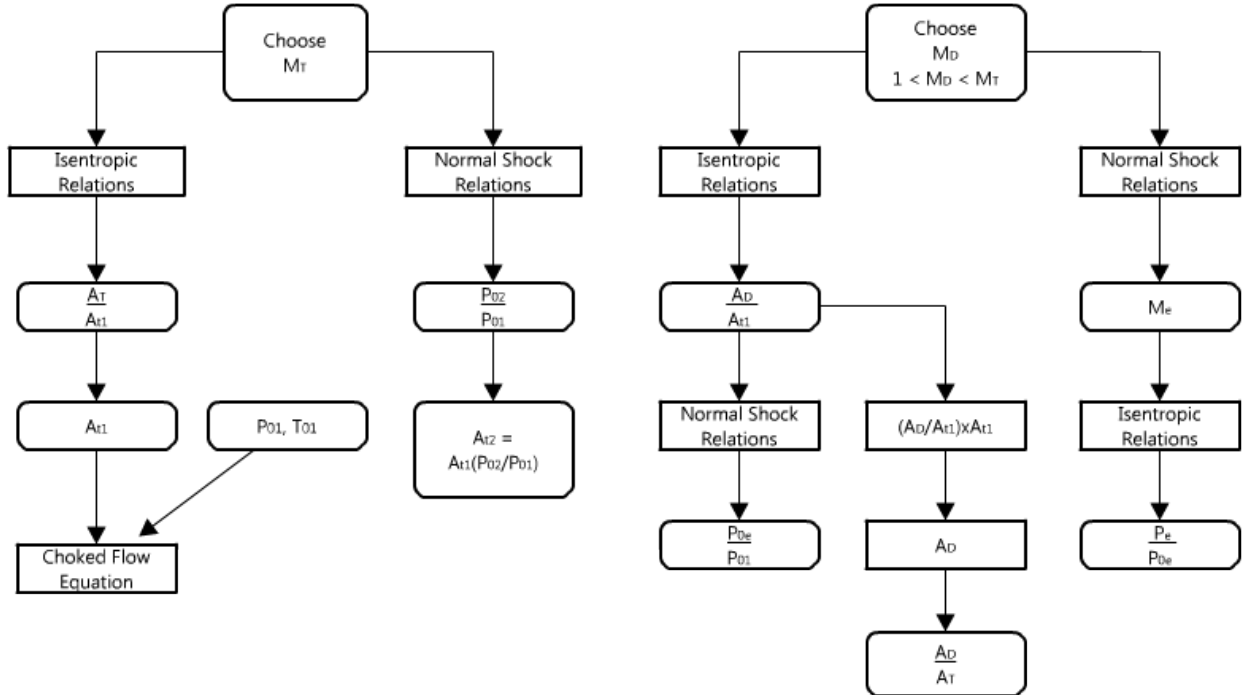


Figure 3.9: Diffuser Test Time Calculation Flowchart

number was arbitrarily chosen for the flow of air through the diffuser (M_D). Using this Mach number, the ratio of diffuser area to the area of the first throat (A_D/A^*) was found from isentropic relations. From the normal shock relations for this Mach number, the ratio of the stagnation pressure at the exit plane to the stagnation pressure of the lab (P_{0e}/P_{01}) was found. Also from normal shock relations, the Mach number of the air flow downstream of the shock wave was found. Given this value, isentropic relations were used to find the ratio of the static pressure at the exit plane to the stagnation pressure at the exit plane (P_e/P_{0e}). With these pressure ratios, the pressure P_e at which the test is considered over was found.

$$P_e = \left(\frac{P_e}{P_{0e}} \right) \left(\frac{P_{0e}}{P_{01}} \right) P_{01} \quad (3.8)$$

With the mass flow equation and Equation 3.8, the test time relation Equation 3.6 was evaluated. The calculation procedure is illustrated in Figure 3.9.

Several different Mach numbers were chosen for calculations starting with Mach 2 in

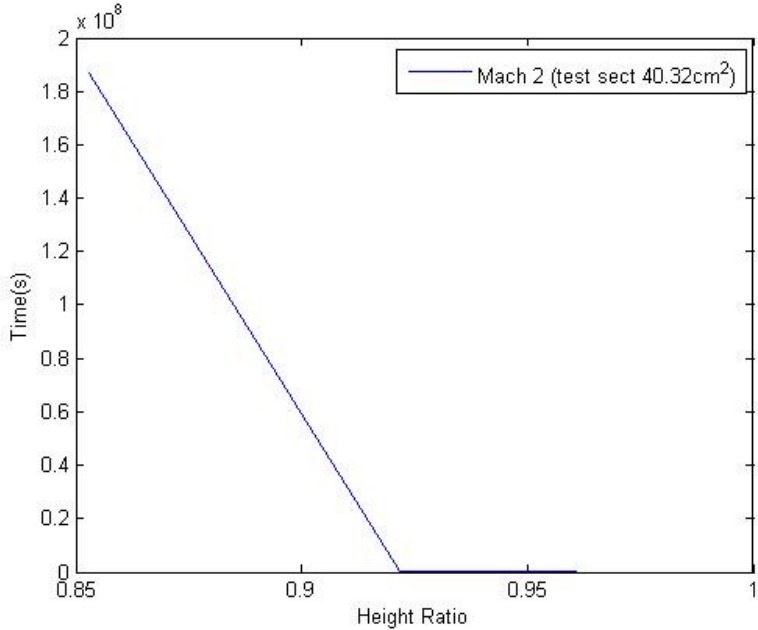


Figure 3.10: Test Time Increase vs. Throat Height Ratio for Mach 2.0

increasing increments of 0.5 up to Mach 3.5. Calculations were performed for two different test section areas. The first test area was the maximum allowable test area, based on previous calculations, of 40 cm^2 . However, it was found that for this test area, with a low Mach number, the area ratio was unreasonably small and there was not enough of an increase in test time for the diffuser to be justifiable. For example, Figure 3.10 shows that the ratio of diffuser height over test section height above 0.925 results in no time increase.

The test section area of 10 cm^2 was found to be an optimal test area with more desirable results, with respect to increased test times, for higher Mach numbers. Figure 3.11 shows that for larger height ratios there is a greater increase in time from 1 second to 3 seconds. As tests will only last on the order of ten seconds, an increase of this magnitude could be very helpful, helping to justify the installation of a diffuser.

Test time increases for a test section of 10 cm^2 with a Mach number of 3.5 ranged from 0.89 seconds to 19.6 seconds. At first glance, an increase of almost 20 seconds seemed promising, but it would result in a height ratio of about 0.14, which is impractically small

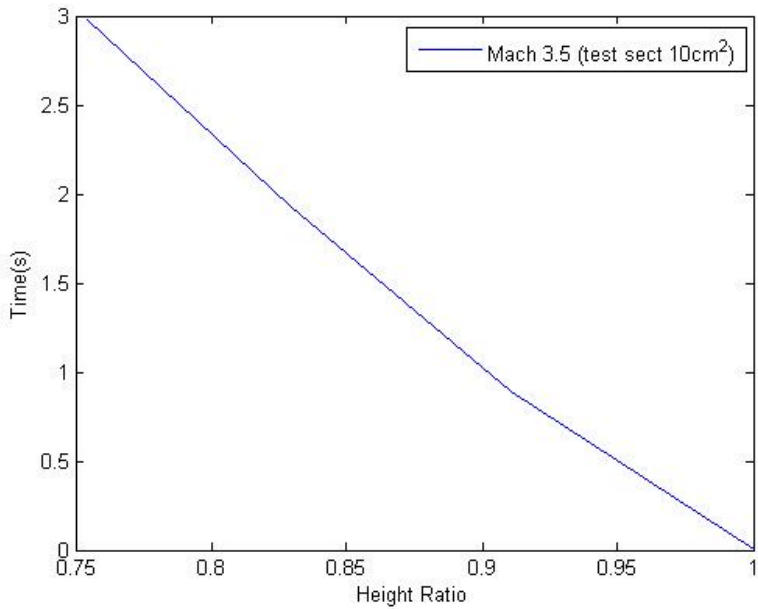


Figure 3.11: Test Time Increase vs. Throat Height Ratio for Mach 3.5

for the collection of data or testing of any model. For this reason, the graphed results were truncated so that all pictured height ratios would be greater than 0.72.

It was important when analyzing this data that the whole project be kept in mind rather than focusing solely on increasing run times. Another consideration when looking at the data was ensuring that there was a great enough difference between the areas of the first and second throats, as a second throat of the same size as the first would defeat the purpose of adding a diffuser.

These preliminary results provided a basis for determining if a diffuser would be designed for the wind tunnel. Though the maximum feasible increase in run time from a diffuser would only be on the order of tens of seconds, it was decided that a diffuser would be incorporated. The theoretical run time for any Mach number was so short that any increase in time was deemed beneficial.

3.1.5 Condensation

As described in Section 2.6, due to the temperature and pressure gradients that arise in the flow through a converging-diverging nozzle, the evaluation of condensation must be considered in further detail. Supersonic wind tunnel design and its efficiency rely heavily on the control and monitoring of the vapor content in the air. If condensation were to occur, it would induce irregularities in the flow characteristics, which could then cause shock waves to occur within the flow thus compromising any data collected.

Temperature change is not instantaneous, which is evident given any experience with heat transfer. Condensation occurs on a molecular level. It is the result of molecules of air colliding with each other and eventually combining to form small droplets of moisture. Greater supercooling is achievable in tunnels with smaller dimensions than in tunnels with larger dimensions [3]. Pope notes a rule of thumb when factoring in the effects of temperature and pressure on condensation. He states that condensation can be considered negligible if the static air temperature reached in the tunnel is no lower than 55°F (30.55°C) below its atmospheric dew point temperature [3].

Figure 3.12 illustrates 0°F supercooling and Figure 3.13 illustrates Pope's rule of thumb with respect to the 55°F (30.55°C) of supercooling. For a given ambient temperature and relative humidity, which can be measured, there is a prescribed dew point temperature. By allowing 0°F (0°C) of supercooling and by allowing 55°F (30.55°C) of supercooling, the minimum allowed static temperature is determined. The ratio of the ambient laboratory temperature (on an absolute temperature scale) and the adjusted dew point, which now becomes the allowable static temperature, is calculated. Inputting this value into the isentropic flow tables results in the maximum achievable Mach number the flow, with those characteristics, can experience before condensation occurs.

The nature of this project dealt with the design of a variable geometry, supersonic wind tunnel. The wind tunnel is expected to operate over a range of Mach numbers up to and including Mach 4. Using Pope's allowance for 55°F (30.55°C) of supercooling, we can see

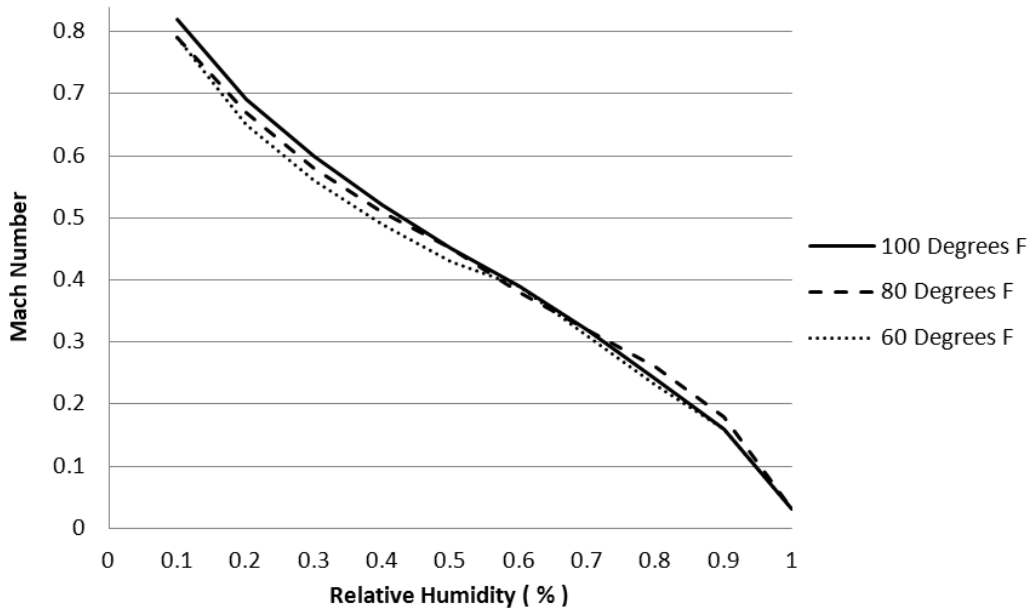


Figure 3.12: Maximum Achievable Mach Number with No Supercooling Allowed

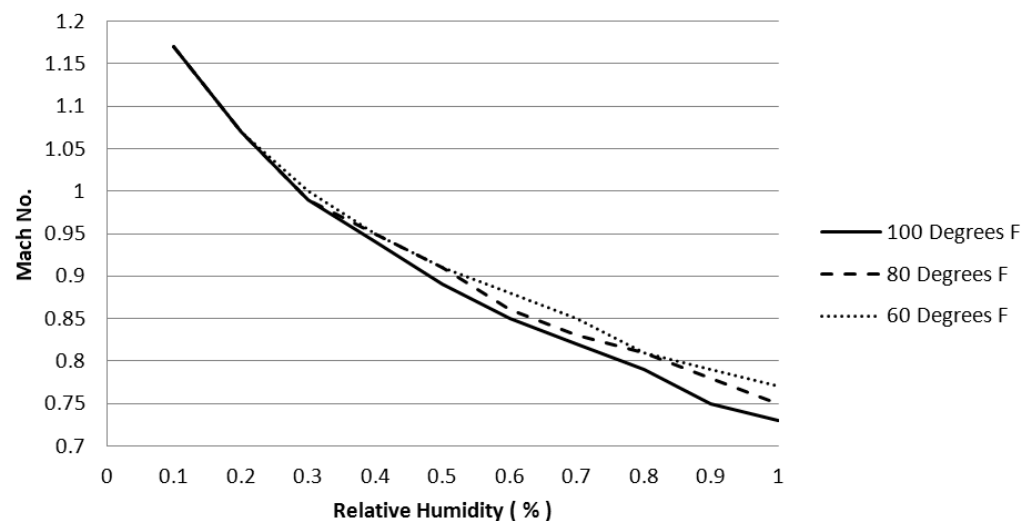


Figure 3.13: Maximum Achievable Mach Number with 55°F of Supercooling

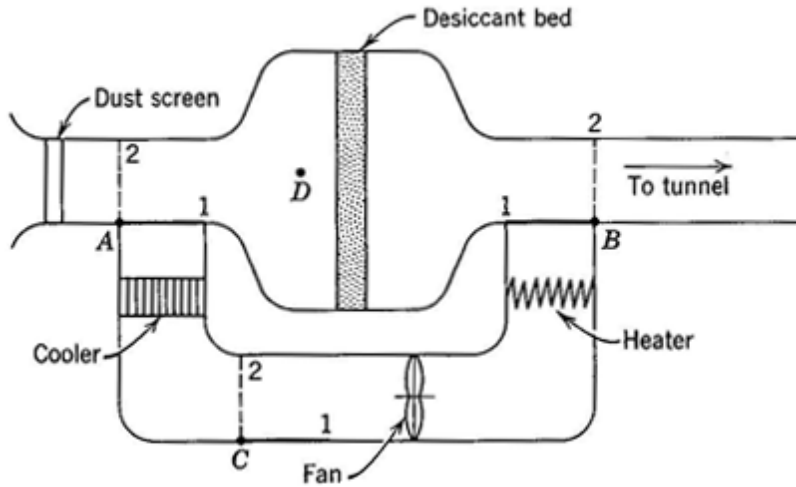


Figure 3.14: Standard Schematic for Dryer (Ref. [3], ©1965, John Wiley & Sons, Inc.)

that the maximum Mach number that can be reached, without condensation, is less than Mach 1.2 (see Figure 3.13). The conclusion reached is that for operating speeds greater than Mach 1.2 condensation will be an issue.

The solution is to design a means by which the incoming air can be conditioned to prevent condensation from occurring. There are two primary ways by which to accomplish this task. The first approach is to heat the air so that when it reaches the prescribed Mach number, the static temperature will be no lower than 55°F (30.55°C) below the dew point temperature. For example, with a dew point of 20°F (479.67°R), 55°F of supercooling corresponds to a static air temperature of -35°F (424.67°R). If the desired Mach number is 3.5, then the total temperature of the incoming air would have to be 1009°F (1469.44°R). This approach is highly unrealistic due to the high temperature requirements. The second approach is to introduce a drying system that will effectively remove moisture from the air before entering the tunnel. The thought behind this approach is that enough moisture will be removed from the air so that the relative humidity of the incoming air is below 10%. Not only is this approach more feasible, but these systems are also relatively cheap and available for purchase.

These dryer systems normally incorporate a desiccant bed of either activated alumina or silica gel that absorbs moisture during operation [3]. Silica gel, which is readily available, would be the material of choice in the design of a drier system for the variable geometry wind tunnel that this project is concerned with. Silica gel is capable of absorbing 0.03 lbs (0.0136 kg) of moisture for every pound (kilogram) of material, has a density of 40 lb/ft³ (639.4 kg/m³), and has a reactivation temperature¹ of 325°F (162.7°C) [3].

Figure 3.14 shows the standard design of an air dryer typically found on supersonic wind tunnels. Not only are they effective, but they are reusable. During operation, all valves are locked at position 1. After the desiccant bed has become saturated, it can be heated, thus regenerating itself. During regeneration of the desiccant, valves ‘B’ and ‘C’ are moved to position 2 to heat the desiccant and allow moisture to escape out the tunnel entrance. Once the temperature at ‘D’ is approximately 250°F (121.1°C), the desiccant can be assumed fully regenerated. Then valve ‘A’ is moved to position 2 and valve ‘C’ moved to position 1 as the cooler is turned on to reduce the desiccant temperature to about 100°F (37.77°C) [3]. It would be impractical to have to regenerate the silica gel after every test run, therefore, the dryer should be designed to work over a series of consecutive test runs. To help design the desiccant bed, a worst-case scenario should be used. Using air at 100°F (37.77°C) and 100% relative humidity, the corresponding partial pressure of vapor is $p_{v1} = 0.953 \text{ lbf/in}^2$ (0.0648 atm). To calculate the exact mass of the water vapor, the humidity ratio must be known. The humidity ratio (ω) is the ratio of mass of vapor to mass of dry air. To find the humidity ratio we input this value of p_{v1} into Equation 3.9 [2].

$$\omega = 0.622 \left(\frac{p_{v1}}{p - p_{v1}} \right) = 0.043 \frac{\text{lb(vapor)}}{\text{lb(dryair)}} \quad (3.9)$$

Once this value of ω is attained, the total mass of moisture m_{v1} , given the mass M of air that has passed through the tunnel, can be found. The mass of air can be calculated using

¹Reactivation temperature refers to the temperature at which the desiccant material must be heated in order to remove any moisture it may have absorbed during use.

the given mass flow rate and duration of a single test run for a specific Mach number. To calculate total mass of moisture to be absorbed, during a single test run, Equation 3.10 is used [2].

$$m_{v1} = \frac{M}{\left(\frac{1}{\omega}\right) + 1} = 0.041M \quad (3.10)$$

Once this is known, the material properties of silica gel can be used to approximate the weight and volume of desiccant needed.

3.2 Variable Contour Ideation

In order for a supersonic wind tunnel to be able to achieve a range of Mach numbers, its contours must be adjustable. The wind tunnel contours, which form the shape of the throat, expansion section, test section, and diffuser, impact the test section Mach number significantly in two ways. First, the test section Mach number is driven by the ratio of the throat area to the test section area; second, the expansion and straightening section shapes determine the presence or absence of shocks in the test section. Since one of the goals of this project was to construct a wind tunnel that could operate at multiple test section Mach numbers, adjustable contours were thus necessary. The adjustability factor, however, creates a significant design challenge. As the contours change shape, the distance between any two points on the contours will also change, necessitating that the contours be capable of changing length. After preliminary designing and deliberating, two ideas were chosen for in-depth consideration.

3.2.1 Axially Shifting Contour Tunnel

The first idea was an axially shifting contour, such as that pictured in Figure 3.15, and originally described in Section 2.4.3.

This tunnel design requires two solid contours, each with a predetermined shape. The

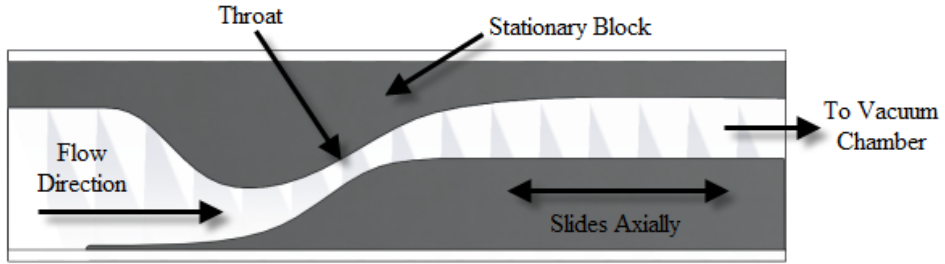


Figure 3.15: Axially Shifting Tunnel

lower contour moves axially down the length of the tunnel while the upper contour remains stationary. A large screw runs through the entire lower contour; by turning this screw, the entire contour moves in a similar fashion to how many vises operate. Any excess lower contour track length beyond the length of the upper contour extends into the chamber and is irrelevant, as flow behavior downstream of the test section need not be uniform, undisturbed flow. The lower contour tapers down to become flush with the track upon which it slides. This permits the track to act as the lower contour in the converging section of the nozzle in the cases in which the throat area is increased. The lower contour is only adjusted in between runs so as not to disturb the flow.

3.2.2 Constant Force Spring Tunnel

The second idea was a tunnel that uses constant force springs (spring treated² metal that exerts the same force regardless of how much it is uncoiled) as the contours (see Figure 3.16).

Unlike the axially shifting tunnel design, both contours in the Constant Force Spring (CFS) Tunnel adjust symmetrically. Two separate constant force springs are used—one for the upper contour and one for the lower contour—and are arranged as mirror images of each other. Part of each spring is unrolled and stretched over its respective flat metal backbone piece (see Figure 3.17). The metal backbone pieces run parallel to the test section and

² Spring treated metal refers to a class of metals, usually steel, which have very high yield strengths and return to their original shape after very large deflections with no permanent deformation [13].



Figure 3.16: Constant Force Spring (1.5 inches wide)

connect perpendicularly to the ends of the wind tunnel. One end of each constant force spring is fixed to the wind tunnel entry piece. The other end of each spring remains coiled inside the vacuum chamber, and uncoils to give the contour extra length when adjusted. The force exerted by the springs constantly pulls the contour towards the coiled end, guaranteeing the absence of slack in the contour when the length of the adjusting sections is at a minimum. For the sections of the springs that comprise the test section and other areas requiring a straight contour, a mechanical slider is used. The slider trucks are inset into the backbone pieces, and the constant force springs are attached so that they are flat against the rails that slide across the trucks. This movement in the straight portions of the contour is necessary in order to be able to adjust the throat, straightening, and expansion sections. Three screws along the expansion section and one on the diffuser adjust the contour shape. The screws are threaded through the backbone pieces, and are attached to the constant force springs in such a way that still allows the spring to slide. By turning the screws, they move up or down and force the springs to do likewise, giving the contour the required shape.

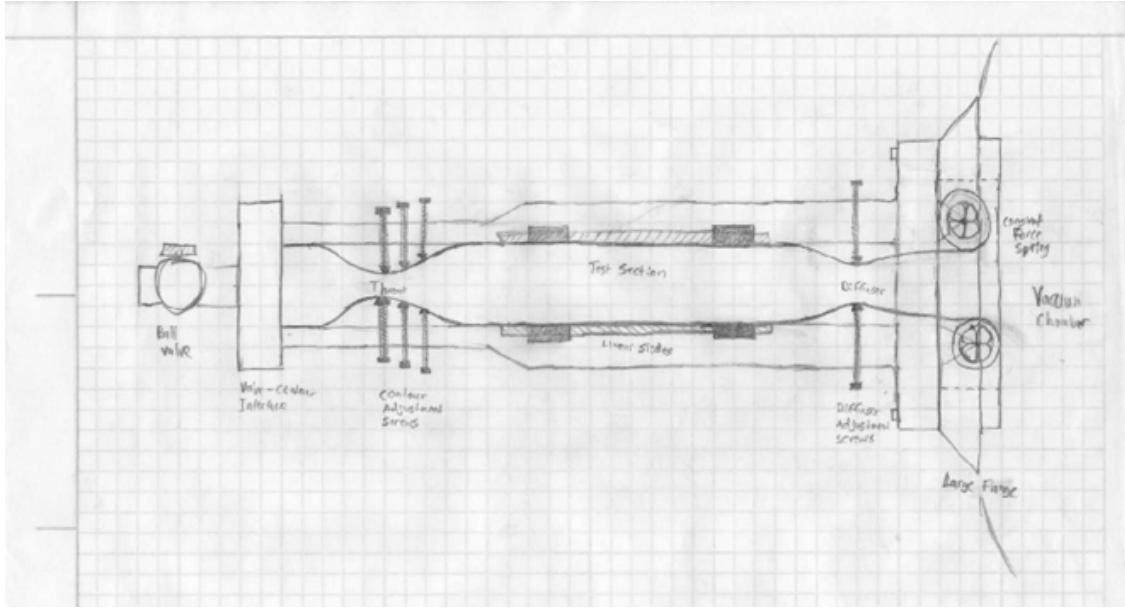


Figure 3.17: Constant Force Spring Tunnel Sketch

3.3 Method of Characteristics Calculations

Following the procedure outlined in Sections 2.3.3 and 2.3.4, an Excel spreadsheet was created to use the MOC to track the progression of Mach waves through the example channel in John & Keith [2]. Afterwards, it was modified to work with any channel divergence angle by ensuring that all cells were based on variables, as opposed to the fixed numerical entries originally used in some of the known cells. The initial Mach number at the minimum throat area was also changed to a more realistic 1.1, rather than the value of 2 originally used. A macro in Excel was created to automate the Goal Seeking action required to calculate the Mach number through iteration of Equation 2.2. The macro minimized the amount of interaction required to change the channel attributes. Following the completion of the Excel spreadsheet, the MOC procedure was ported to a MATLAB script that offered a greater degree of flexibility. The script was designed to allow for a customizable number of points on the initial value line as well as a customizable expansion section length (defined by the number of contour points in the expansion section). The MATLAB code is shown in Appendix C. The code was used to generate contours for Mach 2.5, Mach 3.68, and Mach

4.0. The settings used to generate these contours are located in Appendices D, E, and F. The plots generated are shown in Figures 3.18, 3.19, and 3.20. Note that care must be taken in printing these contours, as they must be printed to scale. The throat height defined in the MOC MATLAB settings must be the same actual height when printed on paper.

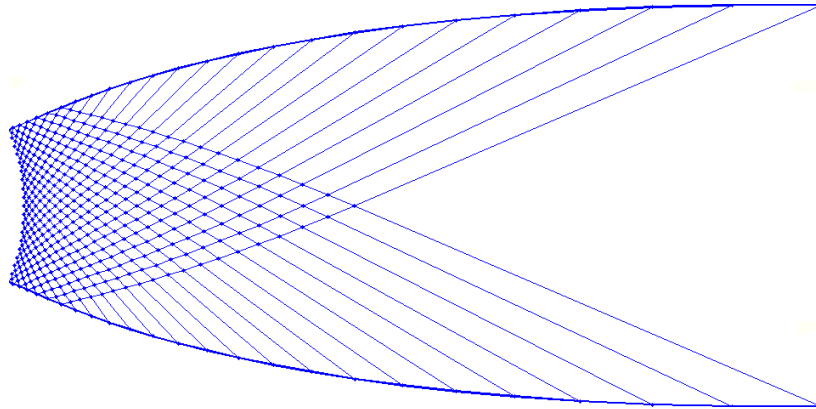


Figure 3.18: Expansion and Straightening Section Contour for Mach 2.5

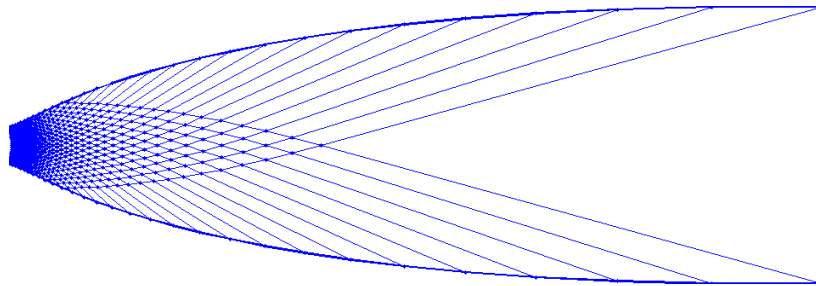


Figure 3.19: Expansion and Straightening Section Contour for Mach 3.68

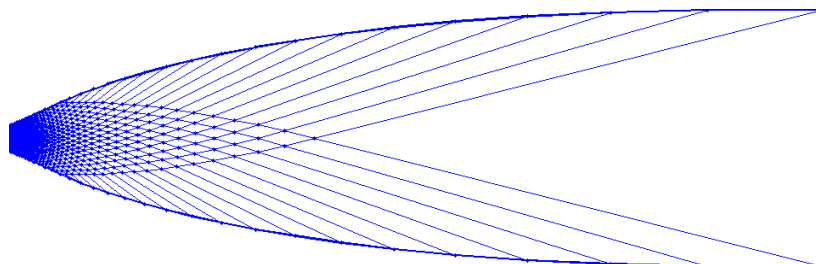


Figure 3.20: Expansion and Straightening Section Contour for Mach 4.0

3.4 Detailed Design

The piece connecting the tunnel to the chamber, the large flange, was the first part to be designed. Since it was desired that the wind tunnel have the ability to reach different Mach numbers in the test section, the final tunnel design was more complicated than that of T1. The main parts of the tunnel were the contour, the backbone and screw adjustments, the diffuser adjuster, the tensioning system, and the ball valve.

3.4.1 Large Flange

At the start of the project, the only available flange ports on the vacuum chamber suitable for tunnel attachment were all of the same, small size. These ports, designed by WPI graduate student Nick Behlman, have a 4 inch diameter viewing port, and use borosilicate glass covers from MDC Vacuum Products, LLC., which are held on by a stainless steel ring, as pictured in Figure 3.21. Attachments, such as wind tunnels, replace the window glass and steel ring, and are affixed using the provided bolt pattern.

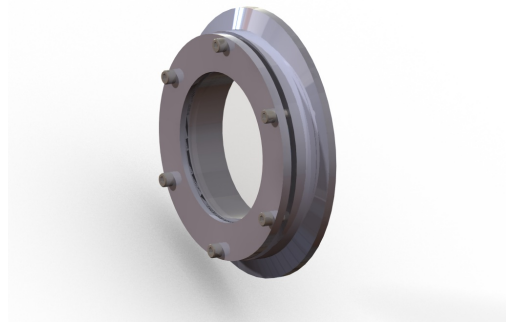


Figure 3.21: Rendering of Standard Flange with 4 inch Viewport

As mentioned in Section 2.5, there is also a large flange on the door of the vacuum chamber, which only had a blank aluminum cover without a viewport. A new windowed flange for this larger port was desired for multiple reasons. A larger viewport would allow for a better view into the chamber, and its axial placement would allow for a different viewing

angle into the chamber from the radially located smaller windows. Being located on the end of the chamber also allows for more room on each side of the tunnel, which is necessary for shadowgraph diagnostics. It would also allow for significantly larger attachments, providing more flexibility for wind tunnel designs and other future experiments.

Window Design

Because the primary objective of the new, large flange was to provide a larger viewing and attachment area, the flange design was based around the new window. Although the viewport glass was a critical design consideration, optics were not as crucial for this viewport as with the smaller flanges, because this window is not intended for use with optical measurement devices. This flexibility broadened the options for allowable materials for the viewport glass. The smaller viewports use glass designed for vacuum chambers, so research began by searching for existing glass solutions from vacuum supply companies. The products that were found were either too small to accommodate the desired viewing area, too expensive for simple viewing purposes, or both.

The second option was to design a viewport window out of clear plastic, able to withstand a full vacuum pressure with reasonably little deformation. The optical quality of plastic would inherently be less than that of glass, but still within acceptable limits for viewing purposes. Two optical plastics were considered: polycarbonate and acrylic. Both are very common in high-strength applications where good optical quality is necessary. Polycarbonate is commonly used in “bulletproof glass” [14], and acrylic is often used for large aquarium tanks and display signs [15].

A nominal diameter of 8 inches (20.32 cm) was originally chosen for the large flange window, and an initial design was modeled in SolidWorks and analyzed under pressure using the built-in stress analysis tools. A simulation was set up to constrain the curved edge to be fixed and subject the window to a full vacuum (14.7 psi) on one face. The first simulations used 3/8 inch thick discs for both polycarbonate and acrylic, as seen in Figure 3.22. Both

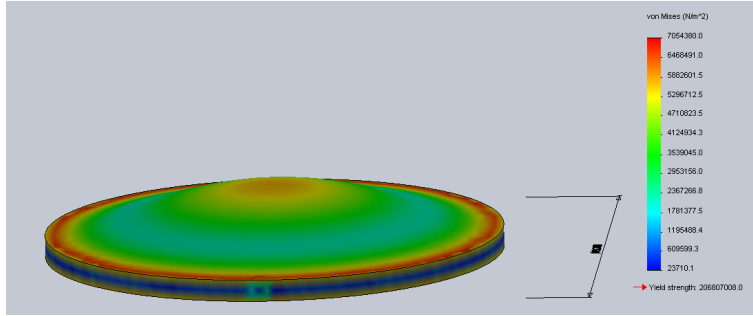


Figure 3.22: Deformation of 8" x 3/8" Thick Acrylic Disk Under 1 atm

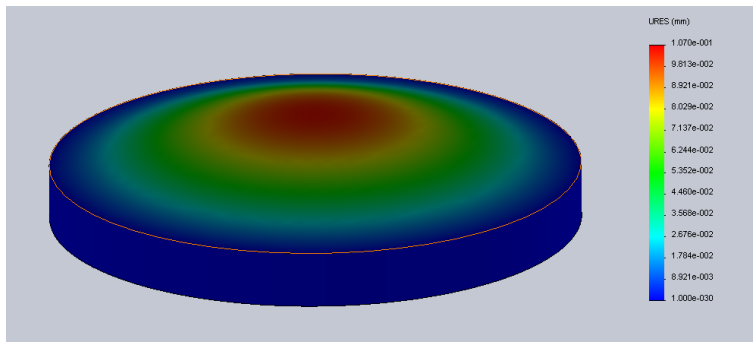


Figure 3.23: Deformation of 9.5" x 1" Thick Acrylic Disk Under 1 atm

were found to have a large enough safety factor (greater than 10) from a stress standpoint, but upon further review both also had unacceptably large deformations. Because both acrylic and polycarbonate had shown similarly acceptable stresses, acrylic was chosen as the material of choice for cost reasons.

An updated design was then analyzed, using a 1 inch thick disc with an overall 9.5 inch diameter disc, and was found to have a factor of safety over 100 on yield strength, and a deformation of 0.1 mm under full vacuum. Figure 3.23 shows the graphical result of the analysis, depicting the deformation of the window under 1 atm (14.7 psi), with a deformation magnification of 225. This design was determined to be satisfactory, and was chosen as the final window for the flange.

Port Cover and Clamp Design

The port cover design was based on the existing blank aluminum cover, so measurements were taken to ensure the new cover reproduced all critical geometry. The only modifications to the geometry were the addition of the viewport hole and associated cuts and bolt patterns. Stainless steel was chosen to replace the aluminum cover for its superior hardness and damage resistance while still maintaining the corrosion resistance.

The overall window clamp design remained similar to that of the small flange, utilizing the same style of ring-clamp to hold the window in place. The interface with the port cover was modified slightly to use eight bolts for better centering of the larger window, as well as a recessed mating pocket to hold the window. The small flange has a recess for the window only on the ring clamp, and thus the window is located only by the bolts. A matching recess in the large flange helps to locate the window, as well as remove all shear forces on the bolts, shown in Figure 3.24.

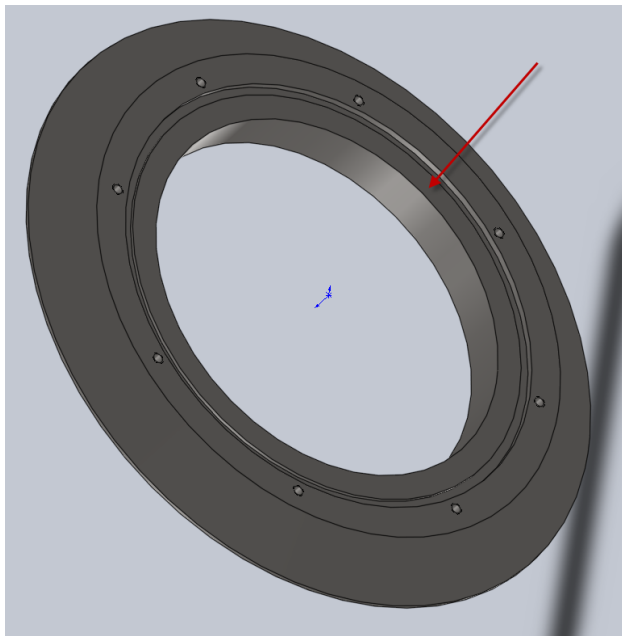


Figure 3.24: Large Flange Window Recess

The ring clamp and port cover recesses both have a 0.75 inch overlap on the acrylic,

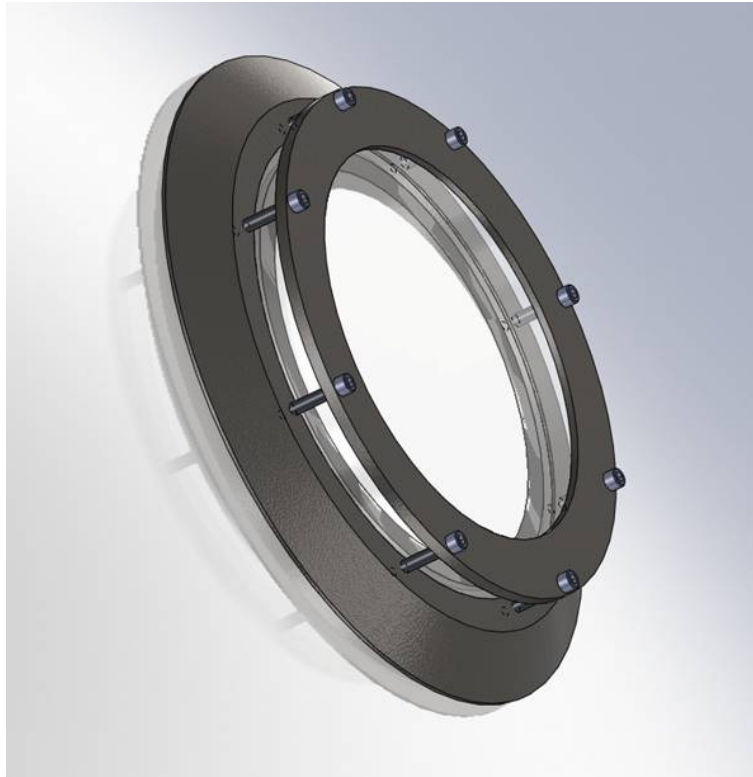


Figure 3.25: Large Flange Final Design

leaving an 8 inch diameter viewable area, which results in an area four times larger than that of the small flange. Similar to the small flange, there is an O-ring between the acrylic window and the port cover to seal against the vacuum. For consistency, the new port cover uses the same O-ring as the aluminum cover to seal against the vacuum chamber. Figure 3.25 shows a CAD rendering of the new flange window attachment.

3.4.2 Wind Tunnel

The final wind tunnel design incorporated many features from the constant force spring concept discussed in Section 3.2.2. The design incorporates a flexible contour controlled with screw adjusters, a spring tensioning system, and an O-ring lining to seal the chamber. Figure 3.26 shows the full CAD assembly in an exploded view.

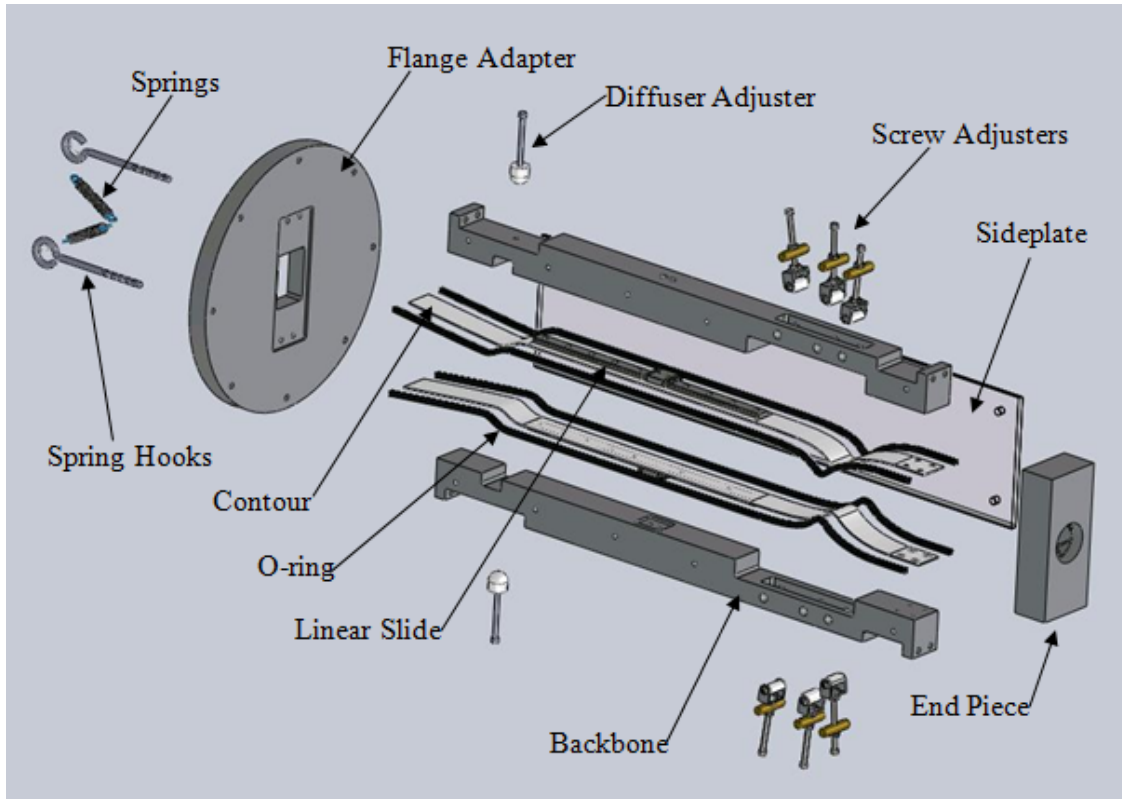


Figure 3.26: Tunnel Exploded View

Variable Contour

The flexible, spline-controlled contour is a critical component for achieving different test section Mach numbers. The initial design concept used constant force springs to provide a tensioned, smooth contour. Further investigation of sample constant force springs demonstrated that off-the-shelf springs were too stiff, and would not flex enough to be workable in this design. High Impact Styrene sheet was investigated at the suggestion of the project advisor, and was found to be a suitable substitute for the contour, although it would not inherently provide a tensioning force.

The contour would be controlled by a screw adjustment system acting at control points. In a manner analogous to the mathematical construct (i.e. a “spline”), these control points define the interface between piecewise, cubic polynomial functions. Stress analysis concepts show that any beam in bending also follows a piecewise cubic function between point loads,

which is equivalent to the styrene contour being pushed upon by the adjustment screws. Using a minimal number of control points, the contour can be manipulated to closely match almost any expansion and straightening curve within a fairly broad range. The control points are defined by blocks of styrene fixed to the contour sheet, which also provide an attachment point for the screw adjustments. The test section is attached to a linear rail (THK, Co. Model RSR-7WM), which holds the contour flat, and allows it to move back and forth slightly to take up the change in length due to the expansion section adjustment.

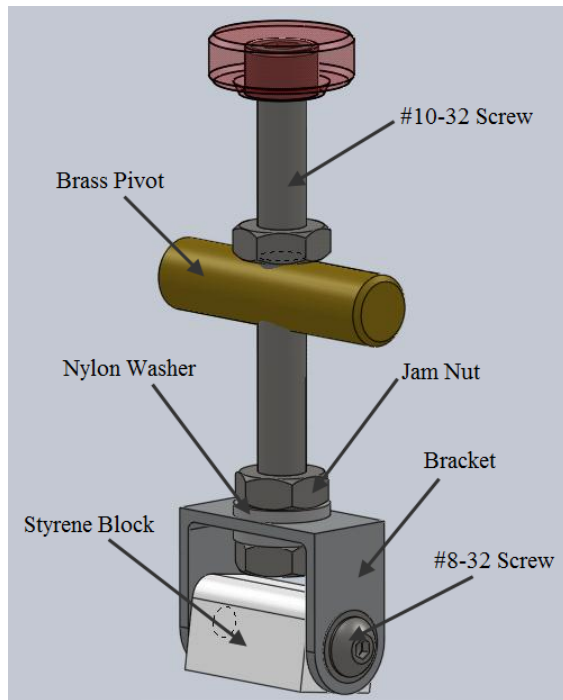


Figure 3.27: Contour Adjuster with #10-32 Screw

Figure 3.27 shows the screw adjustment mechanism for controlling the adjustable sections. The mechanism connects to the contour control points with a bracket and can pivot to accommodate for the angle of the contour.

The two jam nuts and nylon washers are attached to the screw with threadlocking compound (Loctite® 290) on either side of the bracket, allowing the screw to spin inside the bracket while still providing the necessary force to move the bracket and contour.

The brass plug is threaded so that the screw moves in and out when turned, and can

pivot to accommodate translation of the control point along the contour as it changes. A jam nut is threaded above the brass pivot, which can be screwed against it to lock the screw in place. The plug is inserted through a hole in the tunnel backbone, providing a fixed pivot.

Variable Contour Tensioning

In order to ensure that the styrene contours take on the desired shapes, a system was needed to create tension in the contours, pulling them in the direction of the vacuum chamber. To accomplish this, a very simple spring system was devised to pull on the contours. This system consists of an eye hook screw mounted on the chamber side of the contour, and a simple extension spring. The extension spring is connected between the eye hook screw and the second eye hook on the contour. Although this creates additional deflection in the contour, the deflection is downstream of the diffuser and it only creates a positive area change, so the deflection will not cause the flow to choke again. The tensioning system is shown in Figure 3.28.

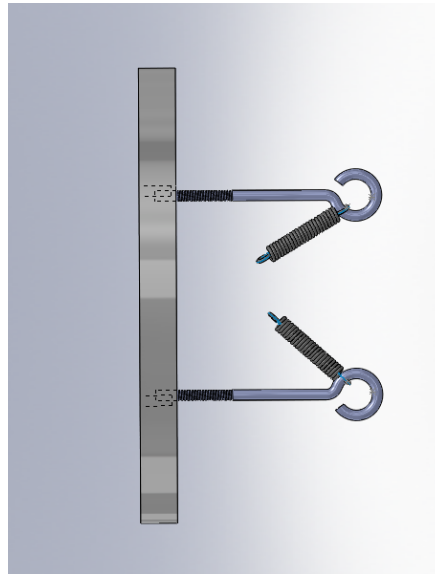


Figure 3.28: Spring Contour Tensioning System

Sealing

The most challenging issue to deal with in this project involved the sealing of the wind tunnel. The wind tunnel must be able to hold a reasonable vacuum in order to allow the vacuum pumps to pump down the chamber to desired pressures. Tunnel leaks made it difficult to reach the intended 50 milliTorr pressure, and they also detracted from test time by acting as an additional inlet. After Peter Moore's tunnel was tested, it became clear just how difficult it is to seal a wind tunnel against a vacuum.

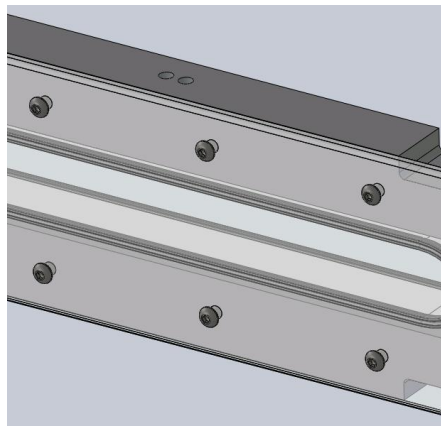


Figure 3.29: Side Plate Screw Attachment

The wind tunnel design for this project offers more difficulty in terms of sealing because of the nature of its variable geometry. Double-sided scotch tape would be an ineffective and impractical means of creating a sufficient seal on the variable geometry tunnel; instead, O-ring material is attached to either side of the flexible polystyrene. The side plates were then screwed onto the backbone with sufficient compression to generate a seal (Figure 3.29). The “quad” O-ring stock has the profile of a cross (Figure 3.30) and is attached to the contours with silicone to create an effective seal.



Figure 3.30: “Quad” O-Ring Profile, nominal 3/16 in. square

4. Testing

The assembling and testing of the wind tunnel made by the previous MQP, referred to as T1 (“Tunnel 1”), was part of this project and was done while simultaneously designing and building T2 (“Tunnel 2”). T1 was tested four times, and each test revealed areas for improvement. T2 was never tested, but the assembly process, which was ultimately more difficult than anticipated, was a success.

4.1 Peter Moore’s Tunnel

Part of this project involved testing T1 and fixing any of its operational problems. As a result, it was determined that this particular design has several disadvantages and advantages. One major issue was that properly sealing the tunnel was extremely difficult. Additionally, the tunnel was designed so that it could only achieve one Mach number. For the same reason, however, the overall design was mechanically simple. Another positive characteristic of this tunnel was that preparing for a run and attaching it to the vacuum chamber was fairly easy. In sum, the four test runs performed with the first tunnel design revealed its flaws, which were fixed, and its benefits, both of which were taken into consideration while assembling the second design.

4.1.1 Test One: Systemic Leaks

The initial assembly of T1 used the gasket materials purchased as part of that project (1/16 inch Buna-N sheet rubber) between the end pieces and the contour blocks, and 3M brand double stick Scotch tape to attach and seal the acrylic side-plates to the contour blocks. The copper pipe and ball-valve assembly (which are soldered together) was attached to the upstream end piece and sealed with Amazing GOOP® brand sealant. The final assembled tunnel is pictured in Figure 4.1.



Figure 4.1: T1 Assembled on VTF

The tunnel's first runs were conducted with no accompanying diagnostic equipment and were videotaped for future analysis. The objectives of the first runs were to:

- Test the effectiveness of the various sealing methods
- Assess the various design and construction techniques
- Observe any condensation phenomena that might occur

Leaks were immediately discovered during the first chamber pump-down, during which the tunnel produced a siren-like wail. The pumping was halted, and electrical tape was used to cover all possible leak points in an effort to both minimize the leakage and help identify the problem spots. Figure 4.2 shows the tape covering on the chamber-side gasket.

The tape was an effective temporary fix, allowing the chamber to be pumped down to 70 Torr. This pressure represented an operational limit, as the pumping speed was not high enough to maintain vacuum against the leaks at lower pressures. The tape also greatly reduced the noise from the tunnel, and revealed that the leaks were almost entirely through the gaskets on the ends, not through the scotch tape on the side-plates.

The tunnel was run twice during this test with the 70 Torr initial pressure. Both runs took approximately 40 seconds to bring the chamber back to atmospheric pressure. Curiously,

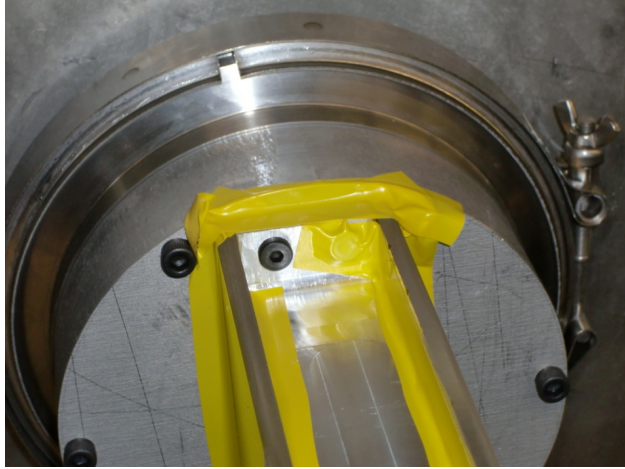


Figure 4.2: Tape on flange side gasket

there was a total absence of fogging and other condensation effects, suggesting the (reservoir) air in the laboratory had low humidity or that the tunnel was perhaps not reaching the anticipated Mach number (and corresponding low static temperature in the test section). Because the tunnel was not instrumented for these tests, the lack of condensation meant that there was nothing to observe visually. Both runs, however, exhibited noticeable changes in the pitch of the sound of the flow after approximately 13 seconds, which was assumed to correspond to the tunnel un-choking.

The tunnel still produced a severe whine when under vacuum, indicating that leaks were present and emanating from a vibrating source. This was determined to be from an incomplete seal at the gaskets, allowing air to rush under and causing the gasket to vibrate like a musical reed. The edges of the gaskets were also observed being pulled into the tunnel slightly when under vacuum (Figure 4.3 and Figure 4.4), another indication of poor sealing. The proposed solution was to install thicker gasket material to allow more compression of the rubber and a tighter seal. In particular, the cause was hypothesized to be the acrylic side-plates, which were not being compressed enough against the rubber.

The test-time calculation, introduced in Section 3.1.2 was modified to verify that steady-state, supersonic flow at the design Mach number was achieved. The calculations indicated



Figure 4.3: Valve End Gasket



Figure 4.4: VTF End Gasket

that the maximum allowable chamber pressure for steady-state conditions was 120 Torr; pressures higher than this would cause a shock to form somewhere inside the tunnel. In other words, 120 Torr was the back pressure that corresponds with the “end of test” as defined previously. The initial chamber pressure used for these tests was below this maximum, and thus the desired test conditions should have been present in the tunnel for approximately 2 seconds. Without further instrumentation, there is no way the actual test time could be determined or operation of the tunnel at its design Mach number of 3.68 verified.

Several modifications were proposed to fix the leaks, including using vacuum grease or Amazing GOOP® sealant around the gaskets. Ultimately, the decision was made to re-cut the gaskets out of thicker material (3/32 inch Buna-N sheet rubber).

4.1.2 Test Two: Thicker Gaskets

Because the sealing gaskets were pulled into the tunnel, the second design iteration featured thicker (3/32” Buna-N sheet rubber) gaskets that would theoretically be more compressible to seal better. This test run continued to make use of the electrical tape as a temporary sealant along the window side plates. The results of this test run were both disappointing and enlightening. On one hand, the thicker gaskets were pulled into the tunnel to a greater extent than they were in the previous test. The entire width of the gasket on each side was pulled in, whereas only a portion of the gasket was pulled in during the previous test. On the other hand, a slight misalignment in the gasket resulted in it becoming pinched along the side between the window and the end piece. On the part that was pinched, it was noticed that the gasket did not get pulled in at all. From these observations, it was decided to cut new gaskets from the original thinner material that would be intentionally oversized so that they would be pinched on all sides. Although this run proved that thicker gaskets performed significantly worse than the thinner, sturdier gaskets used previously, important observations were made that resulted in functionally significant changes for the next test run.

4.1.3 Test Three: Pinched Gaskets & Screw Hole Leakage

The third tunnel test run examined the effectiveness of the intentionally oversized gaskets. As described in the previous section, it was observed that oversized gaskets were pinched between the window or backbone and the respective end piece, which prevents the gaskets from being pulled into the tunnel. This test was also the first to use a more permanent solution to the leakage along the tunnel length than the electrical tape. GE Silicone II clear caulk was applied on the outside edge of the tunnel backbone along its length against the window plate, as illustrated in Figure 4.5.



Figure 4.5: T1 Caulking

During this test, it was observed that the oversized gaskets worked perfectly, completely preventing them from being pulled into the tunnel. With this fix and the additional seal of the caulking, it was possible to pump the tunnel down as low as 20 Torr. It was determined that while leaking had been significantly reduced via the fixes implemented over the course of the previous test runs, there was still non-negligible leakage that prevented the tunnel from being pumped down to the 50 milliTorr pressures for which it had originally been designed. After careful examination, it appeared that the continued leaks were the result of air entering through the screw holes. As a solution to this, it was decided that the next run would feature small O-rings under each of the screws attaching the backbones to their respective end pieces.

4.1.4 Test Four: Backbone Corner Leakage

The purpose of this test was to determine if the O-rings inserted under the screws after the previous test run would finally create a sufficient seal to pump the chamber down to lower pressures. After pumping down the vacuum chamber, pumping stalled at 17 Torr and audible leaks continued to occur. At this point it was determined that continued leaks were through two problem areas. The corners on the outside of the backbones near each end appeared to be insufficiently caulked, contributing to some of the leaking. The sides of the window plates also appeared to be posing a problem due inherently to the design, which does not provide a force to seal the windows against the backbones and end pieces. To solve the former issue, additional caulking was applied at the offending backbone corners. To help alleviate the latter issue, C-clamps were used to add a compressive force to hold the side plates. Even with these clamps, however, the tunnel design would not allow for complete vacuum sealing.

4.2 Variable Geometry Tunnel Construction

Due to increased mechanical complexity, the assembly process for the second generation tunnel, T2, was significantly more involved than T1. The variable geometry tunnel has over 140 individual parts, compared to the 16 used in T1. Due to this mechanical complexity, many issues were encountered during the manufacturing and assembly of T2. Problems occurred with several aspects of the particularly complex contour and adjuster system, from material and part availability to the very involved assembly procedure.

Due to the unavailability of polystyrene blocks of the necessary size, the adjuster attachment blocks had to be redesigned to be made from 0.5 inch diameter styrene rod, which greatly increased the difficulty of manufacturing the throat blocks. Ultimately, the throat curve (Figure 4.6) had to be hand-sanded to shape using a dry and wet sanding process.

Additionally, no bolts for the screw adjusters could be found that were long enough and

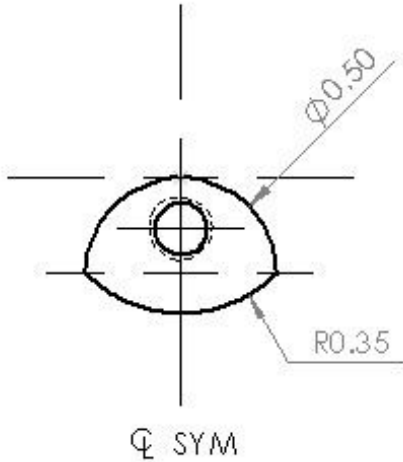


Figure 4.6: Throat block profile

fully threaded, so additional threads had to be cut on the shank of each screw.

Various other assembly aspects required careful setup. The order in which the various components were attached to the contour strips was critical in maintaining correct alignment of all parts. The styrene contour strips were scored and snapped to the correct width, each four feet long. The positions of each styrene block and the linear rails were determined using measurements of the CAD model. The throat block was the first to be attached, and required that the styrene contour strip be pre-bent in order to hold its shape around the block. The block was then attached with a plastic solvent, and held firmly in place by hand for a few minutes. To facilitate the overnight drying, the contour was held in a bent shape with masking tape and left to dry (Figure 4.7).

After the throat blocks were dry, the remaining adjuster blocks and linear rails were attached, aligned with pencil marks on the back side of the contour. The linear rails were attached with quick-dry epoxy, and were masked to ensure that no epoxy got on the bearing surfaces. While one rail was being attached, the sliding “truck” was stored on a separate rail to ensure it remained free of epoxy. The blocks and rails had to be attached before the O-ring to make certain that accurate measurements could be made to align the components.

The most difficult part of the assembly process was attaching the O-ring to the contour



Figure 4.7: Throat Block Fixturing

sides. The attachment process involved applying a thin bead of GE Silicone II clear caulk in one of the O-ring grooves, pressing it against the contour side and wiping along the corner with a paper towel to smooth any over-spill on the contour sides that would come in contact with the flow. The O-ring was then held against the contour with small strips of masking tape and left to dry overnight. To reduce handling time after caulking and the risk of disrupting the O-ring positioning, the second side was done after the first had dried. The final strips were cut to length after being affixed to the backbones.

Additionally, due to the tight curve at the throat, no tape method was sufficient to hold the O-ring in place for the full 24 hour drying cycle. To remedy this, Loctite Quicktite Gel (a quick-dry adhesive) was used to tack down the O-ring around the throat curve. Super glue dries hard, and therefore cannot be used elsewhere along the contour, but was a feasible solution at the throat where the curve geometry is fixed. The super glue was applied in a similar manner to the caulk, but was held in place by hand for 3 minutes to dry. The rest of the O-ring strip was then attached as described above, and a thin bead of caulk was applied around the bend at the throat to ensure that the O-ring was sealed the entire way around the throat.

The process for attaching the contour strips to the adjusters and the backbone was a

complicated and step-wise process; details can be found in Appendix A. The proper assembly order was determined and outlined before the assembly began, using the assembly drawing of the adjuster screws for reference (See Appendix B).

The final assembly operations involved attaching the tensioning system. Once the proper contour length was determined, the contour was trimmed and thin reinforcing strips of 0.050 in. thick aluminum sheet were cut and epoxied to the ends where the tensioning springs attached. A single small hole was drilled in the center of each reinforcing strip, large enough to hook the springs through. The springs were then attached to the end of the strips and the eye bolts on the back side of the flange adapter plate.

Table 4.1 contains a list of all solvents, adhesives and other compounds used in the assembly process.

Table 4.1: Compounds Used for T2 Assembly

Name	Manufacturer	Product Number	Use
Silicone Window & Door Sealant	General Electric	GE5000	O-ring attachment
Plastic Model Cement	Testors Model Master	No. 8872	Styrene block attachment
Super Glue	Loctite	234790	O-ring throat fixturing
Wicking Threadlock	Loctite	29000	Adjuster jam nuts

The final tunnel was assembled with all sideplates, spring tensioners and contours, as seen in Figure 4.8. The system was tested mechanically by adjusting the contours for a range of throat and expansion section shapes.

A few problems were encountered during the assembly process which would need to be fixed in future versions. The cutout in the flange adapter was intended to be a close fit for the O-ring, but ended up being too small and caused the O-ring to pull off of the contour strip. The rest of the O-ring did appear to seal well from visual inspection, although a sixth

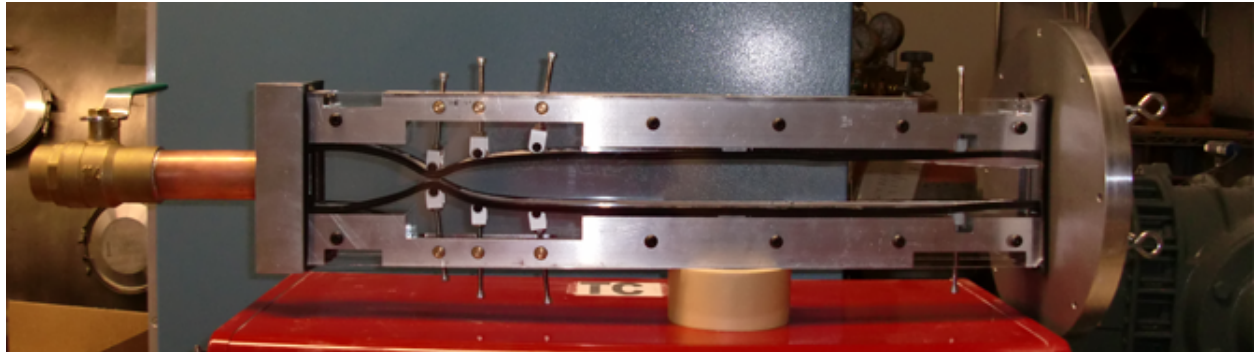


Figure 4.8: Complete Tunnel Assembly

set of sideplate attachment holes would need to be added to the backbone at the expansion section to ensure that it fully seals. In the current state, the sideplate plastic bows outward at that point due to the large distance between attachment points (see Figure 4.9). Lastly, the diffuser adjusters are positioned too close to the end of the linear rail to effectively create a diffuser. This does not prohibit the operation of the tunnel, but is an area for future improvement.

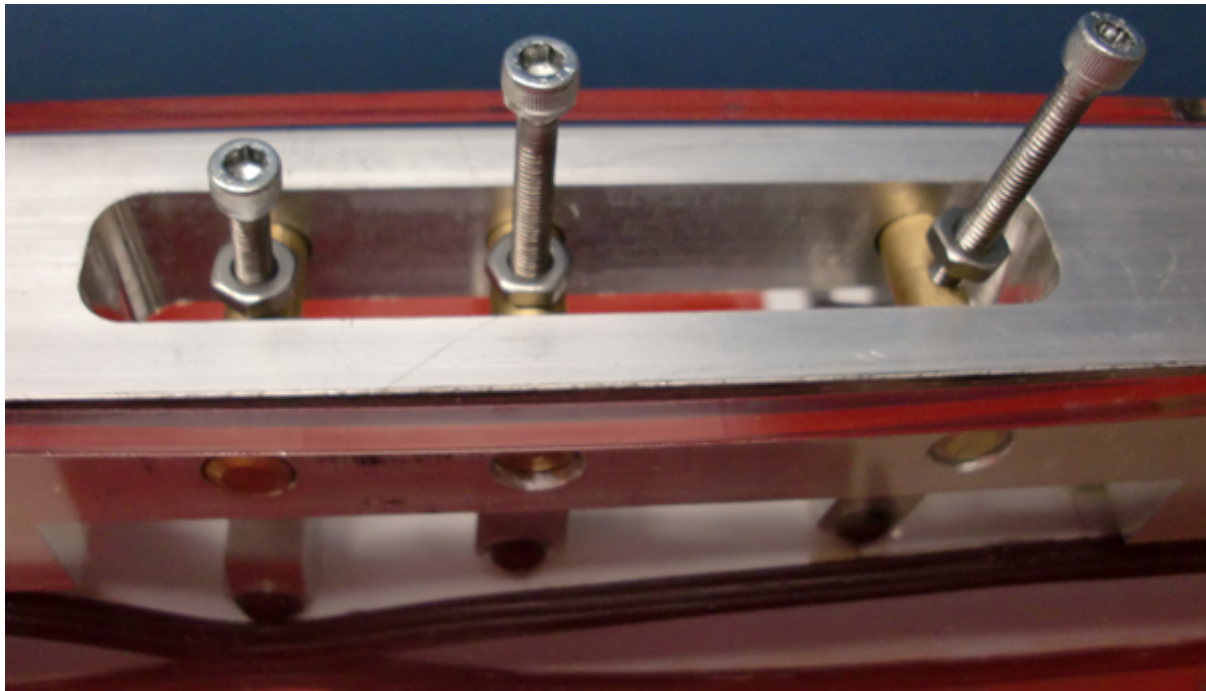


Figure 4.9: Sideplate Gap at Throat

4.3 Large Flange Manufacturing

Numerous problems were encountered in the manufacturing of the large flange, the piece required to attach the tunnel to the VTF chamber. The flange was made of stainless steel, which is a very hard metal, making it difficult to machine. It was quickly discovered that the WPI machine shops were not well equipped to deal with the machining of stainless steel. The clamp ring (the smaller of the two stainless parts) posed no significant manufacturing problems, but took significantly longer to machine than anticipated and required manual grinding to remove flashing and burrs.

The actual port cover itself, which interfaces with the chamber flange, presented significantly more manufacturing issues. Due to the fact that the size of the final part was slightly larger than 1 ft diameter, the stock piece was a flat plate 18 in. x 18 in. x 1.25 in. thick. As such, a very large amount of material had to be removed, which turned out to be an extremely difficult task for the WPI CNC¹ machines. The inner bore was cut on a HAAS VM3 using a large diameter indexable carbide insert mill. The length of the cutting tool and the speed and power limitations of the machine caused the inserts to chip and damage themselves during almost every pass, rendering them useless (Figure 4.10). This slowed the machining process down even more, as it required the operator to stop the machine after every pass to replace the inserts. On-the-fly modification of the code was able to reduce the damage, but was unable to provide a smooth finish on the inside bore.

Following this experience, the part model and drawing was sent out for quotes from local machine shops to find out if the job could be out-sourced to a more capable manufacturing facility. It was determined that out-sourcing the entire part machining process would be prohibitively expensive, but it was within budget to have the outer diameter rough-cut on a water-jet, and returned to WPI for final machining. The WPI shop director agreed that they were capable of doing the final machining on the part after the water-jet process. The WPI machine shop initially encountered problems fitting the part in the desired machine,

¹Computer Numeric Control



Figure 4.10: Damaged Carbide Inserts

but was ultimately able to find a suitable machine. At the time of this writing, the flange was waiting on the last drilling operation for the clamp ring attachment holes.

The acrylic window was purchased pre-cut from Plastics Unlimited, Inc. in Worcester, MA. It was received slightly over-size, and needed to be sanded down around the outer diameter to fit the recesses in the port cover and clamp ring.

5. Recommendations

After completing this project, a number of areas were identified for future improvement. Below is a summary of the recommendations in the areas of tunnel sealing, diagnostics and overall tunnel design. Should any future design and testing be performed, it is suggested that these improvements been carefully considered.

5.1 Sealing the Tunnel

One of the issues experienced during tunnel assembly was with affixing the O-ring material to edges of the polystyrene strips. In subsequent projects, it is recommended that a different method for attaching the quad O-ring—or a different sealing method entirely—be used with this design. The caulk was difficult to use; it did not adhere to the O-ring material very well. Since it takes about 24 hours to dry, keeping it secured to the polystyrene required caulking a couple inches of the O-ring and taping it onto the strip, one section at a time. A flexible, fast drying adhesive would have worked better. Additionally, the compression of the window against the O-ring was the only means of sealing the tunnel. It may be beneficial for projects in the future to find a better way to ensure that there are no leaks in the design. One such method would be to move the valve downstream of the test section (further described in Section 5.3), so that the tunnel contour itself does not have to seal. This method was discussed originally for this project, but deemed unfeasible for a variety of reasons. First, it would have required a separate support system for the tunnel so that the ball valve was not forced to bear the entire cantilevered weight of the tunnel. In addition, further calculations would have to be performed to ensure that the valve itself did not act as a throat and prevent the test section from reaching supersonic speeds.

5.2 Axially Shifting Tunnel Design

Another recommendation involves taking a different approach to the wind tunnel's basic design. The axially shifting tunnel described earlier in Section 3.2.1 may be easier to construct and more reliable to use. Designing the contours would be much easier; once the method of characteristics is properly applied, the shape for each contour can be easily determined. Since each contour is of a fixed shape and made of one solid piece of material, they would be easier to manufacture than the combined contour and backbone of the current design. Additionally, since they have fewer moving parts, the chance of component failure is reduced. Finally, an axially shifted tunnel would probably be easier to seal because it would have a much larger area for sealing. The entire side of the contours could be compressed against the window instead of just the small O-ring area. As described in Section 5.1, using caulk to affix the O-ring material to the sides of the polystyrene strips was difficult and messy. The axially shifting tunnel would remove many of those difficulties.

5.3 Ball Valve Assembly

The ball valve, used to seal the tunnel off from atmospheric pressure and start each run, was placed upstream of the entire tunnel in both the tunnel in this project as well as Peter Moore's design. This design has advantages and disadvantages. One advantage of this design is that it allows for objects to be inserted into the tunnel from downstream, inside the vacuum chamber. Another advantage of upstream placement is that designers need not worry that the valve could act as a second throat downstream, choking the flow and forcing it to go subsonic. This design also has nontrivial disadvantages. The most significant of these is the need to create a nearly perfectly vacuum sealable tunnel design. An upstream valve means that the entire tunnel length must be pumped down to vacuum pressures along with the chamber itself. Without a perfectly sealed tunnel, it can be difficult to pump the chamber down to sufficiently low pressures.

Placement of the ball valve downstream of the test section results in a reversal of the advantages and disadvantages. With a downstream valve, the tunnel need not necessarily be as well-sealed, since the vacuum chamber would be pumped down independently of the tunnel. This is a significant advantage, because properly sealing the tunnel can be very difficult. Attempts to seal T1 with various gaskets, O-rings, and other sealants have only been met with a degree of success. At the time of writing, the leakage has been significantly reduced but not entirely eliminated. Additionally, care must be taken in ensuring that the valve is sized appropriately to ensure that it does not force the flow to re-choke, keeping it from going supersonic. Finally, it will inhibit the use of test equipment or models from being inserted from downstream, inside the vacuum chamber. Even so, the advantages might outweigh the disadvantages and future projects might consider this design change if any additional tunnels are to be built.

5.4 Shadowgraph Imagery

As indicated in Section 2.7.2, a shadowgraph is a type of simple flow imaging system that was investigated for use in this project. A shadowgraph system would make any large density gradients in the flow visible, effectively allowing for the visualization of shocks. This would have been a very useful tool to have had, as it likely would have helped confirm supersonic operation as well as precisely indicate the end of test period (when the shock wave travels back up the test section). Without pressure or imaging diagnostics, the tunnel's actual operating conditions have to be assumed to match the calculated conditions. Although the shadowgraph was highly desirable for this project, investigation of the equipment revealed that it was far too expensive to fit into the project budget. This effectively ruled out the use of shadowgraph imagery for this project. If any future projects focus on wind tunnel development, it could be highly beneficial to reinvestigate the possibility of purchasing the materials required for shadowgraph imaging.

References Cited

- [1] Anderson J. D. *Modern Compressible Flow with Historical Perspective, 3rd Ed.* New York: McGraw-Hill; 2003.
- [2] John J, Keith T. *Gas Dynamics, 3rd Ed.* New Jersey: Pearson Prentice Hall; 2006.
- [3] Pope A., Goin K. *High Speed Wind Tunnel Testing.* New York: John Wiley & Sons; 1965.
- [4] Benson T. *Closed Return Wind Tunnel* [document on the Internet]. National Aeronautics and Space Administration; 2009 May 07 [cited 2009 October 07]. Available from: <http://www.grc.nasa.gov/WWW/K-12/airplane/tuncret.html>
- [5] Benson T. *Blowdown Wind Tunnel* [document on the Internet]. National Aeronautics and Space Administration; 2009 May 07 [cited 2009 October 07]. Available from: <http://www.grc.nasa.gov/WWW/K-12/airplane/tunblow.html>
- [6] *High Speed Wind Tunnel and Test Systems Design Handbook* [document on the Internet]. Lockheed Martin Missiles and Fire Control; 2002 May 06. [cited 2009 November 15]. Available from: <http://www.lockheedmartin.com/data/assets/13617.pdf>
- [7] Liepmann H.P. *An Analytical Design Method for a Two-Dimensional Asymmetric Curved Nozzle.* [document on the internet]. Air Research and Development Command U.S. Air Force Contract AF-33(038)-23070, E.O. No.460-31-14; 1953 [cited 2009 October]. Available from: <http://hdl.handle.net/2027.42/6302>
- [8] Series 1700 Mechanical Booster Vacuum Pumps, Series MB Two-Stage Vacuum Pumps. Bulletin 536. Penwalt Corp.; 1980.
- [9] Moran M. J., Shapiro H. N. *Fundamentals of Engineering Thermodynamics, 6th Ed.* New York: John Wiley & Sons, Inc.; 2008.

- [10] Benson T. *Pitot-Static Tube* [document on the Internet]. National Aeronautics and Space Administration; 2009 October 28 [cited 2010 February 10]. Available from: <http://www.grc.nasa.gov/WWW/K-12/airplane/Pitot.html>
- [11] Evans S. Professor of Engineering. Personal Communication. October 1, 2009.
- [12] Moore P. *Design of a Supersonic Wind Tunnel*. Major Qualifying Project. Worcester Polytechnic Institute; 2009.
- [13] Oberg E., Franklin J. D., Holbrook H. L. *Machinery's Handbook, 26th Ed.*, New York: Industrial Press Inc.; 2000.
- [14] *Specialty Film and Sheet* [document on the Internet]. SABIC Innovative Plastics; 2008 [cited 2009 October 10]. Available from: http://kbam.geampod.com/KBAM/Reflection/Assets/Thumbnail/7034_16.pdf
- [15] *Monterey Bay Habitat* [document on the Internet]. Monterey Bay Aquarium Foundation; 2009. [cited 2009 October 10]. Available from: <http://www.montereybayaquarium.org/efc/mbayhabitat.aspx>
- [16] Wikipedia contributors [Pressure Sensor]. Wikipedia, The Free Encyclopedia; ID: 343071436 [updated 2010 February 10 02:34 UTC ; cited 2010 February 15]. Available from: http://en.wikipedia.org/w/index.php?title=Pressure_sensor&oldid=343071436.
- [17] Low-Cost Silicon Pressure Sensor with Millivolt Output. Pressure, Strain and Force Products [document on the Internet]. Omega Engineering, Inc.; [cited 2010 February 15]. Available from: <http://www.omega.com/Pressure/pdf/PX137.pdf>.

Appendix A: Assembly Procedure

Contour-Backbone Assembly Procedure

1. The brass pivots are inserted into the backbone.
2. A single jam nut is threaded to the top of each adjuster screw.
3. The adjuster screws are threaded through the pivots.
4. A second jam nut and nylon washer is threaded in order onto each adjuster screw.
5. The adjuster brackets are fitted onto the adjuster screws.
6. Another set of nylon washers and jam nuts are threaded onto the screws, in that order, such that the adjuster bracket is sandwiched by two nylon washers in between each nut.
7. The jam nuts on either side of the bracket are tightened so that the bracket is firm, but can still spin. Green (wicking) Loctite threadlocking compound is applied to the jam nuts and left to dry.
8. The styrene attachment blocks are fit between each corresponding adjuster bracket. A button head screw with a metal washer is threaded into each block to secure the adjuster in place. A very small bead of purple Loctite threadlocker may be applied to the screws to keep them from loosening during repeated use.
9. The upstream end of the contour is attached to the backbone with four countersunk #6 screws, with a small amount of epoxy between the backbone and the contour. A small shim of styrene sheet is inserted between the screws, sandwiched by the contour strip and backbone. This is to prevent the contour from bowing inward when the screws are tightened.
10. The diffuser adjuster and linear rail are then threaded and attached.

Appendix B: Part and Assembly Drawings

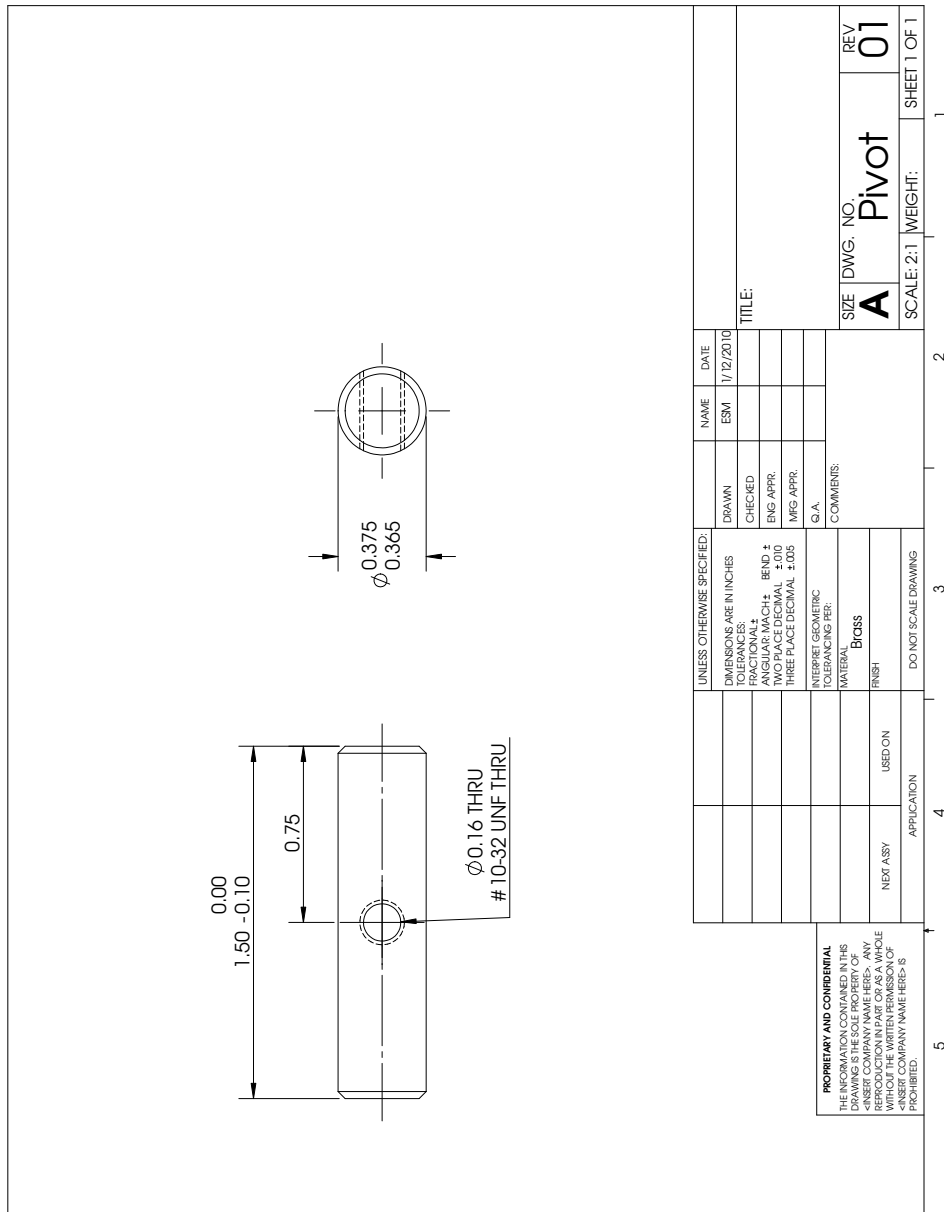


Figure B.1: Adjuster Pivot

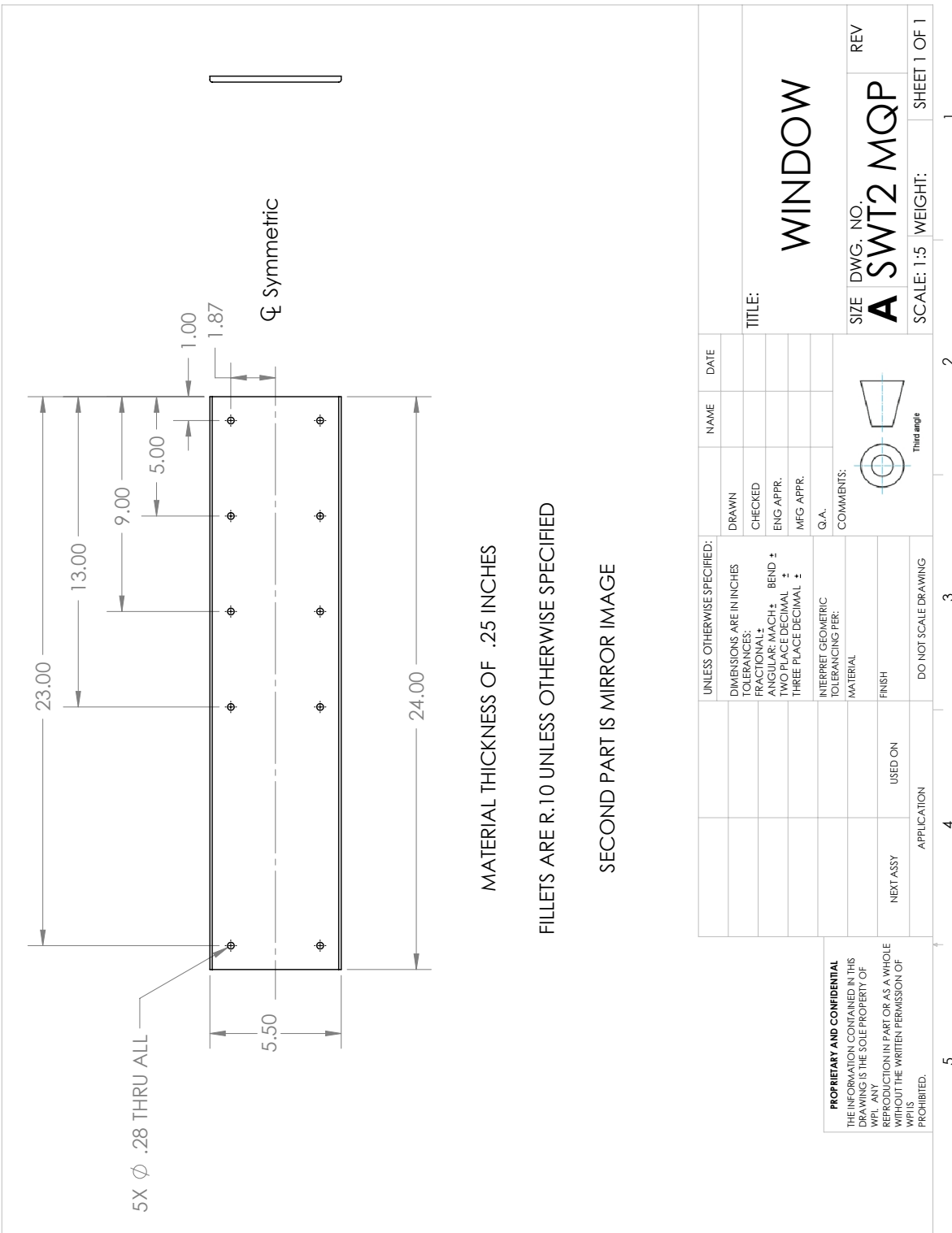


Figure B.2: Side Plate Drawing

The diagram illustrates the exploded view of the Adjuster Assembly. Components are labeled with callouts:

- ① PS Block
- ② Screw Bracket
- ③ Pivot
- ④ Narrow FW 0.25
- ⑤ SBHCSCREW 0.164-32x0.25-HX-N
- ⑥ Preferred Narrow FW 0.164
- ⑦ MSHXNUT 0.190-32-S-N
- ⑧ HX-SHCS 0.19-32x2.5x2.5-N

ITEM NO.	PART NUMBER	Thro at/Q TY.
1	PS Block	1
2	Screw Bracket	1
3	SBHCSCREW 0.164-32x0.25-HX-N	2
4	Preferred Narrow FW 0.164	6
5	Narrow FW 0.25	2
6	Pivot	1
7	MSHXNUT 0.190-32-S-N	3
8	HX-SHCS 0.19-32x2.5x2.5-N	1

		DIMENSIONS ARE IN INCHES						
		TOLERANCES: FRACTIONAL \pm ANGULAR: MACH \pm BEND \pm			DRAWN	NAME	DATE	
		TWO PLACE DECIMAL \pm THREE PLACE DECIMAL \pm			ESM		1/31/2010	
					CHECKED			
					ENG APPR.			
					MFG APPR.			
					Q.A.			
					COMMENTS:			
PROPRIETARY AND CONFIDENTIAL THE INFORMATION CONTAINED IN THIS DRAWING IS THE SOLE PROPERTY OF <INSERT COMPANY NAME HERE>. ANY REPRODUCTION IN PART OR AS A WHOLE WITHOUT THE WRITTEN PERMISSION OF <INSERT COMPANY NAME HERE> IS PROHIBITED.		MATERIAL				SIZE A DWG. NO. Screw Assembly		REV. 02
NEXT ASSY	USED ON	FINISH				SCALE:1:4	WEIGHT:	SHEET 1 OF 1
APPLICATION		DO NOT SCALE DRAWING						

Figure B.3: Adjuster Assembly

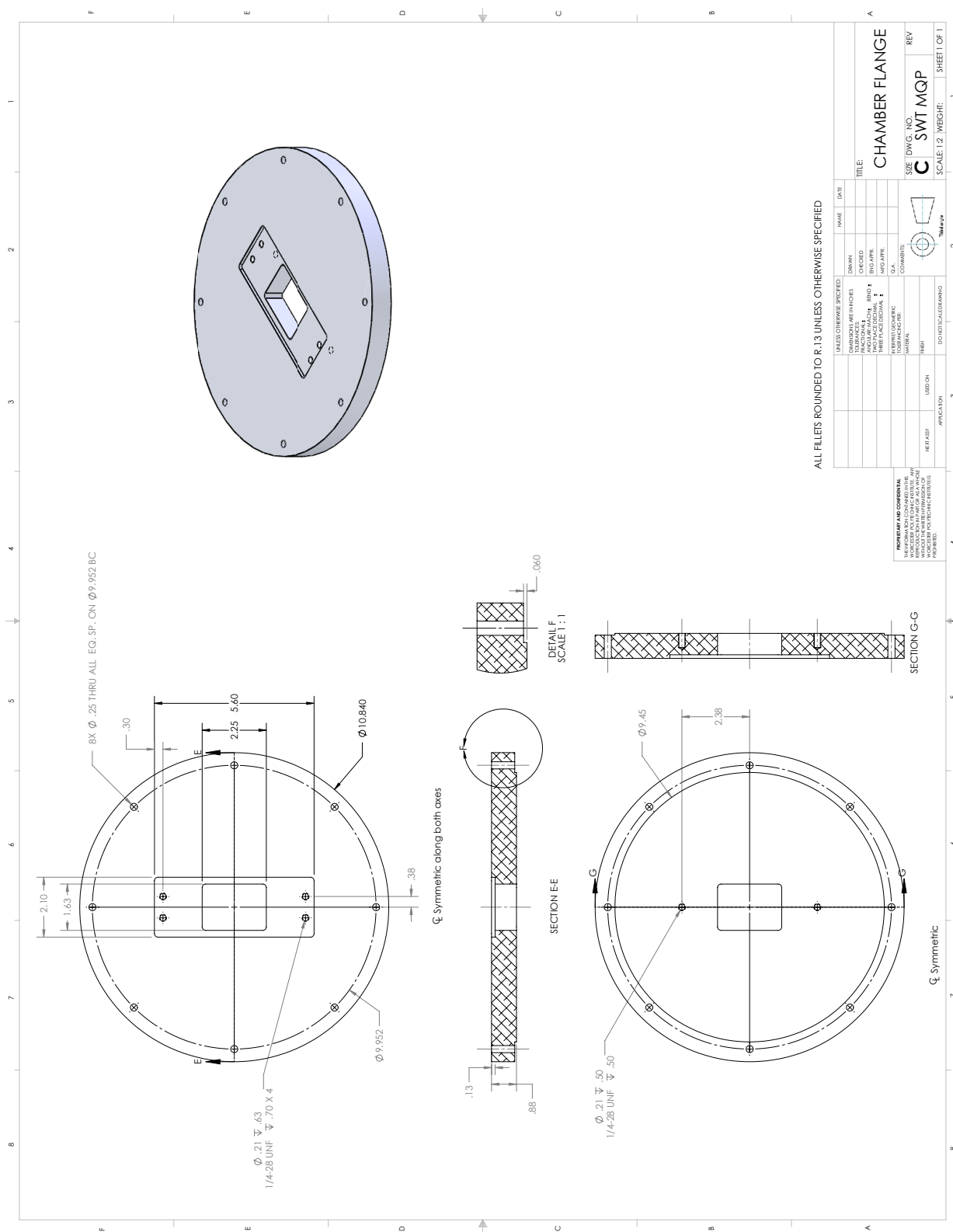


Figure B.4: Chamber Flange

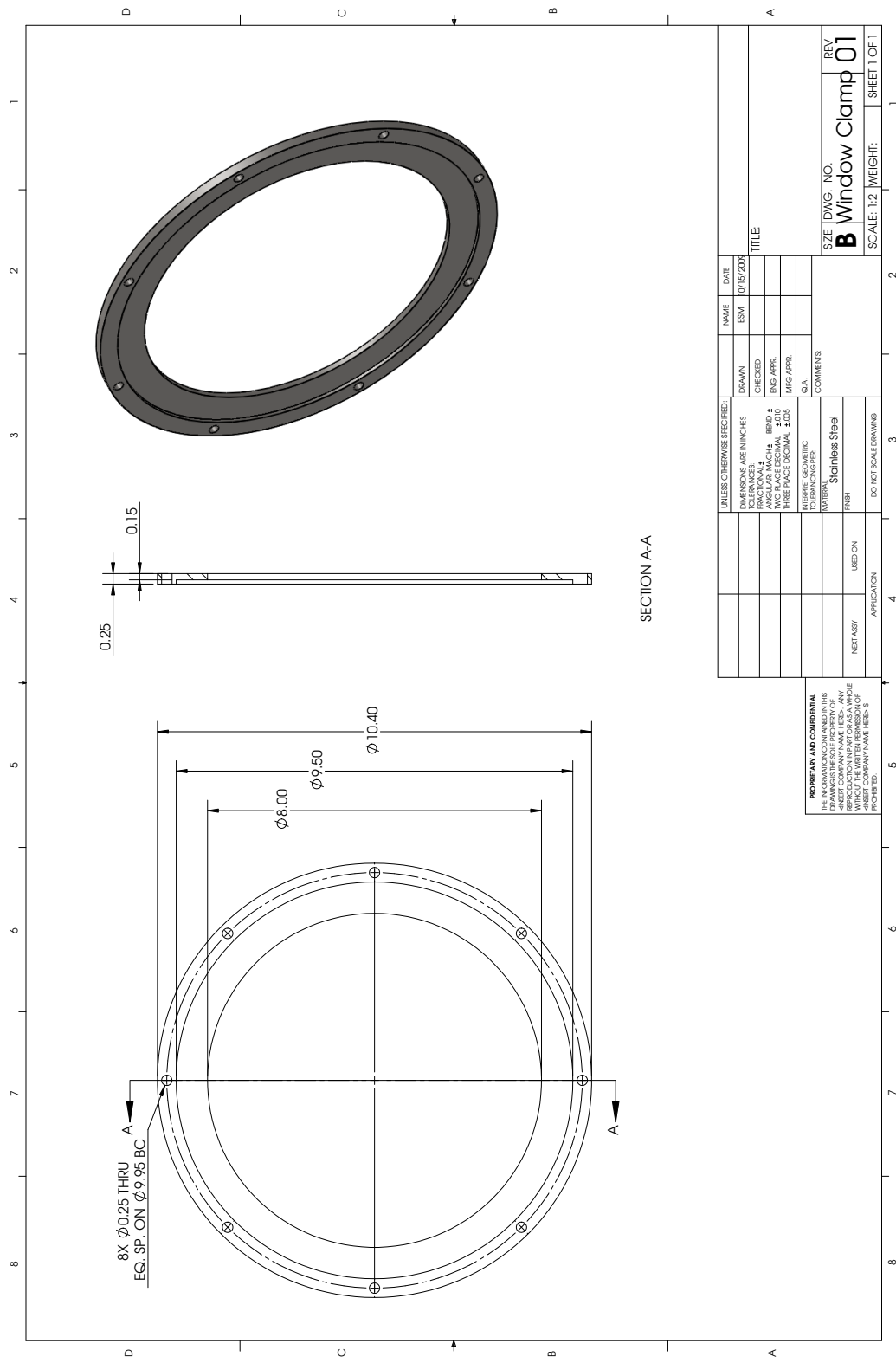


Figure B.5: Window Clamp

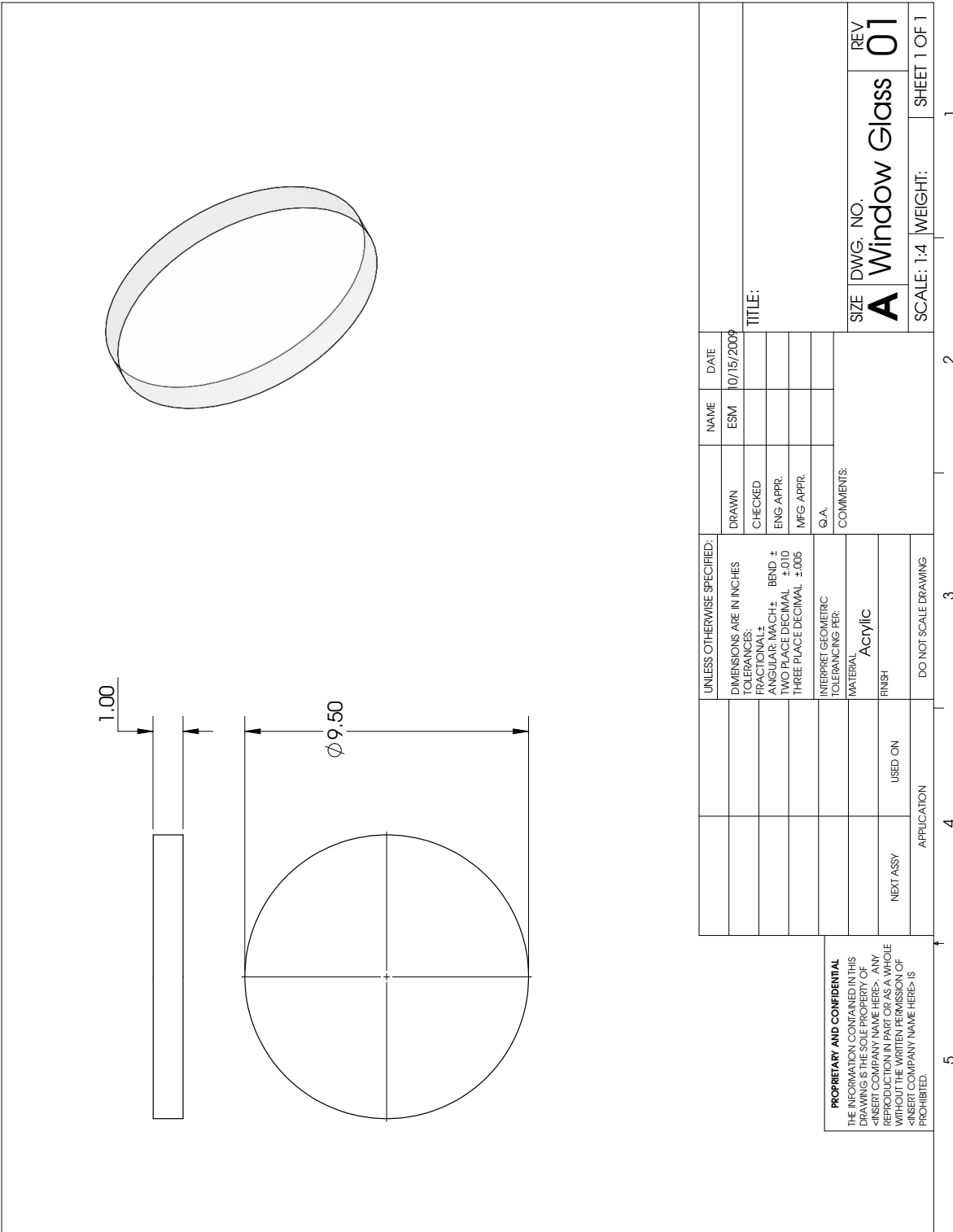


Figure B.6: Window Glass

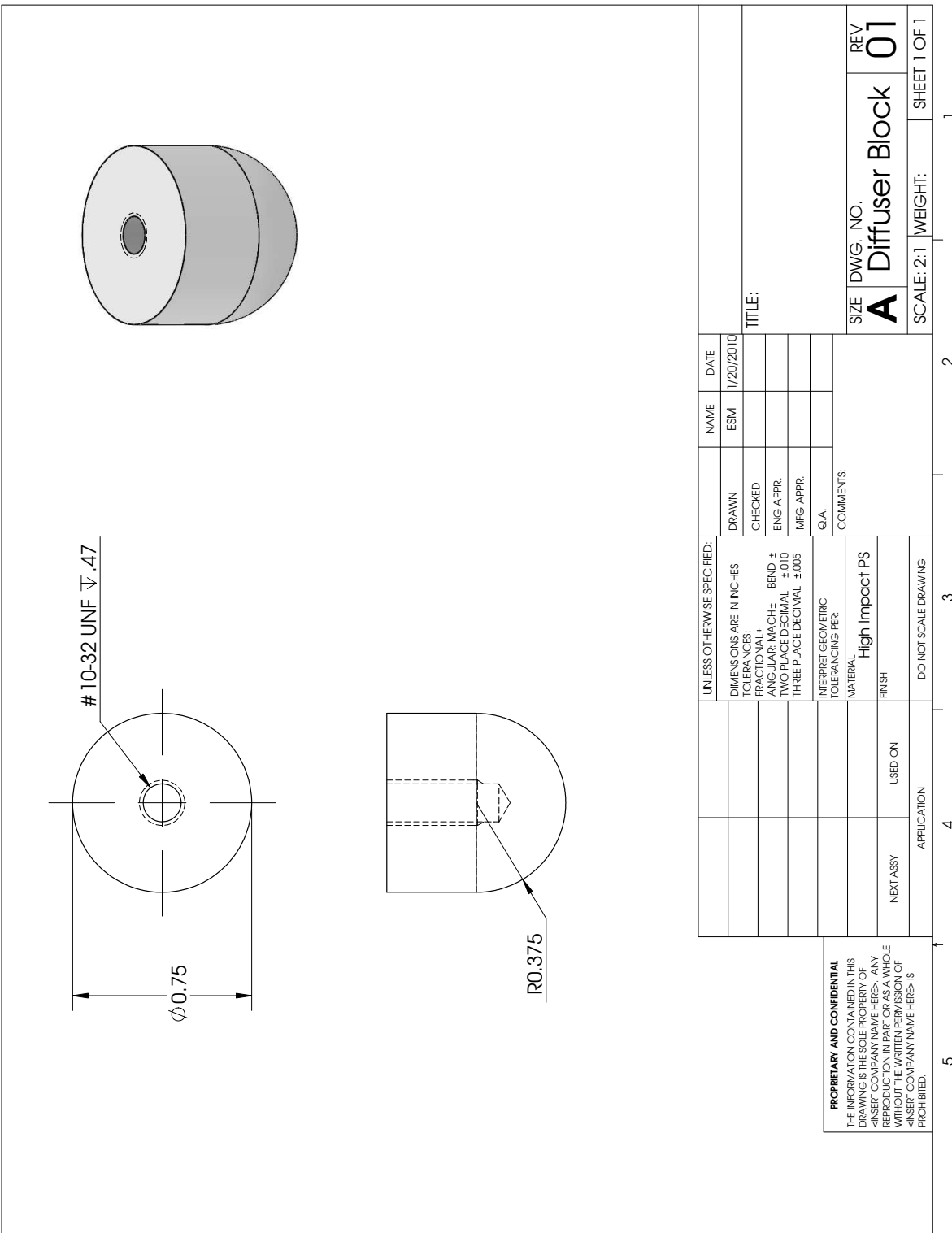


Figure B.7: Diffuser Block

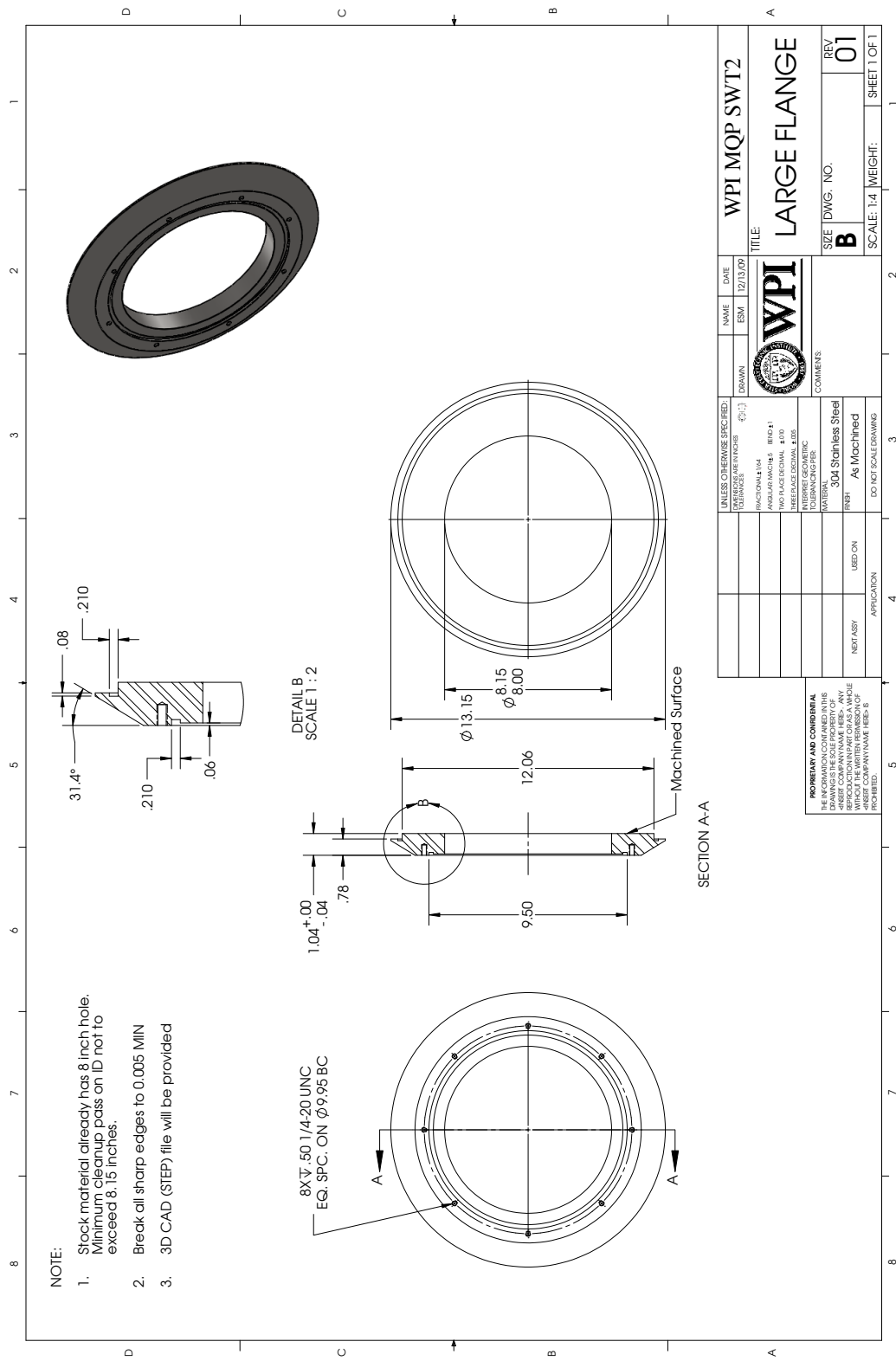


Figure B.8: Large Flange

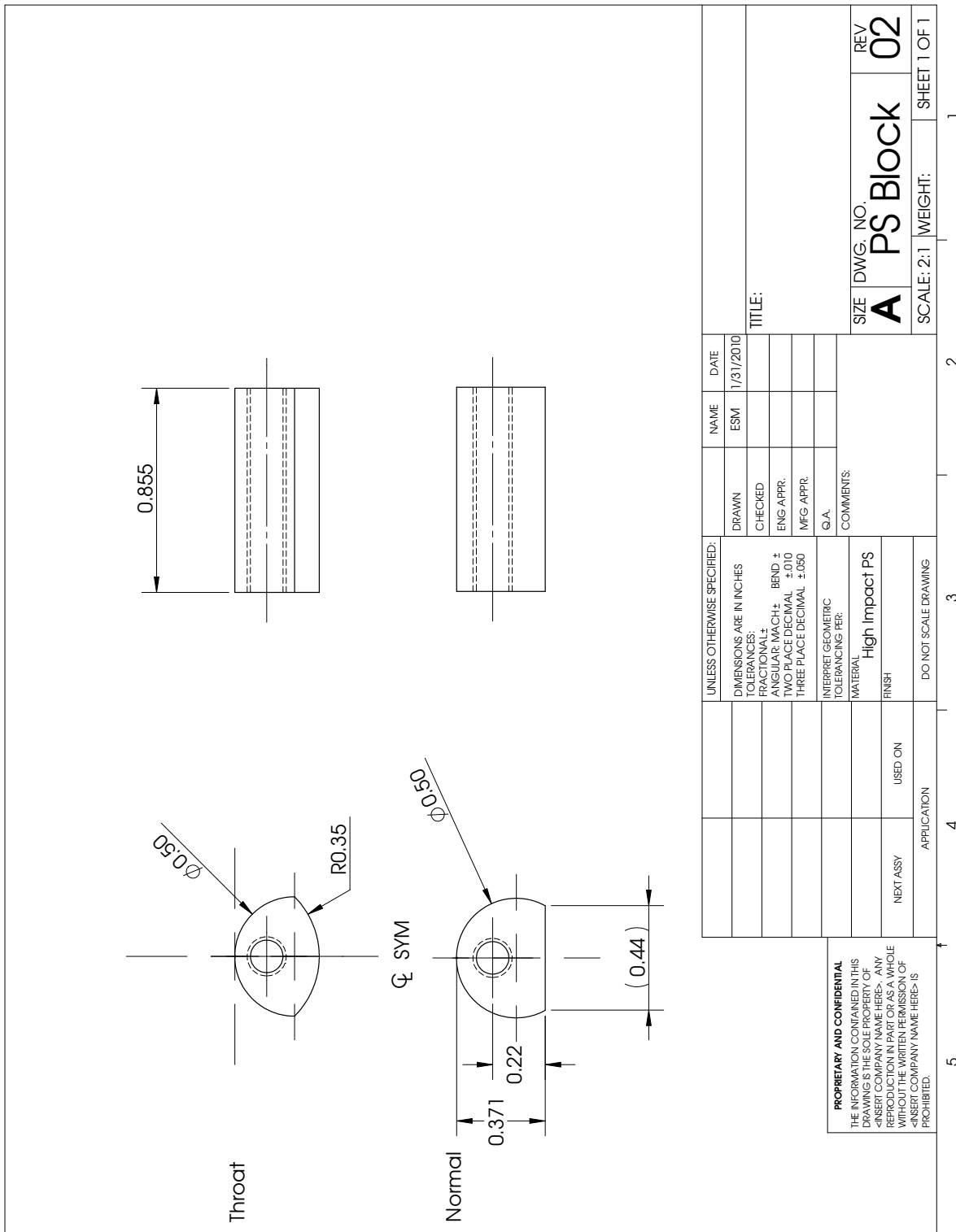


Figure B.9: Polystyrene Block

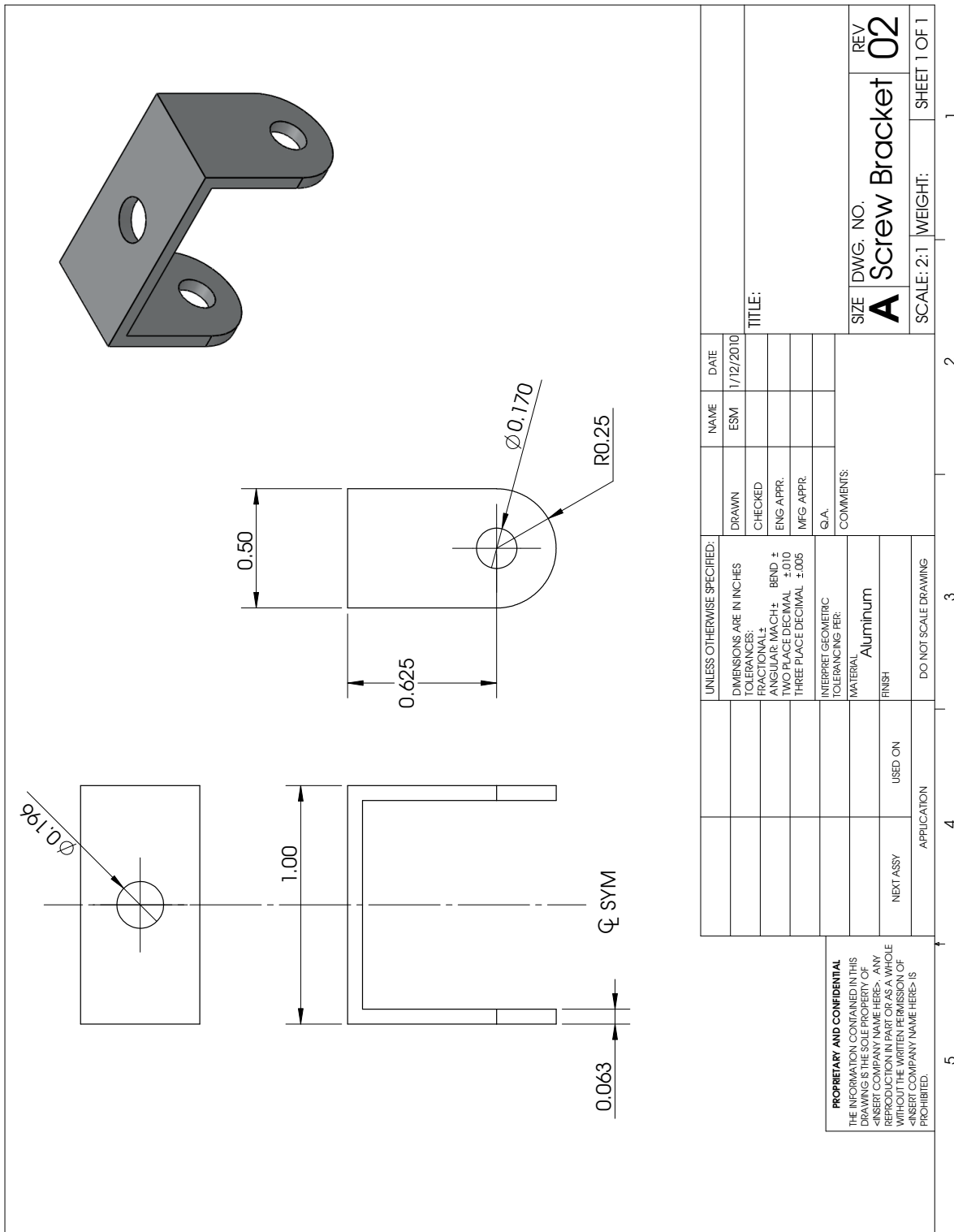


Figure B.10: Screw Bracket

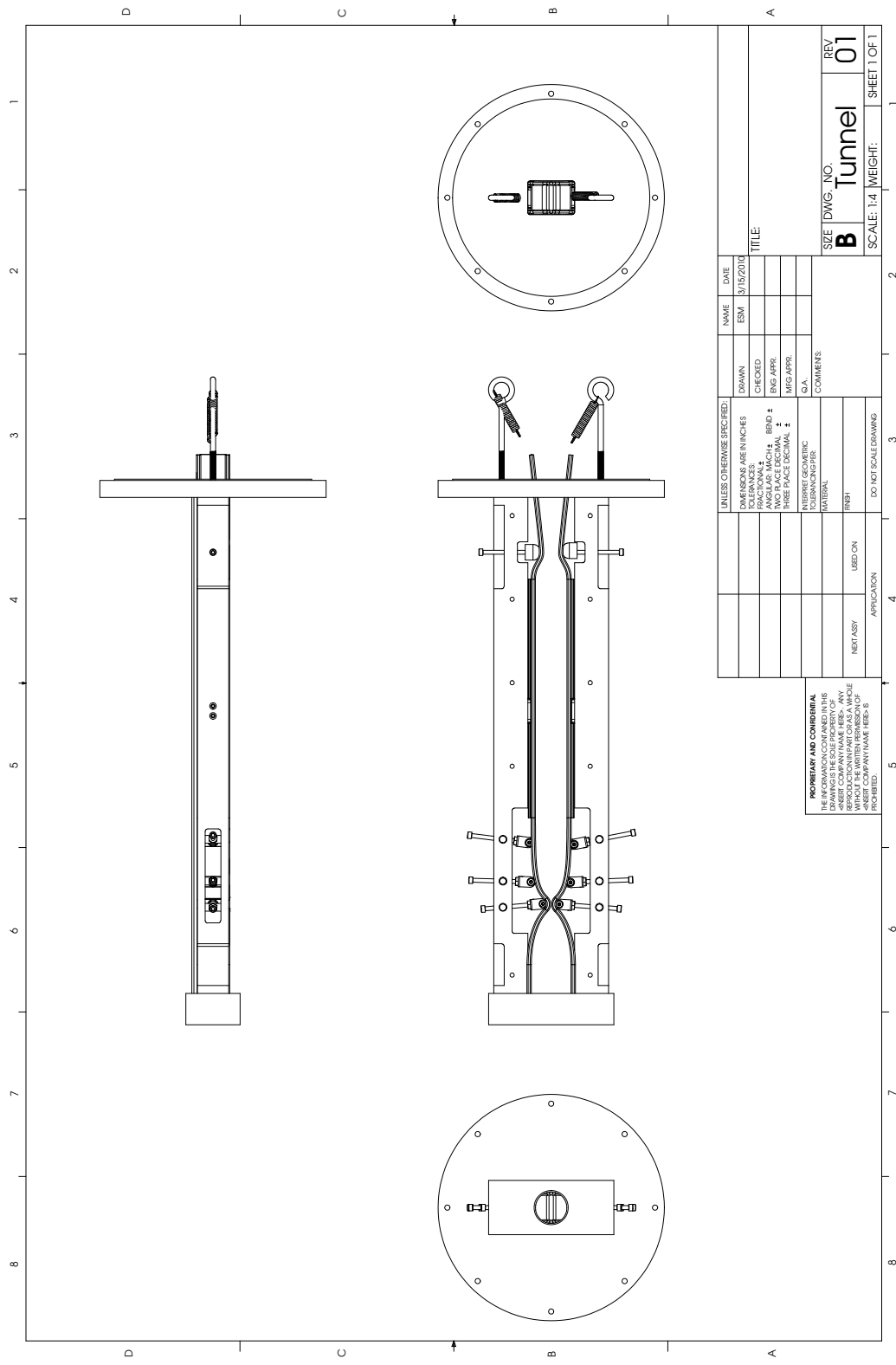


Figure B.11: Complete Tunnel Drawing

Appendix C: MOC MATLAB Code

```
%% Supersonic Wind Tunnel Contour Design
% Brian Earley
% MQP 2009-2010
% JB3-SWT2
% This script uses the Method of Characteristics to calculate the shape of
% a supersonic expansion and straightening contour. The script can be
% configured for varying channel divergence angles and any number of points
% on the initial value line at the throat.

clear all; close all; clc;

%% Calculation Configuration
% Channel divergence angle in degrees:
alpha=24;
% Total height of the entire throat:
throatheight=.25;
% Number of points on the initial value line, or number of angular divisions:
num_divisions=10;
% Number of points along the contour in the expansion region:
num_expcontourpts=5;
% Ratio of specific heats of the gas:
gamma=1.4;
% Initial Mach number at the throat:
mach_initial=1.1;
% Generate Table
% If this is set to 1, a variable "table" will be created to organize the
% output data, which can be exported with xlswrite(filename,table). This
% also duplicates all data, so it may be turned off for large calculations.
generate_table=1;

%% Load Configuration
% Optionally, overwrite the above values with a config file.
%configM25; % Comment out this line to use the set values instead.

%% Basic Maths
disp('Generating Characteristic Mesh... ');
% Points in expansion section
deltaalpha=alpha/(num_divisions-1);
num_exppts=num_expcontourpts*num_divisions+(num_expcontourpts-1)*(num_divisions-1);
% Internal straightening section points
num_intstrtpts=num_divisions*(num_divisions-1);
% Contour points of straightening section
num_contourstrtpts=2*(num_divisions-1);
% Points in straightening section
num strtpts=num_intstrtpts+num_contourstrtpts;
% Total number of points
num_pts=num_exppts+num strtpts;

%% Generate Points Arrays
points=1:1:num_pts;
```

```

expcontourpts=1:(2*num_divisions-1):num_exppts;
expcenterpts=num_divisions:(2*num_divisions-1):num_exppts;
strtcontourpts=num_pts-2*(num_divisions-1)+1:1:num_pts;
strtcenterpts=zeros(size(1:num_divisions-1));
strtcenterpts(1)=num_exppts+2*(num_divisions-1);
for h=2:num_divisions-1
    strtcenterpts(h)=strtcenterpts(h-1)+2*(num_divisions-h);
end
contourpts=[expcontourpts strtcontourpts];
centerpts=[expcenterpts strtcenterpts];

%% Preallocate Variables
alfa=zeros(num_pts,1);
nu=zeros(num_pts,1);
CI=zeros(num_pts,1);
CII=zeros(num_pts,1);
M=zeros(num_pts,1);
mu=zeros(num_pts,1);
alfaplusmu=zeros(num_pts,1);
alfaminusmu=zeros(num_pts,1);
mI=zeros(num_pts,1);
mII=zeros(num_pts,1);
x=zeros(num_pts,1);
y=zeros(num_pts,1);
Apoint=zeros(num_pts,1);
Bpoint=zeros(num_pts,1);
pointtype=zeros(num_pts,1);

%% Determine Point Type & Associated Points
% Point Types:
% Type 1: Contour Points
% Type 2: Centerline Points
% Type 3: All Interior Points
strtdivisions=num_divisions; % Used to determine next point to decrease divisions
nextdecreasepoint=num_exppts+num_divisions; % Set first point of division decrease
arcmaxima=zeros(2*(num_divisions-1),1);
arcindex=0;
for f=num_divisions+1:num_pts
    if(min(abs(contourpts-f))==0)
        pointtype(f)=1;
        if (f<num_exppts)
            % Expansion Region
            Apoint(f)=f+1-2*num_divisions;
            Bpoint(f)=f+1-num_divisions;
        else
            % Straightening Region
            if (f==strtcontourpts(1))
                Apoint(f)=num_exppts+1-num_divisions;
            else
                Apoint(f)=f-1;
            end;
        end
    elseif (min(abs(centerpts-f))==0)
        pointtype(f)=2;
    end
end

```

```

if (f<num_exppts)
    % Expansion Region
    Apoint(f)=f-num_divisions;
    Bpoint(f)=f+1-2*num_divisions;
else
    % Straightening Region
    if (f==nextdecreasepoint)
        % This condition only applies to the last centerline point
        strtdivisions=strtdivisions-1;
    end
    Apoint(f)=f-strtdivisions;
    Bpoint(f)=f-2*strtdivisions;
    if (f~=nextdecreasepoint)
        arcindex=arcindex+1;
        arcmaxima(arcindex)=f+1;
        arcindex=arcindex+1;
        arcmaxima(arcindex)=f+strtdivisions;
    end
    nextdecreasepoint=f+strtdivisions;
end
else
    pointtype(f)=3;
    if (f<num_exppts)
        % Expansion Region
        Apoint(f)=f-num_divisions;
        Bpoint(f)=f+1-num_divisions;
    else
        % Straightening Region
        if (f==nextdecreasepoint)
            strtdivisions=strtdivisions-1;
        end
        Apoint(f)=f-strtdivisions;
        Bpoint(f)=f+1-strtdivisions;
    end
end
end
% Assign B points to straightening section contour points based on arcmaxima
Bpoint(strtcontourpts)=arcmaxima;
% Bugfix for last centerline point in expansion region
Bpoint(num_exppts)=num_exppts+1-2*num_divisions;

%% Initial Value Line Points
disp('Calculating Initial Value Line...');

alfacounter=alpha-deltaalpha;
% Point 1
alfa(1)=alpha;
M(1)=mach_initial;
nu(1)=sqrt((gamma+1)/(gamma-1))*atan(sqrt(((gamma-1)/(gamma+1))*(M(1)^2-1)))-...
atan(sqrt(M(1)^2-1));
CI(1)=alfa(1)+nu(1);
CII(1)=alfa(1)-nu(1);
mu(1)=asin(1/M(1));
alfaplusmu(1)=alfa(1)+mu(1);
alfaminusmu(1)=alfa(1)-mu(1);

```

```

mI(1)=0; mII(1)=0;
y(1)=throatheight/2;
x(1)=y(1)/tan(alfa(1)*pi/180);
RIVL=sqrt(x(1)^2+y(1)^2);
% All Other IVL Points
for q=2:num_divisions
    alfa(q)=alfacounter;
    M(q)=mach_initial;
    nu(q)=sqrt((gamma+1)/(gamma-1))*atan(sqrt(((gamma-1)/(gamma+1))*(M(q)^2-1)))-...
        atan(sqrt(M(q)^2-1));
    CI(q)=nu(q)+alfa(q);
    CII(q)=nu(q)-alfa(q);
    mu(q)=asin(1/M(q));
    alfaplusmu(q)=alfa(q)+mu(q);
    alfaminusmu(q)=alfa(q)-mu(q);
    mI(q)=0; mII(q)=0;
    y(q)=RIVL*sin(alfa(q)*pi/180);
    x(q)=RIVL*cos(alfa(q)*pi/180);
    if (q==num_divisions)
        % If centerline point, set alfacounter to next intermediate value
        alfacounter=alpha-0.5*deltaalpha;
    else
        alfacounter=alfacounter-deltaalpha;
    end
end

%% Start Expansion Section Points
disp('Calculating Expansion Section... ')
for k=num_divisions+1:num_exppts
    if (pointtype(k)==1)
        % Contour point
        alfa(k)=alpha;
        alfacounter=alpha-deltaalpha; % Reset alfa counter
        CII(k)=nu(Bpoint(k))-alfa(Bpoint(k));
        nu(k)=CII(k)+alfa(k);
        CI(k)=nu(k)+alfa(k);
        nu_rad=nu(k)*pi/180;
        Mtemp=1;
        mlow=1;
        mhigh=10;
        for b=1:100,
            Mtemp=(mlow+mhigh)/2;
            temp3 = sqrt(Mtemp^2-1);
            temp2 = atan(sqrt((gamma-1)/(gamma+1))*temp3);
            temp1 = temp2*sqrt((gamma+1)/(gamma-1))-atan(temp3);
            if (temp1 > nu_rad), mhigh = Mtemp; end
            if (temp1 < nu_rad), mlow = Mtemp; end
        end
        M(k)=Mtemp;
        mu(k)=asin(1/M(k));
        alfaplusmu(k)=alfa(k)+mu(k);
        alfaminusmu(k)=alfa(k)-mu(k);
        mI(k)=tan(alfa(k)*pi/180);
        mII(k)=tan(0.5*pi/180*(alfaplusmu(Bpoint(k))+alfaplusmu(k)));
    end
end

```

```

elseif (pointtype(k)==2)
% Center point
alfa(k)=0;
alfacounter=alpha-0.5*deltaalpha;
CI(k)=nu(Apoint(k))+alfa(Apoint(k));
nu(k)=CI(k)-alfa(k);
CII(k)=nu(k)-alfa(k);
nu_rad=nu(k)*pi/180;
Mtemp=1;
mlow=1;
mhigh=10;
for b=1:100,
    Mtemp=(mlow+mhigh)/2;
    temp3 = sqrt(Mtemp^2-1);
    temp2 = atan(sqrt((gamma-1)/(gamma+1))*temp3);
    temp1 = temp2*sqrt((gamma+1)/(gamma-1))-atan(temp3);
    if (temp1 > nu_rad), mhigh = Mtemp; end
    if (temp1 < nu_rad), mlow = Mtemp; end
end
M(k)=Mtemp;
mu(k)=asind(1/M(k));
alfaplusmu(k)=alfa(k)+mu(k);
alfaminusmu(k)=alfa(k)-mu(k);
mI(k)=tan(0.5*pi/180*(alfaminusmu(Apoint(k))+alfaminusmu(k)));
mII(k)=tan(alfa(k)*pi/180);
else
% All other points
alfa(k)=alfacounter;
alfacounter=alfacounter-deltaalpha;
CI(k)=nu(Apoint(k))+alfa(Apoint(k));
CII(k)=nu(Bpoint(k))-alfa(Bpoint(k));
nu(k)=(1/2)*(CI(k)+CII(k));
nu_rad=nu(k)*pi/180;
Mtemp=1;
mlow=1;
mhigh=10;
for b=1:100,
    Mtemp=(mlow+mhigh)/2;
    temp3 = sqrt(Mtemp^2-1);
    temp2 = atan(sqrt((gamma-1)/(gamma+1))*temp3);
    temp1 = temp2*sqrt((gamma+1)/(gamma-1))-atan(temp3);
    if (temp1 > nu_rad), mhigh = Mtemp; end
    if (temp1 < nu_rad), mlow = Mtemp; end
end
M(k)=Mtemp;
mu(k)=asind(1/M(k));
alfaplusmu(k)=alfa(k)+mu(k);
alfaminusmu(k)=alfa(k)-mu(k);
mI(k)=tan(0.5*pi/180*(alfaminusmu(Apoint(k))+alfaminusmu(k)));
mII(k)=tan(0.5*pi/180*(alfaplusmu(Bpoint(k))+alfaplusmu(k)));
end
x(k)=(y(Apoint(k))-y(Bpoint(k))+mII(k)*x(Bpoint(k))-mI(k)*x(Apoint(k)))/(mII(k)-mI(k));
y(k)=y(Apoint(k))+mI(k)*(x(k)-x(Apoint(k)));
end

```

```

%% Start Straightening Section Points
disp('Calculating Straightening Section... ')
for k=num_exppts+1:num_pts
    if (pointtype(k)==1)
        % Contour point
        alfa(k)=alfa(Bpoint(k));
        CII(k)=nu(Bpoint(k))-alfa(Bpoint(k));
        nu(k)=CII(k)+alfa(k);
        CI(k)=nu(k)+alfa(k);
        nu_rad=nu(k)*pi/180;
        Mtemp=1;
        mlow=1;
        mhigh=10;
        for b=1:100,
            Mtemp=(mlow+mhigh)/2;
            temp3 = sqrt(Mtemp^2-1);
            temp2 = atan(sqrt((gamma-1)/(gamma+1))*temp3);
            temp1 = temp2*sqrt((gamma+1)/(gamma-1))-atan(temp3);
            if (temp1 > nu_rad), mhigh = Mtemp; end
            if (temp1 < nu_rad), mlow = Mtemp; end
        end
        M(k)=Mtemp;
        mu(k)=asind(1/M(k));
        alfaplusmu(k)=alfa(k)+mu(k);
        alfaminusmu(k)=alfa(k)-mu(k);
        mI(k)=tan(alfa(k)*pi/180);
        mII(k)=tan(0.5*pi/180*(alfaplusmu(Bpoint(k))+alfaplusmu(k)));
    elseif (pointtype(k)==2)
        % Center point
        alfa(k)=0;
        CI(k)=nu(Apoint(k))+alfa(Apoint(k));
        nu(k)=CI(k)-alfa(k);
        CII(k)=nu(k)-alfa(k);
        nu_rad=nu(k)*pi/180;
        Mtemp=1;
        mlow=1;
        mhigh=10;
        for b=1:100,
            Mtemp=(mlow+mhigh)/2;
            temp3 = sqrt(Mtemp^2-1);
            temp2 = atan(sqrt((gamma-1)/(gamma+1))*temp3);
            temp1 = temp2*sqrt((gamma+1)/(gamma-1))-atan(temp3);
            if (temp1 > nu_rad), mhigh = Mtemp; end
            if (temp1 < nu_rad), mlow = Mtemp; end
        end
        M(k)=Mtemp;
        mu(k)=asind(1/M(k));
        alfaplusmu(k)=alfa(k)+mu(k);
        alfaminusmu(k)=alfa(k)-mu(k);
        mI(k)=tan(0.5*pi/180*(alfaminusmu(Apoint(k))+alfaminusmu(k)));
        mII(k)=tan(alfa(k)*pi/180);
    else
        % All other points

```

```

if (min(abs(arcmaxima-k))==0)
    % Point is in arcmaxima
    % The first point will be on the arc of maxima
    [zero,arcindex]=min(abs(arcmaxima-k));
    alfacounter=alpha-0.5*arcindex*deltaalpha;
    alfa(k)=alfacounter;
else
    % Point is a regular internal point
    alfacounter=alfacounter-deltaalpha;
    alfa(k)=alfacounter;
end
CI(k)=nu(Apoint(k))+alfa(Apoint(k));
CII(k)=nu(Bpoint(k))-alfa(Bpoint(k));
nu(k)=(1/2)*(CI(k)+CII(k));
nu_rad=nu(k)*pi/180;
Mtemp=1;
mlow=1;
mhigh=10;
for b=1:100,
    Mtemp=(mlow+mhigh)/2;
    temp3 = sqrt(Mtemp^2-1);
    temp2 = atan(sqrt((gamma-1)/(gamma+1))*temp3);
    temp1 = temp2*sqrt((gamma+1)/(gamma-1))-atan(temp3);
    if (temp1 > nu_rad), mhigh = Mtemp; end
    if (temp1 < nu_rad), mlow = Mtemp; end
end
M(k)=Mtemp;
mu(k)=asind(1/M(k));
alfaplusmu(k)=alfa(k)+mu(k);
alfaminusmu(k)=alfa(k)-mu(k);
mI(k)=tan(0.5*pi/180*(alfaminusmu(Apoint(k))+alfaminusmu(k)));
mII(k)=tan(0.5*pi/180*(alfaplusmu(Bpoint(k))+alfaplusmu(k)));
end
x(k)=(y(Apoint(k))-y(Bpoint(k))+mII(k)*x(Bpoint(k))-mI(k)*x(Apoint(k)))/(mII(k)-mI(k));
y(k)=y(Apoint(k))+mI(k)*(x(k)-x(Apoint(k)));
end

%% Perform Flow Property Calculations
AoverAstar=y(contourpts)/(5*throatheight);
Mvariance=zeros(size(AoverAstar));
for l=1:size(AoverAstar,1)
    % Iterate the Area Mach relation to solve for Mach number
    mlow=1; mhigh=10; % Initial high and low guesses
    for k=1:100
        MachNo=(mlow+mhigh)/2;
        AAstar=(1/MachNo)*((2/(gamma+1))*(1+((gamma-1)/2)*MachNo^2))^((gamma+1)/(2*(gamma-1)));
        if (AAstar > AoverAstar(l))
            mhigh=MachNo;
        else
            mlow=MachNo;
        end
    end
    Mvariance(l)=MachNo;
end

```

```

PoverP0=(1+(gamma-1)/2.*Mvariance).^( -gamma/(gamma-1));
ToverT0=(1+(gamma-1)/2.*Mvariance).^-1;

%% Plot Contours
figure(1)
plot(x(contourpts),y(contourpts),'LineWidth',2)
hold on
plot(x(contourpts),-y(contourpts),'LineWidth',2)

%% Plot Characteristic Lines
refpointsA=[Apoint(num_divisions+1:num_pts),points(num_divisions+1:num_pts)'];
refpointsB=[Bpoint(num_divisions+1:num_pts),points(num_divisions+1:num_pts)'];
line(x(refpointsA).',y(refpointsA).', 'Color','b')
line(x(refpointsB).',y(refpointsB).', 'Color','b')
line(x(refpointsA).',-y(refpointsA).', 'Color','b')
line(x(refpointsB).',-y(refpointsB).', 'Color','b')
line([x(1) x(num_pts)],[0 0], 'Color','white') % Blank out centerline

%% Plot Characteristic Points
hold on
plot(x,y,'.')
hold on
plot(x,-y,'.')
plottitle=['Supersonic Contour Image for Mach ', num2str(max(Mvariance))];
title(plottitle)
axis('equal')

%% Plot Flow Property Variation
figure(2)
subplot(3,1,1)
plot(x(contourpts),Mvariance);
title('Mach Variation')
ylabel('M'), xlabel('Position (in)')
subplot(3,1,2)
plot(x(contourpts),PoverP0);
title('Pressure Variation')
ylabel('P/P_{0}'), xlabel('Position (in)')
subplot(3,1,3)
plot(x(contourpts),ToverT0);
title('Temperature Variation')
ylabel('T/T_{0}'), xlabel('Position (in)')

%% Generate Table for Export
if (generate_table==1)
    table=[points',alfa,CI,CII,M,mu,alfaplusmu,alfaminusmu,mI,mII,x,y];
end

```

Appendix D: MOC Config: Mach 2.5

```
%% Supersonic Wind Tunnel Contour Design
% Method of Characteristics
% Configuration File

% Ideal Mach: 2.5
% Actual Mach: 2.4999

% Channel divergence angle in degrees:
alpha=23.23;
% Total height of the entire throat:
throatheight=.154868;
% Number of points on the initial value line, or number of angular divisions:
num_divisions=10;
% Number of points along the contour in the expansion region:
num_expcontourpts=7;
% Ratio of specific heats of the gas:
gamma=1.4;
% Initial Mach number at the throat:
mach_initial=1.1;
% Generate Table
% If this is set to 1, a variable "table" will be created to organize the
% output data, which can be exported with xlswrite(filename,table). This
% also duplicates all data, so it may be turned off for large calculations.
generate_table=1;
```

Appendix E: MOC Config: Mach 3.68

```
%% Supersonic Wind Tunnel Contour Design
% Method of Characteristics
% Configuration File

% Ideal Mach: 3.68
% Actual Mach: 3.6797

% Channel divergence angle in degrees:
alpha=25.05;
% Total height of the entire throat:
throatheight=.154868;
% Number of points on the initial value line, or number of angular divisions:
num_divisions=10;
% Number of points along the contour in the expansion region:
num_expcontourpts=14;
% Ratio of specific heats of the gas:
gamma=1.4;
% Initial Mach number at the throat:
mach_initial=1.1;
% Generate Table
% If this is set to 1, a variable "table" will be created to organize the
% output data, which can be exported with xlswrite(filename,table). This
% also duplicates all data, so it may be turned off for large calculations.
generate_table=1;
```

Appendix F: MOC Config: Mach 4.0

```
%% Supersonic Wind Tunnel Contour Design
% Method of Characteristics
% Configuration File

% Ideal Mach: 4.0
% Actual Mach: 3.9993

% Channel divergence angle in degrees:
alpha=24.66;
% Total height of the entire throat:
throatheight=.154868;
% Number of points on the initial value line, or number of angular divisions:
num_divisions=10;
% Number of points along the contour in the expansion region:
num_expcontourpts=16;
% Ratio of specific heats of the gas:
gamma=1.4;
% Initial Mach number at the throat:
mach_initial=1.1;
% Generate Table
% If this is set to 1, a variable "table" will be created to organize the
% output data, which can be exported with xlswrite(filename,table). This
% also duplicates all data, so it may be turned off for large calculations.
generate_table=1;
```

Appendix G: Bill of Materials

Table G.1: Bill of Materials: Tunnel Parts

#	Part Description	Material	Qty	Price	Stock Order/Part No.	Vendor
1	Flange Adapter	6061 Al. Alloy	1	\$55.89	13.5"x14.8"x0.875"	Yarde Metals
2	Tunnel Length	6061 Al. Alloy	2	\$20 ea	1.5"x2"x35" Bar	Yarde Metals
3	Entry Piece	6061 Al. Alloy	1	N/A	N/A	Previous MQP
4	Side Plates	Acrylic	2	\$3.50 ea	5"x25"x0.25" Sheet	Plastics Unlimited
5	Contour	High Impact Styrene	1	N/A	48"x6"x0.125" Sheet	Prof. Blandino
6	PS Block & Diffuser Block	High Impact Styrene	8 ft	\$19.12	8720K34	McMaster
7	Quad O-ring	Buna-N	15 ft	\$0.84/ft	1034T13	McMaster
8	SHCS 1/4-28x1	Steel	10		N/A	True Value
9	SBHCS 1/4-20x0.625	Steel	20	N/A	N/A	WPI
10	Linear Rail	N/A	2	N/A	RSR-7WM	Michael Fagan
11	Screw Bracket	6063 Al. Alloy	6ft	\$15.87	4592T31	McMaster
12	SBHCS #8-32x0.375	Steel	12	N/A	N/A	Michael Fagan
13	#8x0.010x0.38 OD Washer	Steel	24		N/A	True Value
14	#10x0.03x0.38 OD Washer	Nylon	12		N/A	Michael Fagan
15	Hex Jam Nut #10-32	Steel	18		N/A	True Value
16	Pivot	Brass	6 ft	N/A	N/A	WPI
17	SHCS #10-32x2.5	Steel	10		90128A961	McMaster
18	#6-32x0.5 CS Machine Screw	Steel	10		N/A	True Value
19	SHCS M4-20mm	Steel	100		91292A121	McMaster
20	Springs	Spring Steel	2		Serv-a-Lite #25	True Value
21	1/4-20 Eye Bolt	Steel	2	\$0.52 ea.	64520	Lowe's
22	Gasket Rubber	Buna-N 35-45 Shore A	2		12"x12"x1/16"	Previous MQP
24	Large Flange Clamp Ring	316 Stainless Steel	1		12"x12"x0.25" Sheet	Yarde Metals
25	Large Flange Base	316 Stainless Steel	1		18"x18"x1.25" Sheet	Yarde Metals
26	Large Flange Window	Acrylic	2	\$68.03 ea	9.5" OD x 1" Disc	Plastics Unlimited

Table G.2: Bill of Materials: Assembly Items

#	Consumables	Vendor	Price
1	Styrene Solvent	Turn 4 Hobbies	\$6
2	Epoxy	True Value	\$4
3	Caulk	Home Depot	\$5
4	Loctite 290 Threadlocker	Orchard Supply Hardware	\$7
5	Loctite Superglue	Home Depot	\$3

Appendix H: Effect of Probe

Introduction

It was decided that some sort of diagnostics instrumentation was needed to confirm supersonic flow in the wind tunnel test section. Two traditional methods of obtaining pressure measurements were explored: tapping into one of the side plates for static pressure ports, and introducing a Pitot tube into the flow for a stagnation pressure reading behind a normal shock. Since the introduction of a probe had a more significant effect on the flow due to its inherent obstruction, its effects on the Mach number were investigated further.

Since a Pitot probe is positioned directly in the flow, it slightly reduces the test section area. Additionally, it is known that the probe would induce a shock in the supersonic flow. To get an understanding of its effects on the test section Mach number, a simple mathematical model was created using Microsoft Excel.

First, it was noted that the probe's frontal area is what plays the critical role in determining effects on Mach number. Using the simple equation for the area of a circle $A = \pi R^2$ and varying the diameter from 0.125 in. to 1.0 in., the probe's frontal area was calculated. The resulting values were subtracted from the original test section area.

Second, since the area of the throat for T1 was fixed, this new value for the test section area also yielded a modified A/A^* area ratio. This modified A/A^* corresponds to a different Mach number for the idealized case of isentropic flow. Therefore, this value was substituted into the Area-Mach Relation and used to iteratively determine the Mach number using Excel's "Goal Seek" feature.

In order to obtain valid data, the probe diameter was kept within a range that was not large enough to cause the flow to choke locally, creating a second throat. Figure H.1 depicts the calculated test section Mach number corrected for the probe's area reduction effects. As expected, the test section Mach number is indeed decreased for a reasonable range of probe

Table H.1: T1 Parameters Used for Analysis

Parameter	Value
Test Section Mach Number	3.68
A_t/A^*	8
Channel Width (const)	1.5 in.
h^*	0.25 in.
Test Section Height	2 in.
Test Section Area	3 in. ²

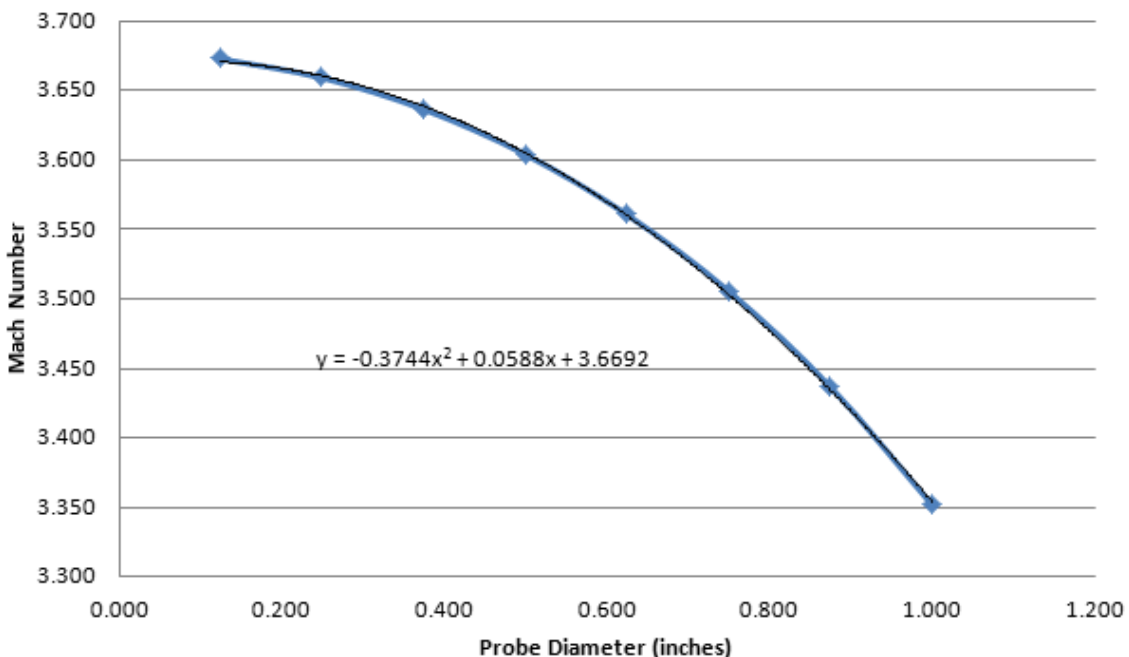


Figure H.1: Mach Number vs. Probe Diameter

diameters introduced into the flow. At first glance, the approximate 0.33 difference in the Mach numbers corresponding to the two probe diameter extremes does not seem to be too significant, but it translates to a 136 m/s or a 304 mph drop in flow velocity.

Since the area ratio is affected, it is necessary to account for the desired probe's geometry in the design process of any fixed geometry tunnel. Based on the results of this analysis, the addition of a probe would inhibit T1 from achieving its design Mach number of 3.68. Fortunately, as in the case for T2, the effects of the obstruction can be corrected with a

variable geometry nozzle.

The analysis was taken a step further to evaluate the percentage in area reduction vs. the percentage Mach number reduction. These results are plotted in Figure H.2. Since the graph

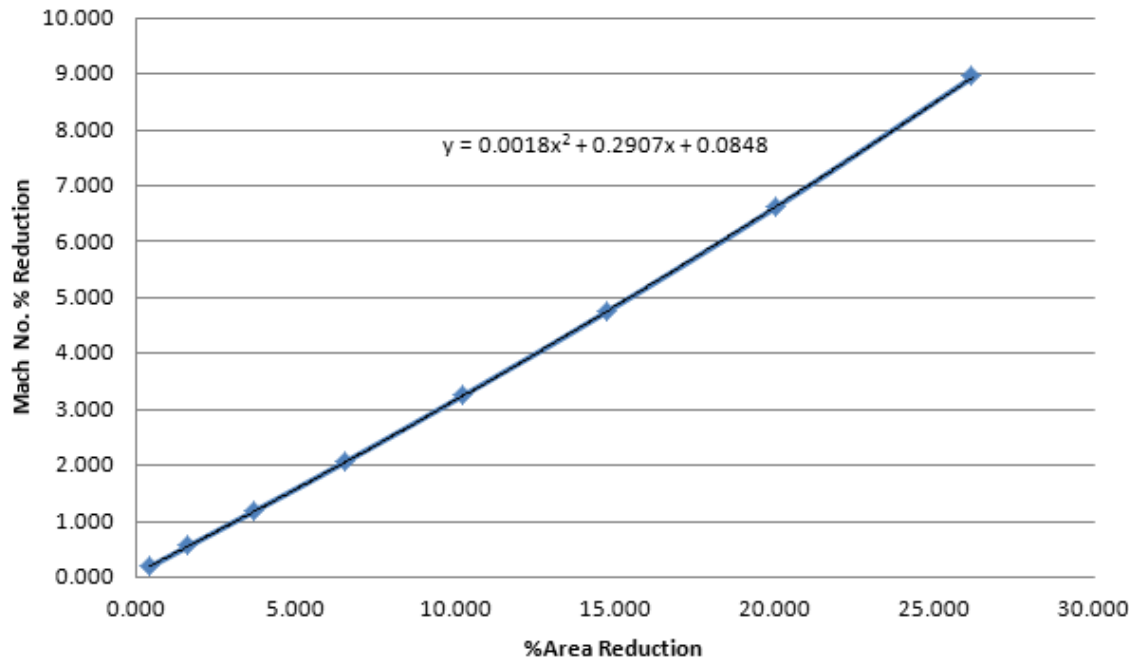


Figure H.2: Percent Reduction in Mach Number vs. Percent Area Reduction Due to Probe

shows a near linear relationship, an equation was fit to it. It turns out for this range, one can expect approximately one-third of the percentage of the area taken up by the probe to be the percentage by which the Mach number will be reduced. This can be used to perform quick calculations. For example: if one expects the probe to take up about 27% of the test section area, then one can expect to see the Mach number reduced by 9% of its nominal value.

Appendix I: Pressure Diagnostics

In running a supersonic wind tunnel, it is important that it is operating at the intended Mach number. This is crucial for designing the tunnel itself, but even more important if any testing of models is intended to be performed in the tunnel. Although there are numerous ways to analyze flow speed, the method chosen for examination in this project utilized static pressure ports to measure the static pressure in the test section. While a preliminary design of a static tube and pressure transducer was investigated, time and budget constraints kept any diagnostics from being completed. It is highly suggested that any groups pursuing a similar venture install a Pitot tube and static pressure port.

For the static port design considered for this wind tunnel, the pressure taps were intended to be holes with diameters on the order of a 1-3 mm drilled into the acrylic windows of the tunnel. On the outer side of the windows, a hole with twice the diameter was to be drilled into the same location to create a counterbore. Hypodermic tubing was to be press fit into the wider hole on the outer side of the window. Flexible rubber tubing was then to be fit over the hypodermic tubing and connected on the other end to the measuring equipment, which for this project would have included a transducer and power supply. Specific dimensions were never finalized, but the basic design could be used in the future.

No design was created for a Pitot tube, but constructing one to supplement the static port would be beneficial in the future. Care must be taken, however, to ensure that the probe diameter is small enough not to affect the test section Mach number (see Appendix H). The Pitot tube could be connected to the same type of measuring device as the static port. For this project, transducers were chosen as the appropriate tool, but the best model of transducer to use was never identified.

In order to measure the pressure being taken by a probe, a pressure transducer must be used. A transducer is a device that converts one type of energy to another [16]. In this application, the conversion would be from mechanical movement to electrical impulse.

Many pressure transducers commonly use a diaphragm to detect changes in pressure as the diaphragm deforms [16]. There were two basic types of pressure transducers considered for this project: those that measure either absolute or differential pressures. The original idea was to use a differential pressure transducer to measure the pressure in the test section relative to the ambient pressure in the room, then use this data to determine a Mach number using the Equation I.1 [2].

$$\frac{P_{02}}{P_2} = \left(1 + \frac{\gamma - 1}{2} M_2^2\right)^{\frac{\gamma}{\gamma-1}} = \left[1 + \left(\frac{\gamma - 1}{2}\right) \left(\frac{M_1^2 + \frac{2}{\gamma-1}}{\frac{2\gamma}{\gamma-1} M_1^2 - 1}\right)\right]^{\frac{\gamma}{\gamma-1}} \quad (\text{I.1})$$

This method may have worked well, but in the interest of potential future developments, it was decided that it would be better to try two absolute pressure transducers. It was theorized that if future projects considered the use of a Pitot probe in the tunnel, it would be more advantageous to have the capability to measure absolute pressure measurement. Equation I.1 was used to evaluate the range of pressures which would be measured for the Mach numbers of interest. These values were then used to identify an absolute pressure transducer that fit within the allotted budget. One candidate transducer was the PX137-015AV from Omega Engineering, Inc. The problem with this instrument was that, upon further inspection of its specifications, it would not give accurate enough readings. The specifications are presented in Table I.1.

Table I.1: Omega Pressure Transducer Specifications [17]

Model No.	Gage Pressure Range	FS ^a Output (@ 12V excitement))
PX137-015AV	15 psia	90 ± 5 mV

^a Full Scale

Concern arose as a result of the 90 ± 5 mV output and the 15 psia range because of how low the pressures in the test section would be. In order to determine the actual effect the 5 mV uncertainty would have, a sensitivity study was conducted. First, a relationship was established between the output of the transducer in volts and the input pressure in units of

pounds per square inch. The result of this relationship was each unit of pressure nominally corresponded to 6 mV, but at any given time could correspond to as much as 6.3 mV or as little as 5.6 mV, which is a very wide range. Next, the expected pressure was converted to the corresponding voltage reading, while incorporating the 5 mV uncertainty, and converted back into units of pressure.

$$\frac{6P_2 - 5}{5.6} = P_{2_{read}} \quad (\text{I.2})$$

$$\frac{6P_2 + 5}{6.3} = P_{2_{read}} \quad (\text{I.3})$$

Finally, the results of Equations I.2 and I.3 were used in Equation I.4 to produce corresponding Mach numbers. The results are listed in Table I.2, where each part of the process described above is carried out in each column. The error for the lower bound uncertainty was unable to be calculated.

$$M_2 = \sqrt{\frac{\left(\frac{P_{02}}{P_2}\right)^{\frac{\gamma-1}{\gamma}} - 1}{\frac{\gamma-1}{2}}} \quad (\text{I.4})$$

The final conclusion was that the uncertainty in the results from these transducers was too great, as illustrated in Figure I.1 and Table I.2. The Mach numbers for the lower bound were not possible to find. These calculations assumed an ambient pressure of 14 psi (P_{02} in Equation I.4), not including any error, since it would be possible to obtain this value using more precise instrumentation. In Equation I.4, P_2 is the independent variable being changed in each case listed in Table I.2.

Table I.2: Error Data for Omega PX137-015AV Pressure Transducer

Case #	P ₂ (psi)	P _{2_{read}} Lower	P _{2_{read}} Upper	P ₀ (psi)	Mach Nominal	Mach Lower	Mach Upper	Error Upper Bound
1	0.100	-0.786	0.889	14	3.939	N/A ^a	2.448	38%
2	0.150	-0.732	0.937	14	3.643	N/A	2.414	34%
3	0.200	-0.679	0.984	14	3.440	N/A	2.382	31%
4	0.250	-0.625	1.032	14	3.285	N/A	2.352	28%
5	0.300	-0.571	1.079	14	3.161	N/A	2.323	26%

^a Unable to evaluate

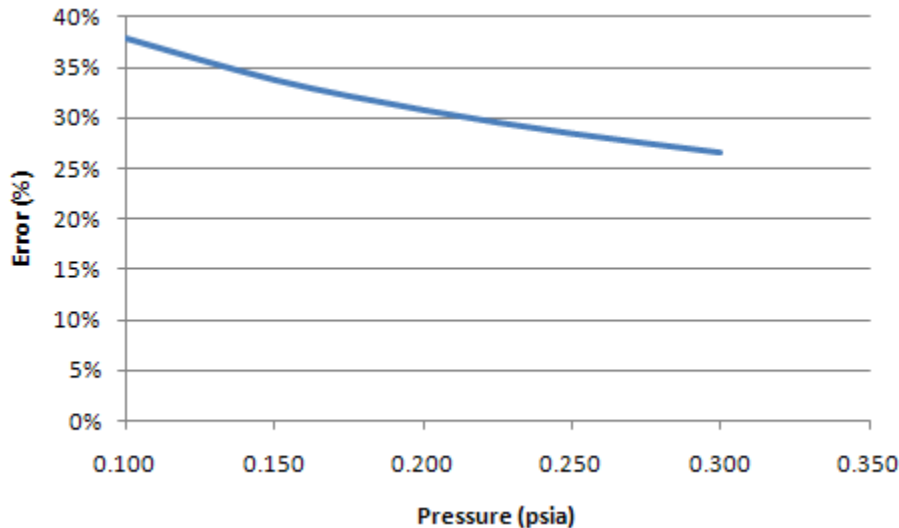


Figure I.1: Pressure (psia) vs. Error

If a Pitot probe and static port were to be used utilized for the pressure diagnostics, it is suggested that an electronics box be designed to house the transducers and necessary connections. As such an arrangement was anticipated for this project, a basic design was created (see Figures I.2 and I.3).

The transducer box was intended to allow for both the Pitot probe and the static pressure port to give readings simultaneously. The tubes running from the body of the Pitot probe and the static tap were to connect to the transducers through slightly oversized holes in the top of the electronic box. The transducers would connect to a data acquisition device via

BNC connectors affixed to the box's lid. The transducers would be powered by an external source plugged into the side of the box. For the purposes of this project, the box was intended to be entirely constructed of metal. Its size, the size of its holes, and the power needed depend entirely on the transducers and thus were not finalized.

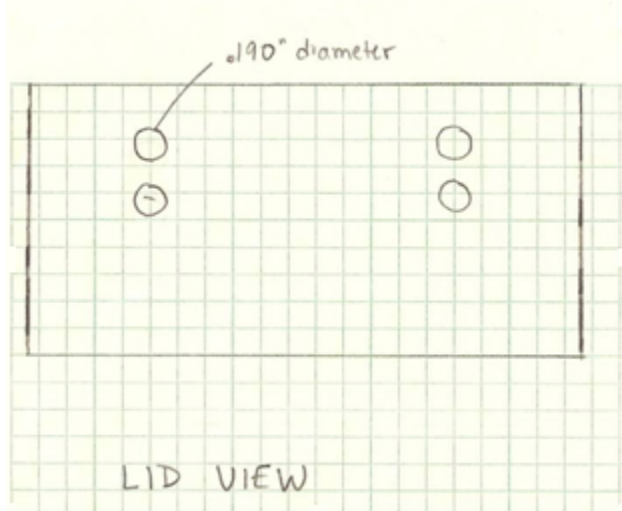


Figure I.2: Transducer Box Lid View

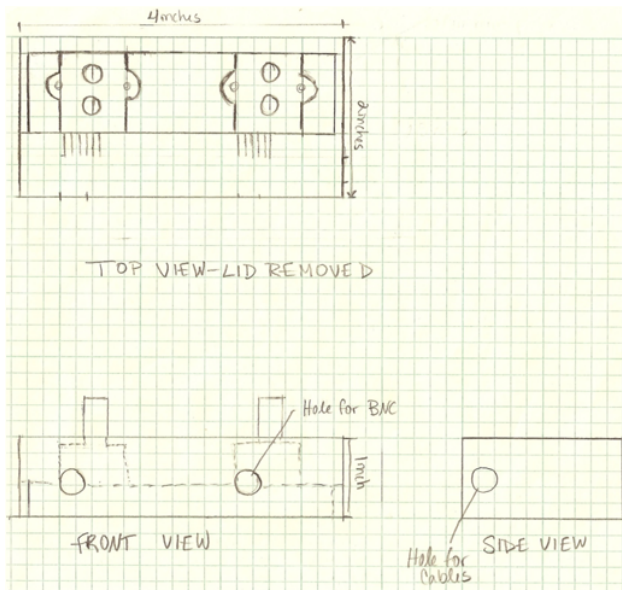


Figure I.3: Transducer Box Views

Appendix J: Psychrometrics Data

Below are the calculations performed to obtain maximum achievable Mach numbers given a range of temperatures (60-100°F) and relative humidities (0-100%). Tables are presented showing increasingly greater amounts of allowable supercooling.

Table J.1: Amount Supercooled vs. Relative Humidity

Mach. No.	Ambient Temp (°F)	Ambient Temp (°R)	Relative Humidity	Dew Point (°F)	Dew Point (°R)	Dew Temp (°R)	Amount Supercooled (°F, °R)	
T ₀ /T								
3.68	3.664	60	519.67	0.1	3	462.67	141.83	320.84
3.68	3.664	60	519.67	0.2	19	478.67	141.83	336.84
3.68	3.664	60	519.67	0.3	29	488.67	141.83	346.84
3.68	3.664	60	519.67	0.4	36	495.67	141.83	353.84
3.68	3.664	60	519.67	0.5	41	500.67	141.83	358.84
3.68	3.664	60	519.67	0.6	46	505.67	141.83	363.84
3.68	3.664	60	519.67	0.7	50	509.67	141.83	367.84
3.68	3.664	60	519.67	0.8	54	513.67	141.83	371.84
3.68	3.664	60	519.67	0.9	57	516.67	141.83	374.84
3.68	3.664	60	519.67	1	60	519.67	141.83	377.84

Table J.2: Maximum Achievable Mach Number with No Supercooling

Ambient Temp (°F)	Ambient Temp (°R)	Relative Humidity	Partial Press. of Gas (lbf/in²)	Partial Press. of Vapor (lbf/in²)	Dew Point (°F)	Dew Point (°R)	T ₀ /T	Mach No.
100	559.67	0.1			34	493.67	1.1337	0.82
100	559.67	0.2	0.9503	0.19006	51	510.67	1.0960	0.69
100	559.67	0.3	0.9503	0.28509	63	522.67	1.0708	0.6
100	559.67	0.4	0.9503	0.38012	71	530.67	1.0546	0.52
100	559.67	0.5	0.9503	0.47515	78	537.67	1.0409	0.45
100	559.67	0.6	0.9503	0.57018	83	542.67	1.0313	0.39
100	559.67	0.7	0.9503	0.66521	89	548.67	1.0200	0.32
100	559.67	0.8	0.9503	0.76024	93	552.67	1.0127	0.24
100	559.67	0.9	0.9503	0.85527	97	556.67	1.0054	0.16
100	559.67	1	0.9503	0.9503	100	559.67	1.0000	0.03
90	549.67	0.1			26	485.67	1.1318	0.81
90	549.67	0.2	0.6988	0.13976	42	501.67	1.0957	0.69
90	549.67	0.3	0.6988	0.20964	55	514.67	1.0680	0.59
90	549.67	0.4	0.6988	0.27952	62	521.67	1.0537	0.52
90	549.67	0.5	0.6988	0.3494	69	528.67	1.0397	0.45
90	549.67	0.6	0.6988	0.41928	75	534.67	1.0281	0.37
90	549.67	0.7	0.6988	0.48916	79	538.67	1.0204	0.32
90	549.67	0.8	0.6988	0.55904	83	542.67	1.0129	0.25
90	549.67	0.9	0.6988	0.62892	87	546.67	1.0055	0.16
90	549.67	1	0.6988	0.6988	90	549.67	1.0000	0.03
80	539.67	0.1			19	478.67	1.1274	0.79
80	539.67	0.2	0.5073	0.10146	35	494.67	1.0910	0.67
80	539.67	0.3	0.5073	0.15219	46	505.67	1.0672	0.58
80	539.67	0.4	0.5073	0.20292	53	512.67	1.0527	0.51
80	539.67	0.5	0.5073	0.25365	59	518.67	1.0405	0.45
80	539.67	0.6	0.5073	0.30438	65	524.67	1.0286	0.38
80	539.67	0.7	0.5073	0.35511	69	528.67	1.0208	0.32
80	539.67	0.8	0.5073	0.40584	73	532.67	1.0131	0.26
80	539.67	0.9	0.5073	0.45657	77	536.67	1.0056	0.18
80	539.67	1	0.5073	0.5073	80	539.67	1.0000	0.03
70	529.67	0.1			11	470.67	1.1254	0.79
70	529.67	0.2	0.3632	0.07264	27	486.67	1.0884	0.67
70	529.67	0.3	0.3632	0.10896	37	496.67	1.0664	0.59
70	529.67	0.4	0.3632	0.14528	45	504.67	1.0495	0.49
70	529.67	0.5	0.3632	0.1816	51	510.67	1.0372	0.43
70	529.67	0.6	0.3632	0.21792	56	515.67	1.0271	0.37
70	529.67	0.7	0.3632	0.25424	60	519.67	1.0192	0.31
70	529.67	0.8	0.3632	0.29056	64	523.67	1.0115	0.23
70	529.67	0.9	0.3632	0.32688	67	526.67	1.0057	0.16
70	529.67	1	0.3632	0.3632	70	529.67	1.0000	0.03
60	519.67	0.1	0.2563	0.02563	3	462.67	1.1232	0.79
60	519.67	0.2	0.2563	0.05126	19	478.67	1.0857	0.65
60	519.67	0.3	0.2563	0.07689	29	488.67	1.0634	0.56
60	519.67	0.4	0.2563	0.10252	36	495.67	1.0484	0.49
60	519.67	0.5	0.2563	0.12815	41	500.67	1.0379	0.43
60	519.67	0.6	0.2563	0.15378	46	505.67	1.0277	0.39
60	519.67	0.7	0.2563	0.17941	50	509.67	1.0196	0.31
60	519.67	0.8	0.2563	0.20504	54	513.67	1.0117	0.23
60	519.67	0.9	0.2563	0.23067	57	516.67	1.0058	0.16
60	519.67	1	0.2563	0.2563	60	519.67	1.0000	0.03

Table J.3: Maximum Achievable Mach Number with 55°F Supercooling

Ambient Temp (°F)	Ambient Temp (°R)	Relative Humidity	Dew Point (°F)	Dew Point (°R)	Allowable Supercooling (55°F)	Allowable Supercooling (°R)	T ₀ /T	Mach No.
100	559.67	0.1	34	493.67	-21	438.67	1.2758	1.17
100	559.67	0.2	51	510.67	-4	455.67	1.2282	1.07
100	559.67	0.3	63	522.67	8	467.67	1.1967	0.99
100	559.67	0.4	71	530.67	16	475.67	1.1766	0.94
100	559.67	0.5	78	537.67	23	482.67	1.1595	0.89
100	559.67	0.6	83	542.67	28	487.67	1.1476	0.85
100	559.67	0.7	89	548.67	34	493.67	1.1337	0.82
100	559.67	0.8	93	552.67	38	497.67	1.1246	0.79
100	559.67	0.9	97	556.67	42	501.67	1.1156	0.75
100	559.67	1	100	559.67	45	504.67	1.1090	0.73
90	549.67	0.1	26	485.67	-29	430.67	1.2763	1.17
90	549.67	0.2	42	501.67	-13	446.67	1.2306	1.07
90	549.67	0.3	55	514.67	0	459.67	1.1958	0.99
90	549.67	0.4	62	521.67	7	466.67	1.1779	0.94
90	549.67	0.5	69	528.67	14	473.67	1.1604	0.9
90	549.67	0.6	75	534.67	20	479.67	1.1459	0.85
90	549.67	0.7	79	538.67	24	483.67	1.1365	0.83
90	549.67	0.8	83	542.67	28	487.67	1.1271	0.79
90	549.67	0.9	87	546.67	32	491.67	1.1180	0.77
90	549.67	1	90	549.67	35	494.67	1.1112	0.74
80	539.67	0.1	19	478.67	-36	423.67	1.2738	1.17
80	539.67	0.2	35	494.67	-20	439.67	1.2274	1.07
80	539.67	0.3	46	505.67	-9	450.67	1.1975	0.99
80	539.67	0.4	53	512.67	-2	457.67	1.1792	0.95
80	539.67	0.5	59	518.67	4	463.67	1.1639	0.91
80	539.67	0.6	65	524.67	10	469.67	1.1490	0.86
80	539.67	0.7	69	528.67	14	473.67	1.1393	0.83
80	539.67	0.8	73	532.67	18	477.67	1.1298	0.81
80	539.67	0.9	77	536.67	22	481.67	1.1204	0.78
80	539.67	1	80	539.67	25	484.67	1.1135	0.75
70	529.67	0.1	11	470.67	-44	415.67	1.2743	1.17
70	529.67	0.2	27	486.67	-28	431.67	1.2270	1.06
70	529.67	0.3	37	496.67	-18	441.67	1.1992	1
70	529.67	0.4	45	504.67	-10	449.67	1.1779	0.94
70	529.67	0.5	51	510.67	-4	455.67	1.1624	0.9
70	529.67	0.6	56	515.67	1	460.67	1.1498	0.87
70	529.67	0.7	60	519.67	5	464.67	1.1399	0.84
70	529.67	0.8	64	523.67	9	468.67	1.1302	0.81
70	529.67	0.9	67	526.67	12	471.67	1.1230	0.78
70	529.67	1	70	529.67	15	474.67	1.1159	0.76
60	519.67	0.1	3	462.67	-52	407.67	1.2747	1.17
60	519.67	0.2	19	478.67	-36	423.67	1.2266	1.07
60	519.67	0.3	29	488.67	-26	433.67	1.1983	1
60	519.67	0.4	36	495.67	-19	440.67	1.1793	0.95
60	519.67	0.5	41	500.67	-14	445.67	1.1660	0.91
60	519.67	0.6	46	505.67	-9	450.67	1.1531	0.88
60	519.67	0.7	50	509.67	-5	454.67	1.1430	0.85
60	519.67	0.8	54	513.67	-1	458.67	1.1330	0.81
60	519.67	0.9	57	516.67	2	461.67	1.1256	0.79
60	519.67	1	60	519.67	5	464.67	1.1184	0.77

Table J.4: Maximum Achievable Mach Number with 180°F Supercooling

Ambient Temp (°F)	Ambient Temp (°R)	Relative Humidity	Dew Point (°F)	Dew Point (°R)	Allowable Supercooling (55°F)	Allowable Supercooling (°R)	T ₀ /T	Mach No.
100	559.67	0.1	34	493.67	-146	313.67	1.7843	1.98
100	559.67	0.2	51	510.67	-129	330.67	1.6925	1.85
100	559.67	0.3	63	522.67	-117	342.67	1.6333	1.78
100	559.67	0.4	71	530.67	-109	350.67	1.5960	1.73
100	559.67	0.5	78	537.67	-102	357.67	1.5648	1.68
100	559.67	0.6	83	542.67	-97	362.67	1.5432	1.65
100	559.67	0.7	89	548.67	-91	368.67	1.5181	1.61
100	559.67	0.8	93	552.67	-87	372.67	1.5018	1.58
100	559.67	0.9	97	556.67	-83	376.67	1.4858	1.55
100	559.67	1	100	559.67	-80	379.67	1.4741	1.54
90	549.67	0.1	26	485.67	-154	305.67	1.7982	2
90	549.67	0.2	42	501.67	-138	321.67	1.7088	1.89
90	549.67	0.3	55	514.67	-125	334.67	1.6424	1.79
90	549.67	0.4	62	521.67	-118	341.67	1.6088	1.75
90	549.67	0.5	69	528.67	-111	348.67	1.5765	1.69
90	549.67	0.6	75	534.67	-105	354.67	1.5498	1.65
90	549.67	0.7	79	538.67	-101	358.67	1.5325	1.63
90	549.67	0.8	83	542.67	-97	362.67	1.5156	1.61
90	549.67	0.9	87	546.67	-93	366.67	1.4991	1.58
90	549.67	1	90	549.67	-90	369.67	1.4869	1.56
80	539.67	0.1	19	478.67	-161	298.67	1.8069	2
80	539.67	0.2	35	494.67	-145	314.67	1.7150	1.89
80	539.67	0.3	46	505.67	-134	325.67	1.6571	1.81
80	539.67	0.4	53	512.67	-127	332.67	1.6222	1.76
80	539.67	0.5	59	518.67	-121	338.67	1.5935	1.72
80	539.67	0.6	65	524.67	-115	344.67	1.5658	1.68
80	539.67	0.7	69	528.67	-111	348.67	1.5478	1.65
80	539.67	0.8	73	532.67	-107	352.67	1.5302	1.63
80	539.67	0.9	77	536.67	-103	356.67	1.5131	1.6
80	539.67	1	80	539.67	-100	359.67	1.5005	1.58
70	529.67	0.1	11	470.67	-169	290.67	1.8222	2
70	529.67	0.2	27	486.67	-153	306.67	1.7272	1.91
70	529.67	0.3	37	496.67	-143	316.67	1.6726	1.83
70	529.67	0.4	45	504.67	-135	324.67	1.6314	1.78
70	529.67	0.5	51	510.67	-129	330.67	1.6018	1.73
70	529.67	0.6	56	515.67	-124	335.67	1.5779	1.7
70	529.67	0.7	60	519.67	-120	339.67	1.5594	1.67
70	529.67	0.8	64	523.67	-116	343.67	1.5412	1.65
70	529.67	0.9	67	526.67	-113	346.67	1.5279	1.62
70	529.67	1	70	529.67	-110	349.67	1.5148	1.61
60	519.67	0.1	3	462.67	-177	282.67	1.8384	2.05
60	519.67	0.2	19	478.67	-161	298.67	1.7399	1.93
60	519.67	0.3	29	488.67	-151	308.67	1.6836	1.85
60	519.67	0.4	36	495.67	-144	315.67	1.6462	1.8
60	519.67	0.5	41	500.67	-139	320.67	1.6206	1.76
60	519.67	0.6	46	505.67	-134	325.67	1.5957	1.72
60	519.67	0.7	50	509.67	-130	329.67	1.5763	1.69
60	519.67	0.8	54	513.67	-126	333.67	1.5574	1.67
60	519.67	0.9	57	516.67	-123	336.67	1.5436	1.65
60	519.67	1	60	519.67	-120	339.67	1.5299	1.63

Table J.5: Maximum Achievable Mach Number with 320°F Supercooling

Ambient Temp (°F)	Ambient Temp (°R)	Relative Humidity	Dew Point (°F)	Dew Point (°R)	Allowable Supercooling (55°F)	Allowable Supercooling (°R)	T ₀ /T	Mach No.
100	559.67	0.1	34	493.67	-286	173.67	3.2226	3.35
100	559.67	0.2	51	510.67	-269	190.67	2.9353	3.1
100	559.67	0.3	63	522.67	-257	202.67	2.7615	2.95
100	559.67	0.4	71	530.67	-249	210.67	2.6566	2.9
100	559.67	0.5	78	537.67	-242	217.67	2.5712	2.8
100	559.67	0.6	83	542.67	-237	222.67	2.5135	2.75
100	559.67	0.7	89	548.67	-231	228.67	2.4475	2.7
100	559.67	0.8	93	552.67	-227	232.67	2.4054	2.65
100	559.67	0.9	97	556.67	-223	236.67	2.3648	2.6
100	559.67	1	100	559.67	-220	239.67	2.3352	2.55
90	549.67	0.1	26	485.67	-294	165.67	3.3179	3.4
90	549.67	0.2	42	501.67	-278	181.67	3.0257	3.17
90	549.67	0.3	55	514.67	-265	194.67	2.8236	3
90	549.67	0.4	62	521.67	-258	201.67	2.7256	2.97
90	549.67	0.5	69	528.67	-251	208.67	2.6342	2.85
90	549.67	0.6	75	534.67	-245	214.67	2.5605	2.77
90	549.67	0.7	79	538.67	-241	218.67	2.5137	2.75
90	549.67	0.8	83	542.67	-237	222.67	2.4685	2.7
90	549.67	0.9	87	546.67	-233	226.67	2.4250	2.7
90	549.67	1	90	549.67	-230	229.67	2.3933	2.65
80	539.67	0.1	19	478.67	-301	158.67	3.4012	3.46
80	539.67	0.2	35	494.67	-285	174.67	3.0897	3.25
80	539.67	0.3	46	505.67	-274	185.67	2.9066	3.07
80	539.67	0.4	53	512.67	-267	192.67	2.8010	3
80	539.67	0.5	59	518.67	-261	198.67	2.7164	2.92
80	539.67	0.6	65	524.67	-255	204.67	2.6368	2.87
80	539.67	0.7	69	528.67	-251	208.67	2.5862	2.8
80	539.67	0.8	73	532.67	-247	212.67	2.5376	2.76
80	539.67	0.9	77	536.67	-243	216.67	2.4907	2.73
80	539.67	1	80	539.67	-240	219.67	2.4567	2.7
70	529.67	0.1	11	470.67	-309	150.67	3.5154	3.53
70	529.67	0.2	27	486.67	-293	166.67	3.1780	3.3
70	529.67	0.3	37	496.67	-283	176.67	2.9981	3.15
70	529.67	0.4	45	504.67	-275	184.67	2.8682	3.05
70	529.67	0.5	51	510.67	-269	190.67	2.7779	3
70	529.67	0.6	56	515.67	-264	195.67	2.7070	2.9
70	529.67	0.7	60	519.67	-260	199.67	2.6527	2.87
70	529.67	0.8	64	523.67	-256	203.67	2.6006	2.83
70	529.67	0.9	67	526.67	-253	206.67	2.5629	2.8
70	529.67	1	70	529.67	-250	209.67	2.5262	2.77
60	519.67	0.1	3	462.67	-317	142.67	3.6425	3.65
60	519.67	0.2	19	478.67	-301	158.67	3.2752	3.37
60	519.67	0.3	29	488.67	-291	168.67	3.0810	3.23
60	519.67	0.4	36	495.67	-284	175.67	2.9582	3.12
60	519.67	0.5	41	500.67	-279	180.67	2.8763	3.07
60	519.67	0.6	46	505.67	-274	185.67	2.7989	3
60	519.67	0.7	50	509.67	-270	189.67	2.7399	2.95
60	519.67	0.8	54	513.67	-266	193.67	2.6833	2.9
60	519.67	0.9	57	516.67	-263	196.67	2.6423	2.87
60	519.67	1	60	519.67	-260	199.67	2.6026	2.83